DENDRON-POLYMER-DENDRON BASED MICELLES AS DRUG DELIVERY SYSTEMS

by

Emine Ece Manavoğlu

B.S. in Chemistry, Boğaziçi University, 2009

Submitted to the Institute for Graduate Studies in
Science and Engineering in partial fulfillment of
the requirements for the degree of
Master of Science

Graduate Program in Chemistry

Boğaziçi University

2011

Canım Aileme,

ACKNOWLEDGEMENT

First of all, I am grateful to my thesis supervisor, Assist. Prof. Rana SANYAL for her guidance and help during my master and undergraduate years and letting me to her group and being my second family.

I would like to extend my thanks to Assoc. Prof. Amitav Sanyal for his helpful discussions regarding all my research for my master and undergraduate programs.

I would like to extend my thanks to Assoc. Prof. Gamze Torun Köse for her careful and constructive review of the final manuscript of my thesis.

I wish to express my great thanks to Bilge Gedik Ulusoy, Ayla Türkekul and Burcu Selen Çağlayan for running me a lot of DLS, STEM and NMR measurements supporting my laboratory work.

I want to thank to all Bogazici University Chemistry Department family and Hülya Metiner, for unforgattable years.

I want to thank to Melike Eceoğlu, Gamze Tanrıver and Serap Yapar for drug synthesis.

Then I want to thank all my present and former labmates, specifically; Nergiz ,Sezin, Oyuntuya, Tuğba, Serap, Merve, Sebla, Özgül, in the first place, for being my best friends and sharing all moments with me during lab work and outside.

I also want to thank Yeliz Yılmaz, Esra Kurmus, Burcu Güre, Elif Özülkü, Filiz Carus, Hanife Terzi for being with me all the times during my graduate studies and giving me support to bear with bad and good circumstances.

My deepest thanks go to my whole family, Abdullah, Gülay and Tuğçe Manavoğlu, my fiancee Sercan Geçici, for believing and supporting me all the time, and showing their endless love every moment.

This research has been supported by The Scientific and Technological Research Council of Turkey (TUBITAK) (107T623).

ABSTRACT

DENDRON-POLYMER-DENDRON BASED MICELLES AS DRUG DELIVERY SYSTEMS

Polymeric micelles are known to be good candidates for drug release systems due to their high loading capacities of inner hydrophobic core as well as unique compatibility in the body.

Micelles from amphiphilic copolymers can be formed in water via self-assembly according to the solubility difference of the hydrophilic and hydrophobic blocks. This kind of polymeric micelles have a narrow size distribution and unique architectured core, where hydrophobic segment forms the inner core and hydrophilic segment of the block copolymer surrounds the core and form the sphere of micelle.

In our study, dendron-polymer-dendron conjugates are prepared via Huisgen type ‘click’ reaction using polyester dendrons and PEG, followed by functionalization of the dendron surface with hydrophobic moiety. This system provides the hydrophobic-hydrophilic-hydrophobic balance neccessary to form the polymeric micelles in aqueous media. Dendron surface was further ornamented with drug molecules to yield the micellar drug delivery system.

ÖZET

İLAÇ SALIM SİSTEMLERİ OLARAK DENDRON-POLİMER-DENDRON YAPISINDAKİ MİSELLER

Polimerik misel yapılar, hidrofobik çekirdek kısmına istenilen hidrofobik molekülü yükleme kapasitesinin çokluğu ve polimer iskeletinden kaynaklanan biyouyumluluk özellikleri nedeniyle ilaç salım sistemleri için ideal olan bir araçtır.

Amfifilik kopolimer yapısındaki miseller su içerisinde herhangi bir dış etken olmaksızın oluşabilme özelliğine sahiptir. Hidrofilik/ hidrofobik bloklardaki çözünürlük farkı sebebi ile oluşan misel yapılar belli bir ölçekte büyüklük dağılımına ve hidrofobik bloğun iç çekirdeği, hidrofilik bloğunsa dış katmanı oluşturduğu eşsiz bir yapıya sahiptir.

Bu tez çalışmasında, dendron-polimer-dendron konjugeleri poliester dendronlar ve PEG polimeri kullanılarak Huisgen tipi ‘klik’ reaksiyonu ile elde edilmiş, sonraki aşamada ise dendron yüzeylerine hidrofobik fonksiyonel gruplar bağlanmıştır. Bu sistem ile, sulu ortamda polimerik misel oluşumu için gerekli olan hidrofobik-hidrofilik-hidrofobik denge sağlanır. Dendron yüzeyleri ilaç molekülleri ile bezenerek, ilaç salım sistemi potansiyeli olan misel yapılar elde edilmiştir.

TABLE OF CONTENTS

LIST OF FIGURES

LIST OF TABLES

LIST OF ACRONYMS/SYMBOLS

J	Coupling constant
ν	Frequency
μ	Wavelength
Bis-MPA	2,2-bis(hydroxymethyl)propionic acid
$CDCl_3$	Deuterated chloroform
CH_2Cl_2	Dichloromethane
CMC	Critical micelle concentration
Comb	Combretastatin
DCC	Dicyclohexylcarbodiimide
DDS	Drug delivery system
DLS	Dynamic light scattering
DMAP	N,N Dimethylaminopyridine
DMF	Dimethylformamide
EPR	Enhanced Permeability and Retention Effect
Et_2O	Diethyl ether
FT-IR	Fourier Transform Infrared
NMR	Nuclear Magnetic Resonance
P	Product
PAMAM	Polyamidoamine
PEG	Poly(ethylene glycol)
PMDETA	N,N,N',N',N''-pentamethyldiethylenetriamine
py	Pyridine
STEM	Scanning transmission electron microscope
TEA	Triethylamine
TEM	Transmission electron microscopy
THF	Tetrahydrofuran

1.INTRODUCTION

1.1 Dendrimers

Dendrimers are tree like three-dimensional structures which are synthesized by repetition of sets of reactions. Due to their well-defined structures they are very useful molecules for nanoscale applications. To control size, shape and flexibility is easy with these dendritic structures. There are two ways to synthesize dendrimers: divergent and convergent routes. Schematic representation of dendrimer synthesis routes can be seen in Figure 1.1.

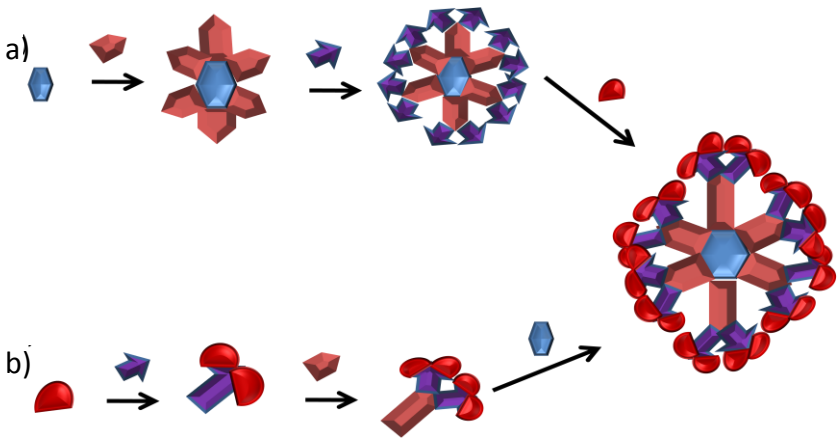

Figure 1.1. Synthesis routes for dendrimers
a) divergent b) convergent method.

In divergent method, (Figure 1.1.a) , the route for growing dendrimer is from core to shell by addition of monomer layer by layer; on the other hand, for covergent route,(Figure 1.1.b), the growth is started from the terminal group toward a focal point. But drawbacks of convergent method such as loss of valuable higher generation dendrons and steric hinderance make this type growth route disfavored [1,2].

Dendrimers are grown using the same starting monomer to get symetrical 3-D shape structures, as given in Figure 1.2., the dendrimers are named according to the number of repeating units like G1, G2, etc., meaning generation number.

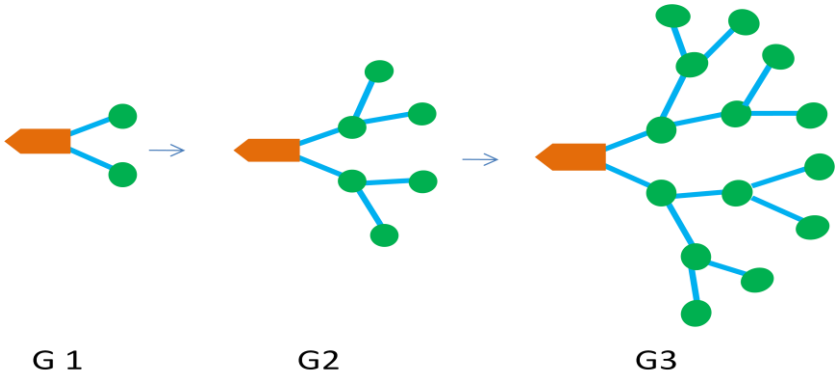

Figure 1.2. Generations of dendrimers.

Besides their structures, the unique properties of dendrimers like high degree of branching, well-defined molecular weight and multivalency, make them good candidates for drug delivery.

For dendrimer growth different types of backbones can be used like amines, polyesters, benzyls, as interested. Aliphatic polyester dendrimers based on 2,2-bis(hydroxymethyl) propionic acid are promising dendrimer backbones for the development of anticancer drug conjugates when they are combined with polymer backbones [3].

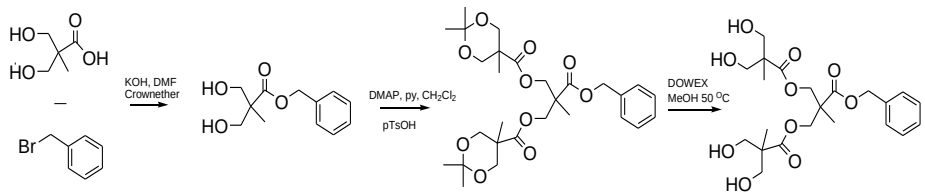

Figure 1.3. G2 benzyl ester dendron synthesized using coupling reaction.

It is very crucial that dendrimers with well-defined architectures lead low polydispersity besides controlled multiplicity of reactive chain ends. Thus, it is possible to design the periphery of a dendrimer by introducing functional groups that makes possible attachments of biomolecules, especially drug molecules. To increase molecular weight of dendrimer system, different types of polymers can also be attached to the core or periphery

using coupling or addition reactions in which Huisgen type 1,3 cycloaddition reaction is in our interest.

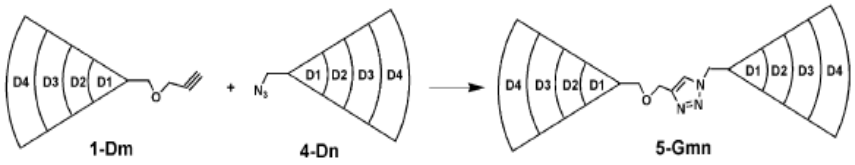

Figure 1.4. Triazole dendrimers via click reaction.

1.2. Azide/ Alkyne CuAAC Cycloaddition Reaction

Briefly, the azide/alkyne click reaction can be defined as a metal-catalyzed type of Huisgen 1,3- dipolar cycloaddition reaction between C-C triple, N-N triple bonds. The relevant products of this reaction are tetrazoles and triazoles [4]. In Cu(I) free click reaction, mainly two products are obtained, namely 1,4 and 1,5 adducts, as given in Figure 1.5. Thanks to K. Barry Sharpless and Morten Meldal, they improved this reaction by using Cu[I] catalyst and achieved to synthesize just 1,4-adduct adduct, at room temperature [5].

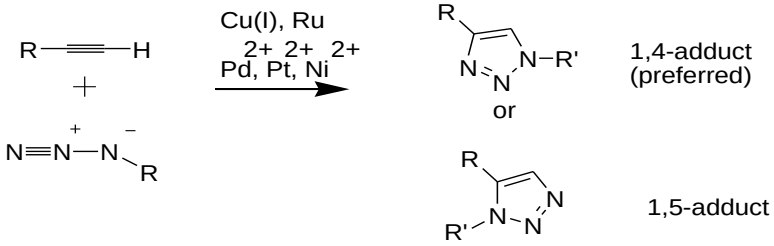

Figure 1.5. Cycloadducts after azide/alkyne click reaction.

Proposed mechanism of azide/alkyne reaction is given in Figure1.6. , this mechanism is proposed by Sharpless, then finally revised by Bock.

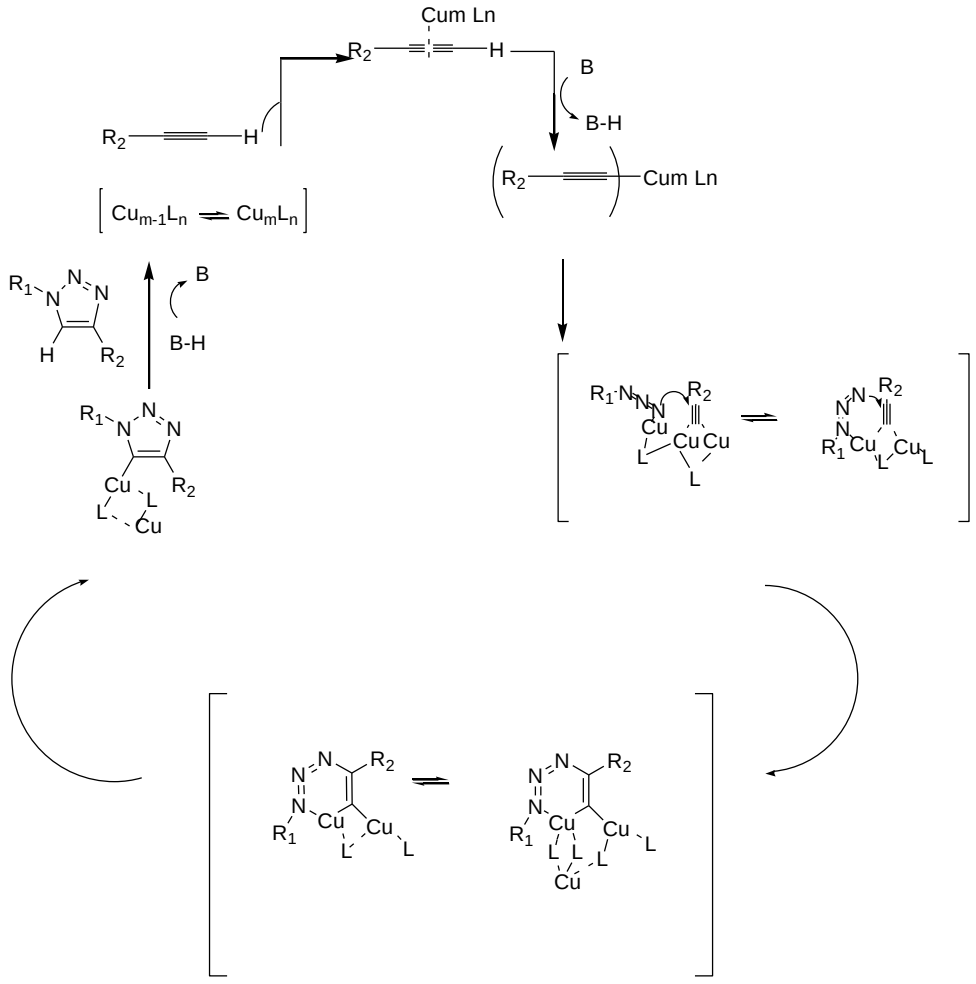

Figure 1.6. Mechanism of CuAAC reaction.

1.3. Dendron Polymer Conjugates Synthesis Using CuAAC Click Reaction

Thanks to one of a kind reliability of the Cu(I) catalyzed ligation of terminal alkynes and azides, a highly efficient route to triazole based dendrimers are now available. Many new type dendron polymer conjugates as AB or AB_2 types have been investigated up to now by different research groups.

Generally, polymer choice for this kind of conjugate systems is poly (ethylene glycol) (PEG) which is a hydrophilic polymer and used for many applications because of its lowering toxicity and immunogenity and better biodistribution characteristics.

By dendron-polymer conjugates, the benefit can be got from both the unique properties of dendrons and polymers at one shot.

Frechet and Hawker has showed the synthesis of first generation of dendronized linear polymers in 2004. As it can be seen in Figure 1.7. [6].

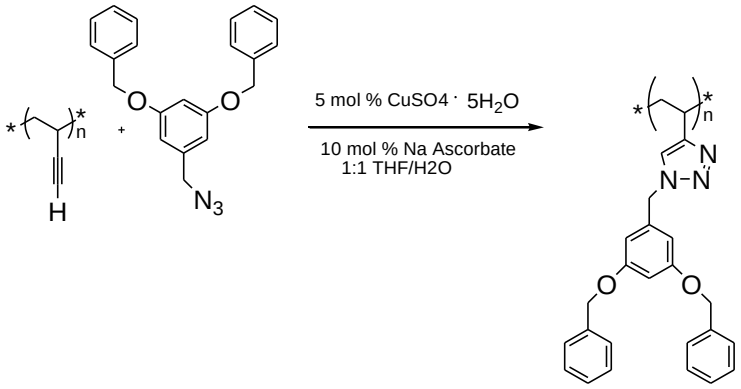

Figure 1.7. Syntetic route to first generation dendronized polymers.

Sanyal Group has studied on PEG and polyester dendrons based ABA type polymer-dendron conjugates using 'click chemistry' for hydrogel formation (Figure 1.8.) [7].

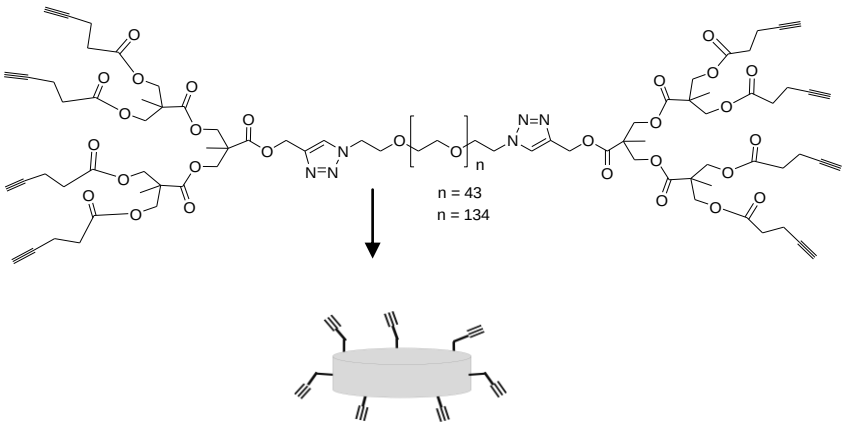

Figure 1.8. Hydrogel formation from PEG-dendron conjugates.

1.4. Polymer- Dendron- Drug Conjugates

In recent years, the great interest for preparation of new polymeric materials for drug delivery systems has brought many new designs and innovative ideas for DDS agents. The problematic properties of some potentially useful low molecular weight drug candidates are the biggest motivating reason for that kind of studies. Many low molecular weight drugs suffer from drawbacks such as poor water solubility, bioavailabilty, as well as rapid elimination [8].

Development of new DDS systems has shown that the attachment of low MW drugs to high MW polymeric backbone can lead to many benefits like improved solubility as well as increased circulation time of the polymer-drug conjugates in plasma [9].

The improved circulation time of the polymer-drug conjugates is the direct outcome of the decreased rate of renal filtration that relates with molecular size, thus molecules with larger hydrodynamic volumes are eliminated more slowly [10].

To enhance the DDS agents in terms of architectural ideality, dendrimers' well defined structures become very important. Via attaching water soluble polymers to dendrimers and thanks to modification facility at the periphery or core of dendrimers, drug molecules can be attached with known amount.

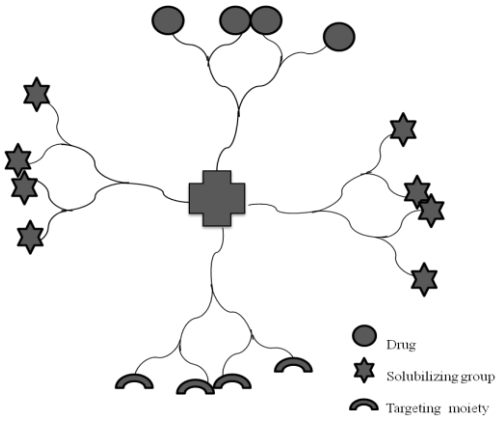

Figure 1.9. Schematic representation of a possible dendritic DDS.

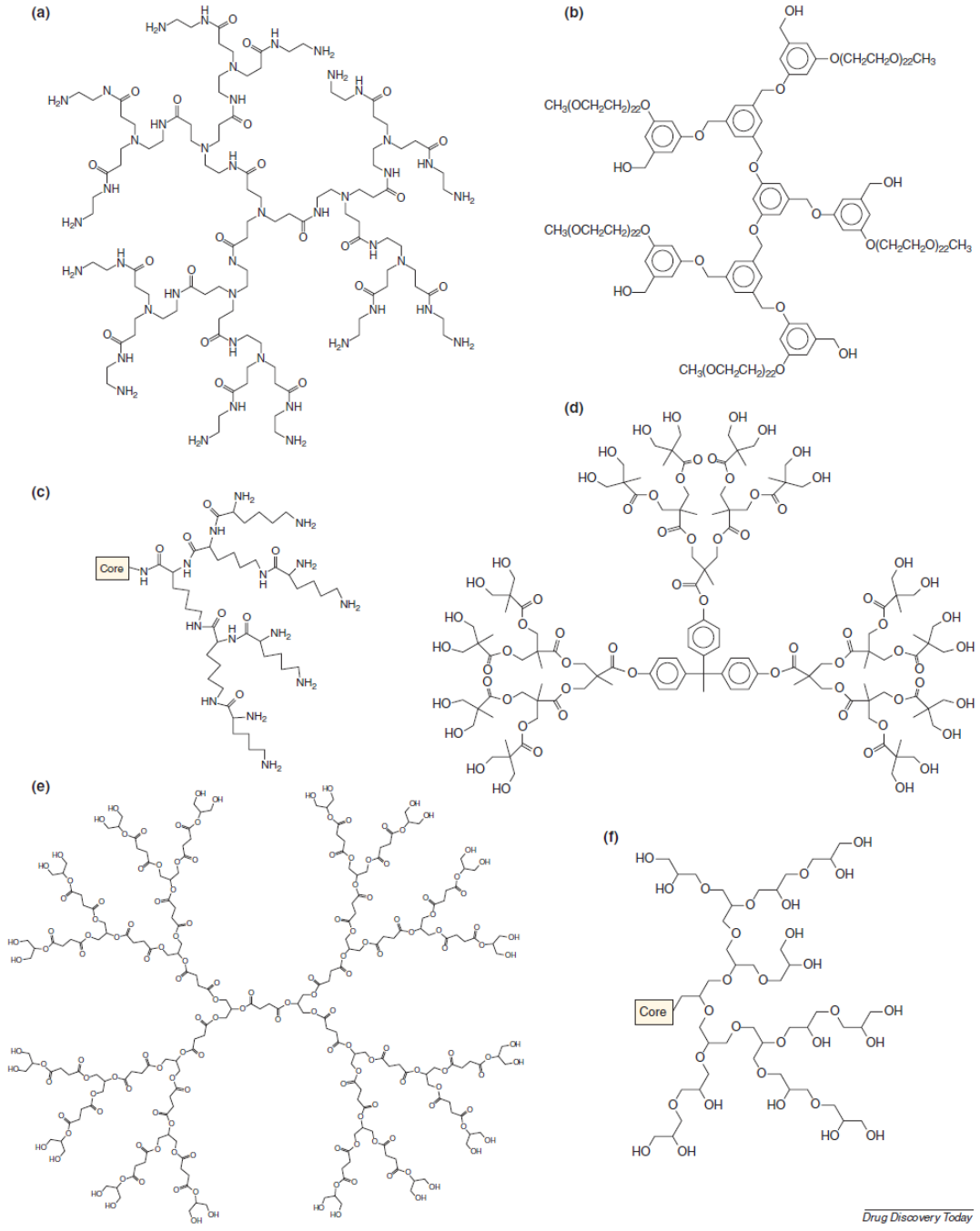

Figure 1.10. Structures of biocompatible dendrimers [11].

In Figure 1.10., there are the structures of biocompatible dendrimers which are clinically tested for drug delivery; (a) PAMAM dendrimer. (b) Polyaryl ether dendron (c)

Polylysine dendron. (d) Polyester dendrimer based on Bis-MPA (e) Polyester dendrimer based on glycerol and succinic acid. (f) Dendritic polyglycerol.

Frechet and coworkers synthesized polyester dendrimer – PEG hybrids for biological applications. They showed that polyester dendrimers do not show any preferential organ accumulation after administration to mice intravenously and rapidly excreted in the urine due to low molecular weights and its compact dendritic architecture (Figure 1.11.).

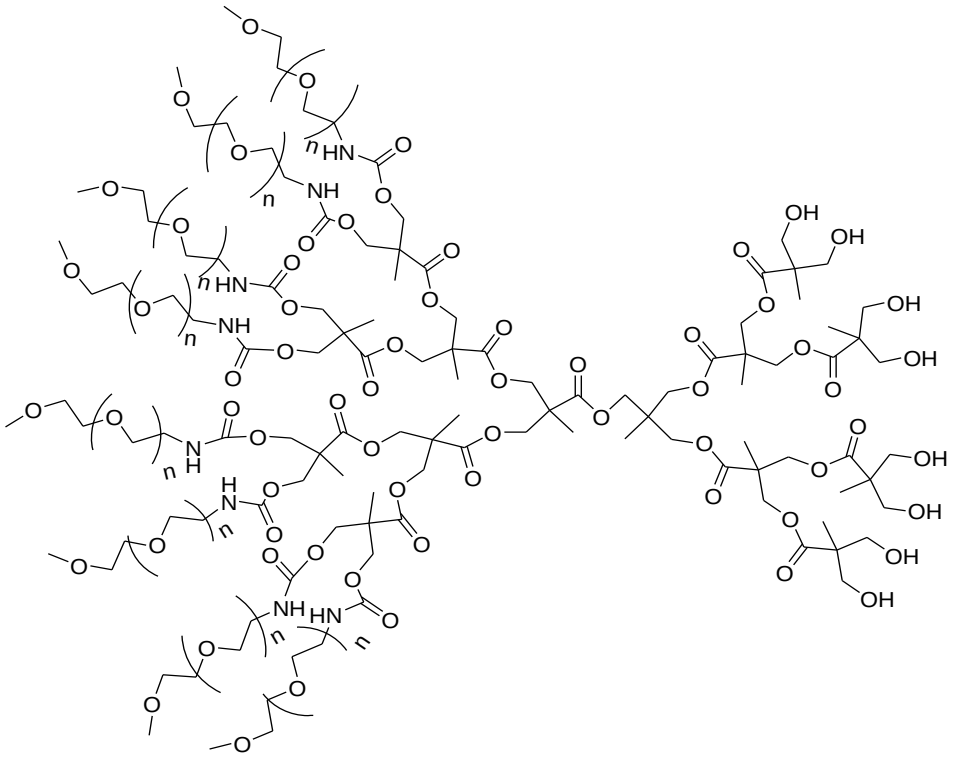

Figure 1.11. Structural representation of G3 polyester dendrimer - PEG hybrids.

Szoka and coworkers has showed the design and synthesis of dendritic polyester systems based on the 2,2-bis(hydroxymethyl)propanoic acid monomer as a possible drug carrier. One of anticancer drug, doxorubicin was attached to polymer-dendron system via pH sensitive linkage (Figure 1.12.) [12].

In recent polymer-drug conjugates' researches, many PEGylated small drug molecules are studied, while some of them became commercially available, for some of them clinical trials still go on. In the review article published in 2009, Veronese and coworkers showed different PEG-drug conjugates [13].

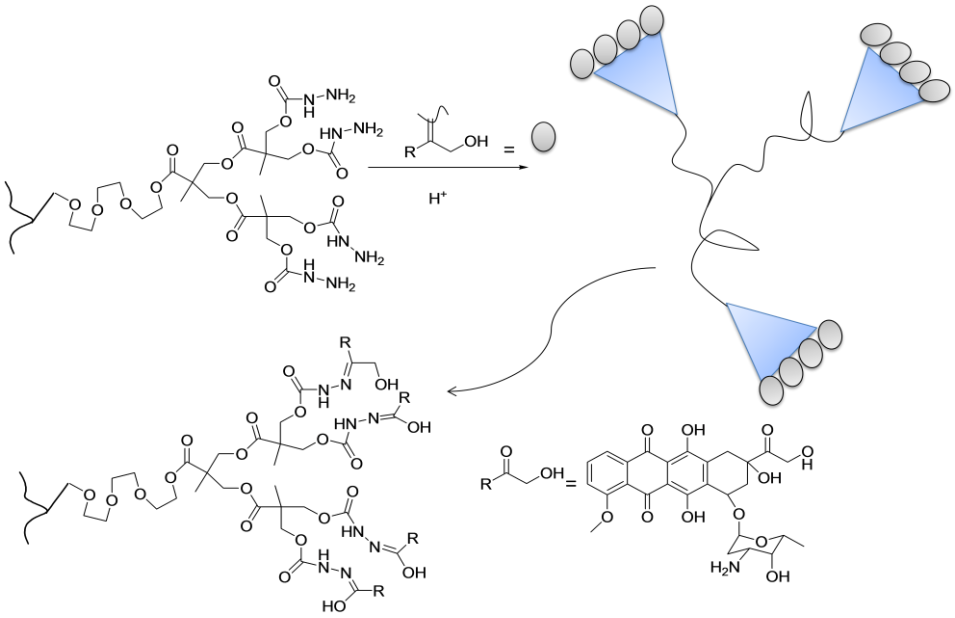

Figure 1.12. Structures of biocompatible dendrimers.

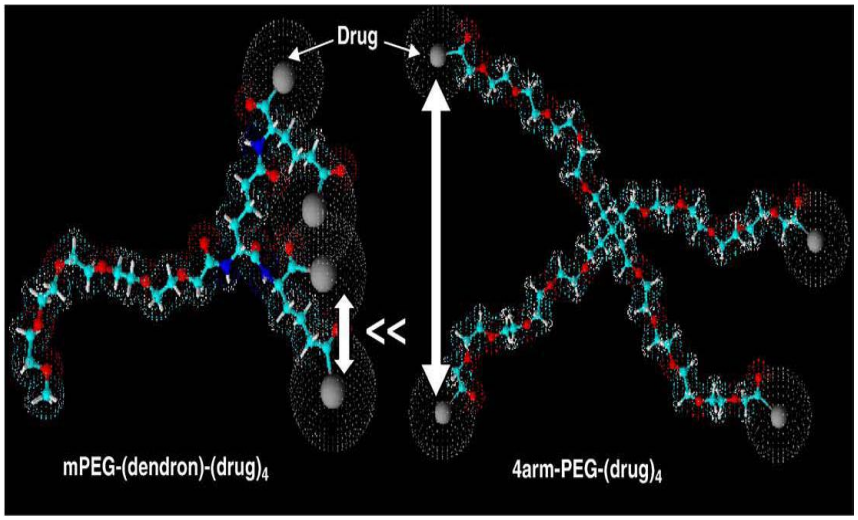

Figure 1.13. Schematic represantation of higher steric entanglement in PEG dendrons with respect to multi-arm PEGs.

1.5. Polymer-Dendron Based Micelles

Today, treatment of cancer by chemotherapy still faces major problems like lack of selectivity of anticancer drugs toward tumor cells; thus cells of gastrointestinal tract and bone marrow are affected by high cytotoxic effects of these drugs. This results in a narrow therapeutic index of many anticancer drugs [14]. Moreover, some resistant tumor cells require higher dosage of treatment which also increase the toxic effects to healthy cells; thus for efficient treatment, different vehicles are neccesary to overcome the difficulties of high dosage anticancer drugs treatment and to decrease toxicity.

Amphiphilic block copolymers which can self-assemble in aqueous media have been a popular studying topic due to their broad application area from biomaterial sciences to surface chemistry [15]. Polymeric micelles are emerging as ideal vehicles for drug delivery [16]. By these nanocarriers, solubility and longevity of drugs can be increased and controlled release by environmental sensitive or external stimuli can be accompanied. Also accumulation of drugs in solid tumors can be offered by enhanced permeability and retention effect [17].

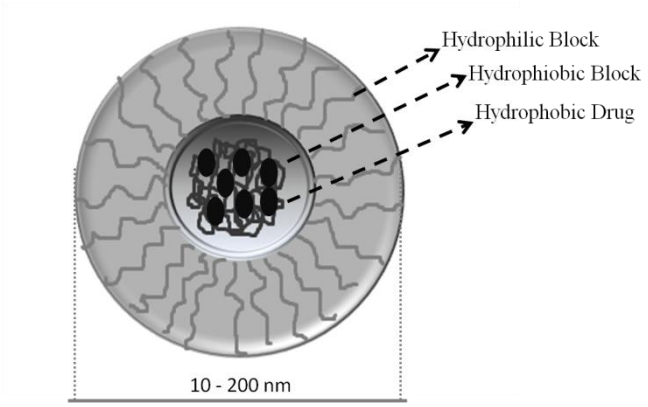

Figure 1.14. A typical structure of a polymer-dendron-drug based micelle.

The typical structure of a polymer-dendron based micelle in water is given in Figure 1.16., the structure of polymeric micelles consist of a core and a shell ; the inner core is the hydrophobic part which encapsulates poorly water-soluble drug and the shell is the hydrophilic part of block copolymer which is usually polyethylene type polymer that protects the drug from aqueous environment and provides polymeric micelle a site specific targeting drug delivery [18].

For targetting the tumor, pharmaceutical drug carriers carrying drug in plasma should possess properties like i) biodegradability, ii) small particle size, iii) high loading capacity, iv) prolonged circulation and accumulation in right pathological site in the body. [19] Also as mentioned before, enhanced permeability and retention effect (EPR) is provided by polymeric micelles, is crucial for targetted drug delivery. The morphology of tumor cell differs from healthy cell in terms of the regulation of epitel cells; where there are holes between sicked cells, there is no deformation between non-tumor cells, so that accumulation of macromolecules like polymeric micelles easily accomponied for targetted drug delivery, the figure for EPR effect is given in Figure 1.15.

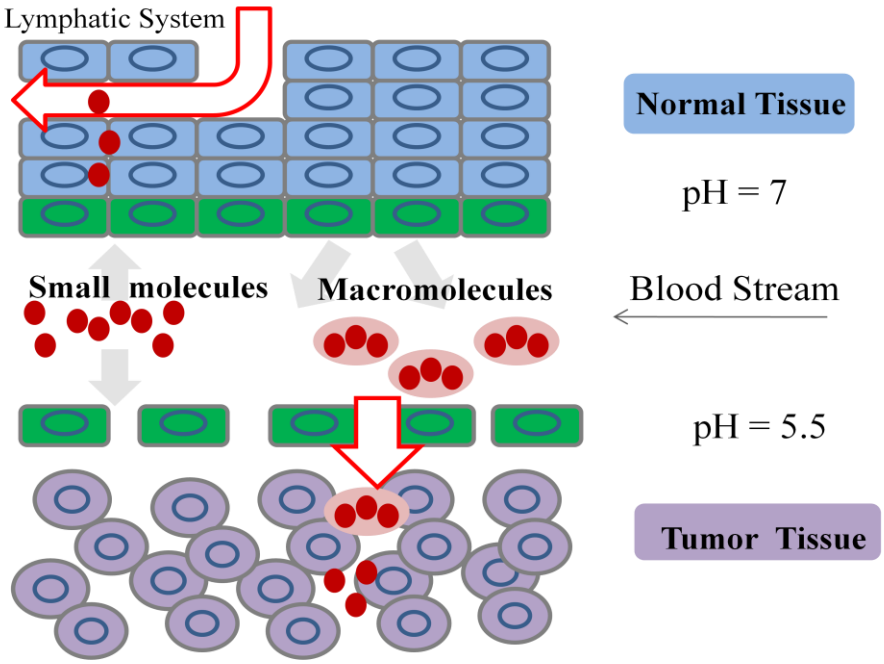

Figure1.15. Scheme of enhanced permeabilty and retention effect.

In the early 1990s, Kataoka's group introduce polymeric micelles as drug delivery systems, via development of doxorubicin-conjugated block copolymer micelle. [20] Polymeric micelles have also been used for delivery of many anticancer agents in preclinical and clinical studies. Liposomes, lipid based drug delivery systems, nanoparticles also reported for solid-tumor targetting agents but they are the victim of acquired drug resistance and poor targeting. Polymeric micelles are the only reported drug delivery systems that establish multi drug resistance using different approaches like passive targeting, ph- sensitive and thermosensetive drug delivery systems [21].

In 2004, Kim and coworkers has showed the micellar characteristics of urethane-amide based dendron-PEG conjugates in water. The mean diameter of this micellar sytems found to be between 90-170 nm range with dynamic light scattering methodology [22].

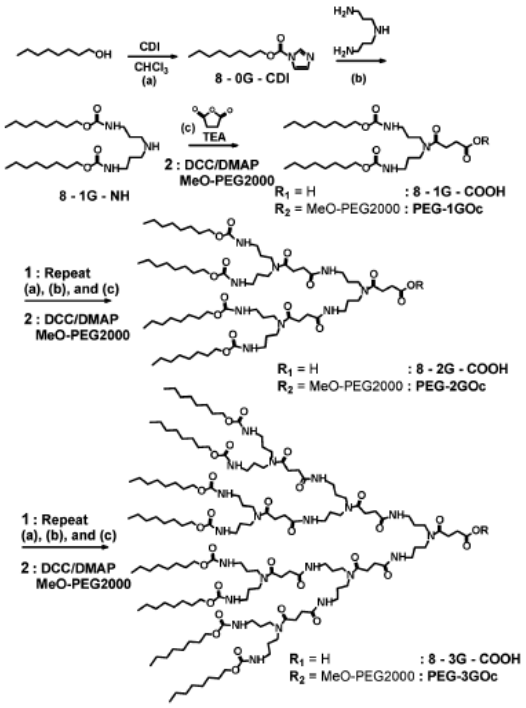

Figure 1.16. Synthesis of dendron-PEG conjugates before micelle formation.

Hammond and coworkers has designed and synthesized an amphiphilic comb-dendritic block copolymer based on poly (*ç-n*dodecyl-L-glutamate) as a hydrophobic comb

block and a hydrophilic polyester dendron block modified with PEG. The critical micelle concentration (CMC) was found to be 10^{-8} M approximately [23].

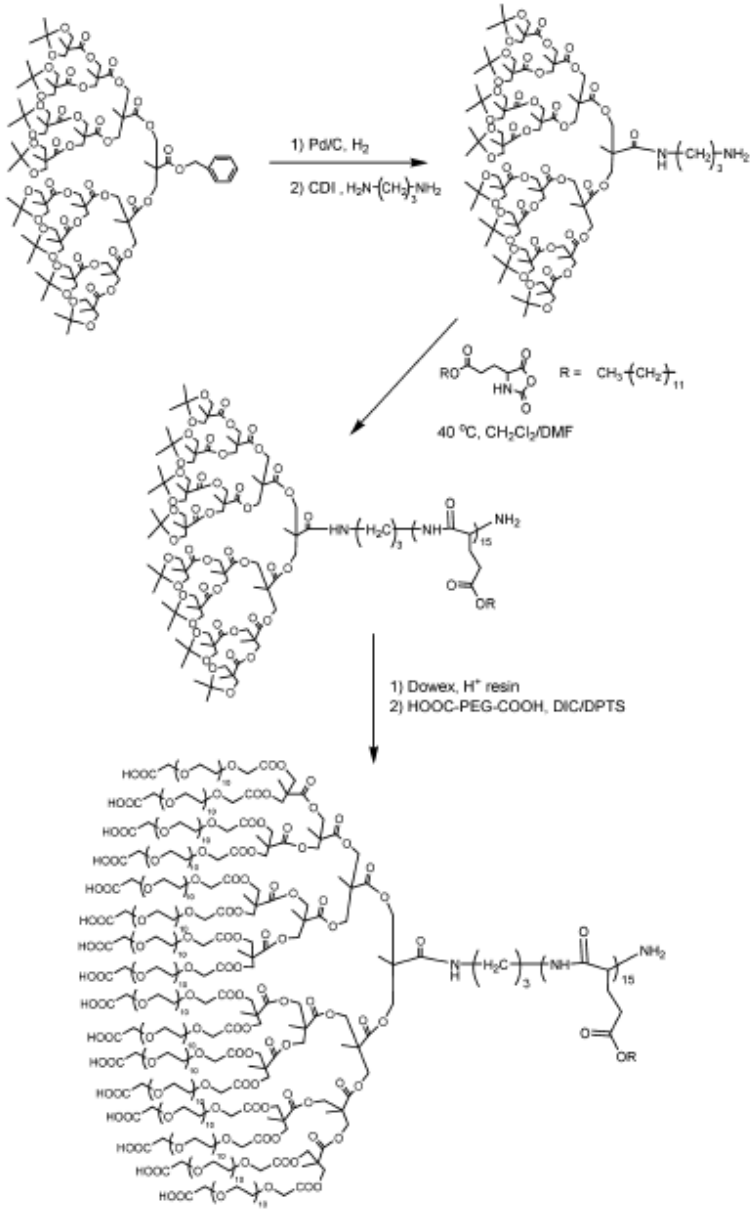

Figure 1.17. Synthetic route of comb-dendritic block copolymer.

These dendritic architectures found to have micellar properties in water via self assembly due to amphiphilicity.

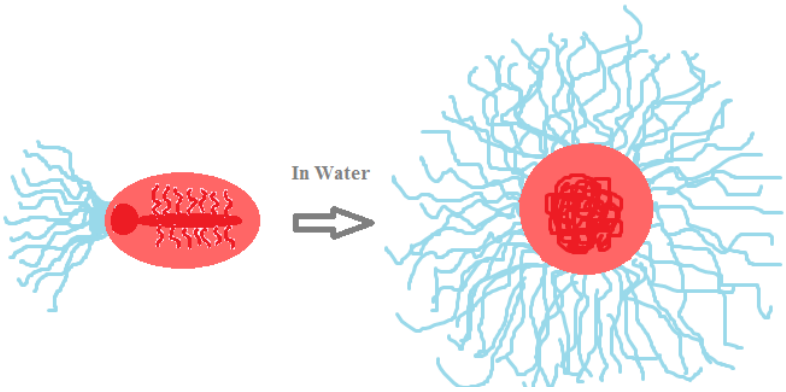

Figure 1.18. Self assembly of dendron-polymer based micelles in water.

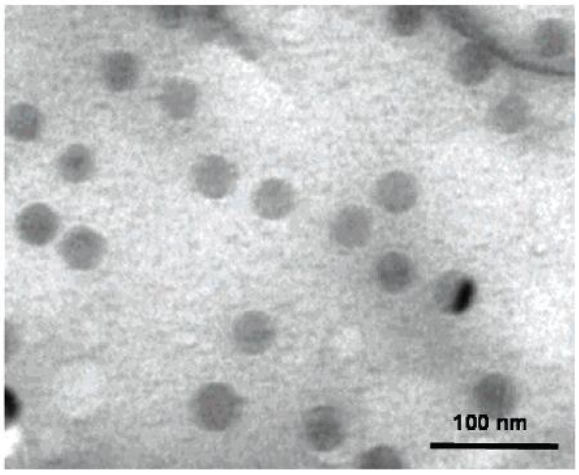

Figure 1.19. TEM image of comb-dendritic micelles.

Liu et al. , explored the potential of dendritic unimolecular micelles in DDS. In their study , they used dendritic unimolecular micelles with a hydrophobic core surrounded by a hydrophilic shell via coupling dendritic hypercores with PEG mesylate. The monomer choice was 4,4-bis(49-hydroxyphenyl) pentanol [24].

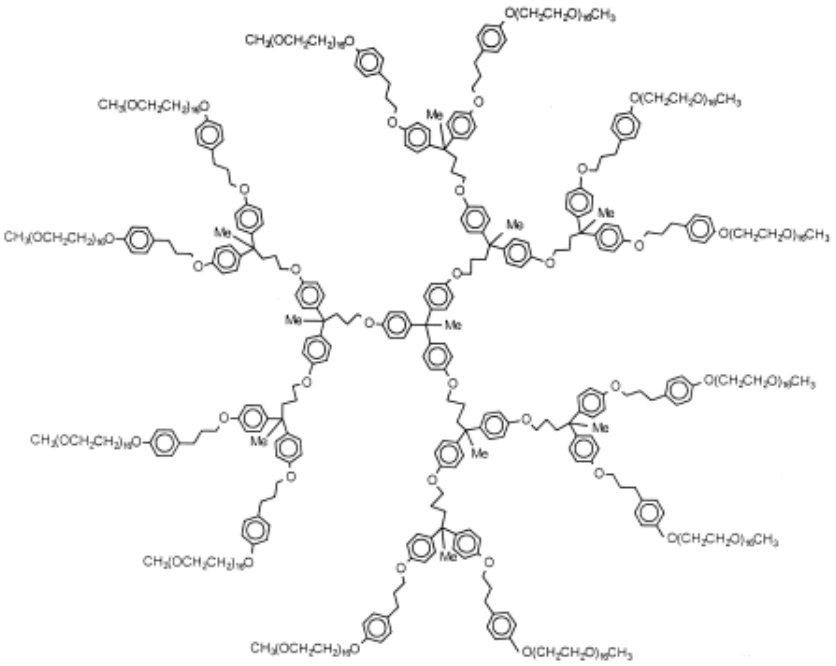

Figure 1.20. Structure of G2 unimolecular dendritic micelle.

The critical micelle concentration (CMC) , the minimum concentration of conjugate that tend to form micelle, is most commonly performed technique to evaluate the thermodynamic stability of the micelles in aqueous solutions. CMC measurements generally performed using the fluorescence method with pyrene as the probe since pyrene preferentially partitions into the hydrophobic core of micelles in water. Moreover, pyrene's long excited-state lifetime and spectral sensitivity to the surrounding medium makes it a good candidate for fluorescence studies. Generally, excimer fluoresence measured by the excimer-to-monomer ratio (I_E/I_M) provides highly localized information because the excimer is only formed when aromatic rings of pyrene closely approach each other within 4-5 A^o. Amphiphilic polymers generally have lowered CMC values, usually 10^{-6} M [25-32].

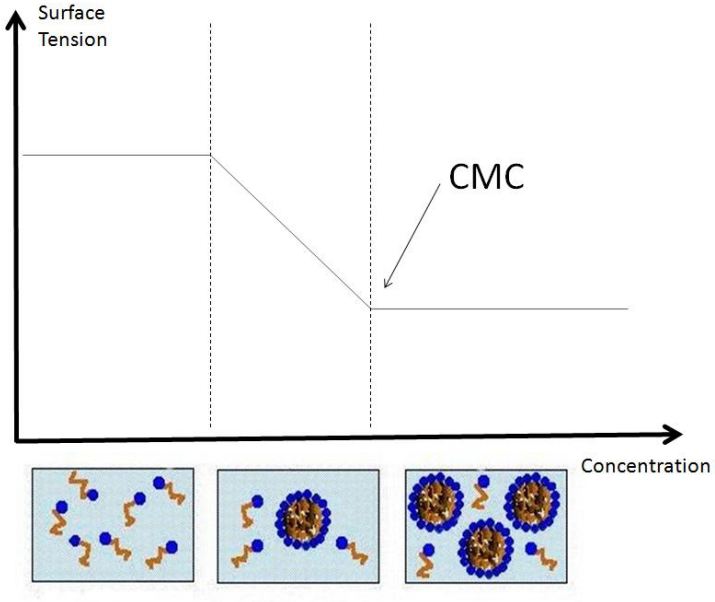

Figure 1.21. Represantation of CMC.

Yang et al. has reported PEG-PAMAM unimolecular micelle systems. He claimed that high molecular weight PEG attached micelles would tend to agglomerate even at relatively low concentrations. The entangled PEG arms disrupted the stability of the network at the surface and these long arms may tend to penetrate into other micelles and occupy the inner space instead of guest molecules. Thus partial loss of inner space occurs due to agglomeration [33].

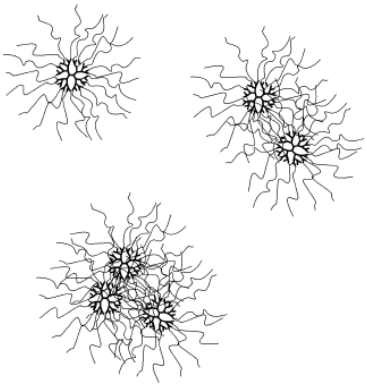

Figure 1.22. Schematic diagram of micelle agglomeration.

2. AIM OF THE STUDY

2.1. Micelle Formation From ABA Block Copolymers

Micelles have high potential for carrying hydrophobic molecules , thus they are good candidates for drug delivery systems. To get micellar structures, hydrophobic/hydrophilic blocks must be used in the design. In this study, we tried to introduce a novel micellar structure, using dendron-polymer-dendron conjugates. Using dendron-polymer-dendron conjugates brings multivalent, well defined architectural properties, besides biocompatible and biodegradable facilities to the system. For our design, we used biodegradable polyester dendrons and attached them to bifunctional biocompatible polyethylene glycol polymer chain using Huisgen type click reaction. Due to surface properties of polyester dendrons, alkyne functionality was brought to the system. This system is an amphiphilic design. So that, conjugates tend to form micellar structures in water via self-assembly. We tried to get micellar structures and the result were as expected.

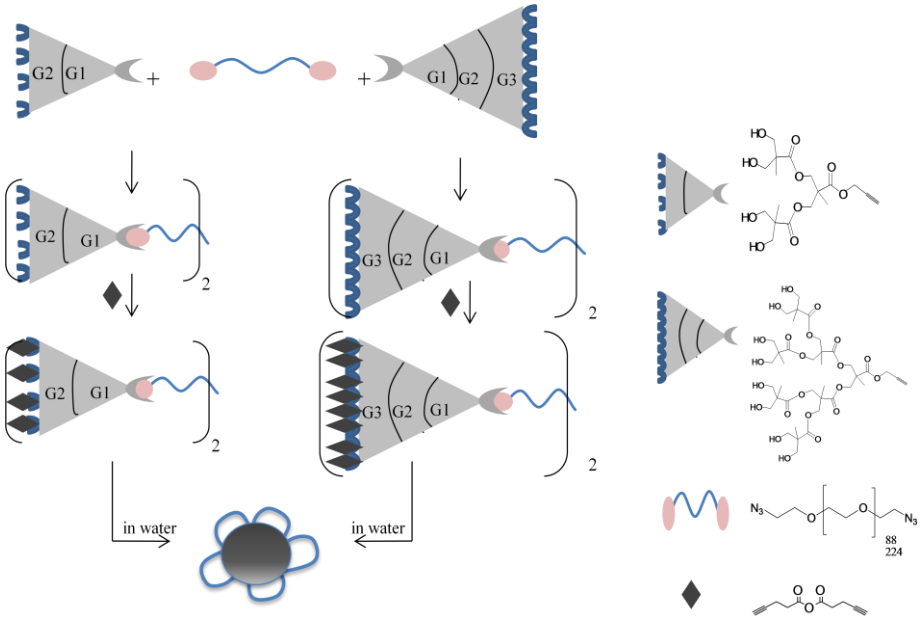

Figure 2.1. General scheme for micellar structures of ABA copolymers.

2.2. Micellar Structures from Drug Conjugated ABA Copolymers

After the synthesis of ABA copolymers they become available to one more click reaction in the presence of azide bearing molecule due to alkyne functionality at dendrons' surfaces. We introduce azido-COMB molecule to the generation 2 and 3 polyester dendron conjugated PEG10K copolymers and COMB functionalized drug conjugates were synthesized. Micelle formation from these drug conjuagetes was performed via self-assembly in water.

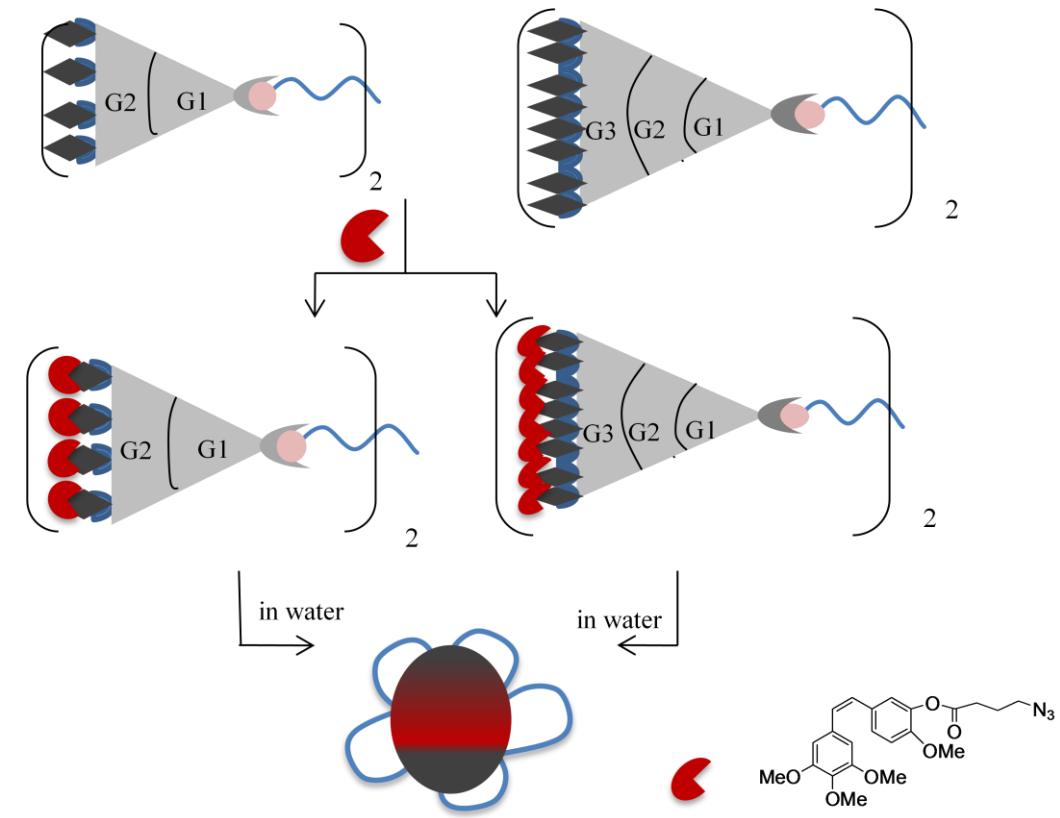

Figure 2.2. General scheme for micellar structures of drug conjugates copolymers.

3. RESULTS AND DISCUSSION

3.1. Preparation of ABA Triblock Copolymers

In order to obtain ABA triblock copolymers, biodegradable polyester dendrons and biocompatible PEG polymer were conjugated via Huisgen type [3+2] cycloaddition reaction in the presence of Cu(I)Br. Two generations of the polyester dendrons, namely G2 and G3 were used in this study. The molecular weights of PEG that were used in experiments were 4000 and 10000 Da. Starting from PEGdiol, 4K and 10K, mesylated PEG products, then bisazido PEGs 3 and 4 were obtained.

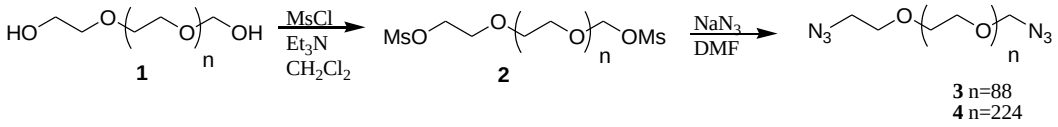

Figure 3.1. Synthesis of bisazido PEGs.

Polyester dendrons 5 and 6 were synthesized according to literature. Then, dendron-polymer-dendron combinations were synthesized via the Huisgen type [3+2] "click" reaction, in the presence of Cu(I)Br and PMDETA in THF (Figure 3.2.) The conjugates are named according to the dendron generation used and the length of PEG chain, for instance, p 9 means generation three polyester bearing sixteen hydroxy functional groups on the surface as the A block and the PEG's molecular weight is 4000 Da as the middle B block.

After the synthesis of ABA type conjugates, functionalization to the surface of the dendrons were done using 4-pentynoic anhydride 3c using DMAP and pyridine in dry CH_2Cl_2. Via this acylation reaction the surface hydroxy groups on the dendrons changed to have alkyne functionality. These funtionalized copolymers named as p 15, where R group represents the alkyne unit. 4-pentynoic anhydride was synthesized using 4-pentynoic acid via DCC coupling reaction. In Figure 3.3. synthesis scheme of 4-pentynoic acid can be seen.

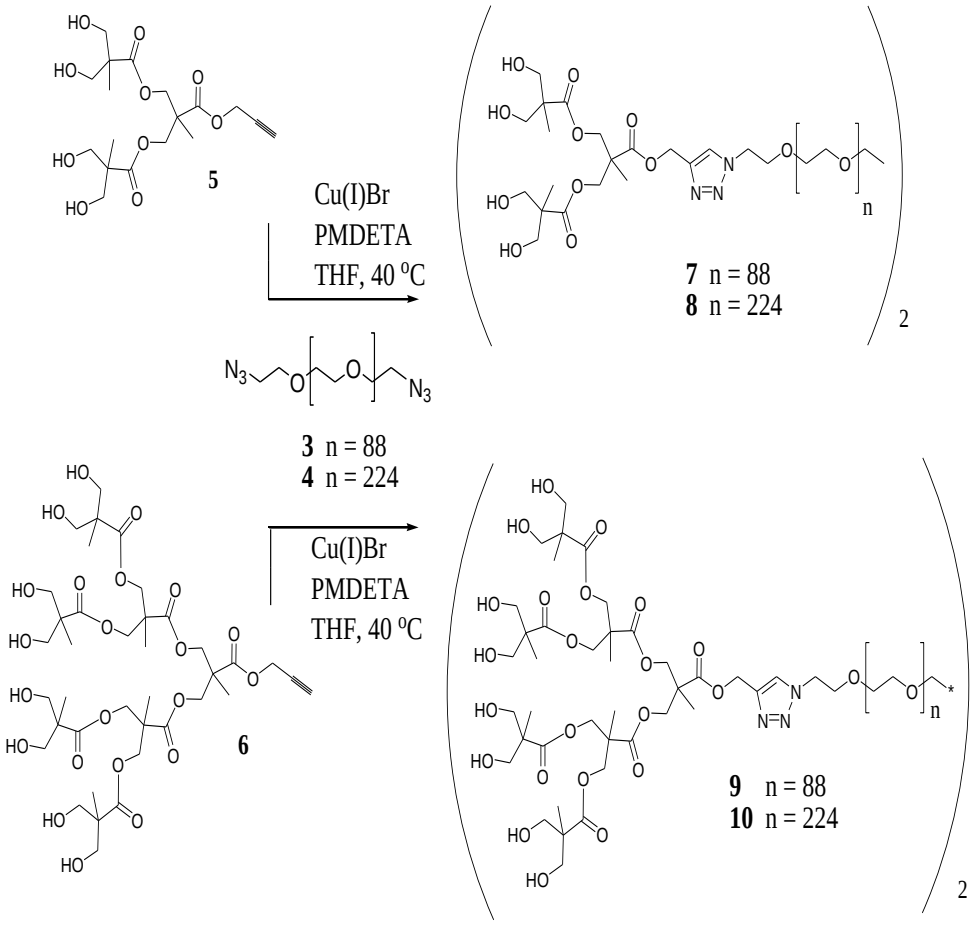

Figure 3.2. Synthesis of ABA triblock copolymers.

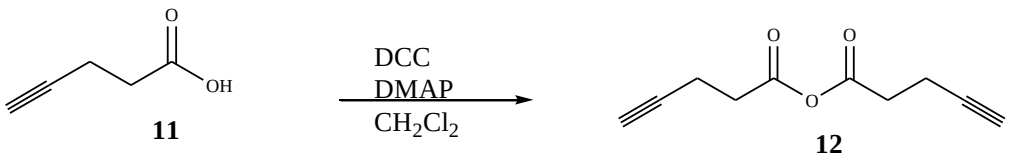

Figure 3.3. Synthesis of 4-pentynoic acid.

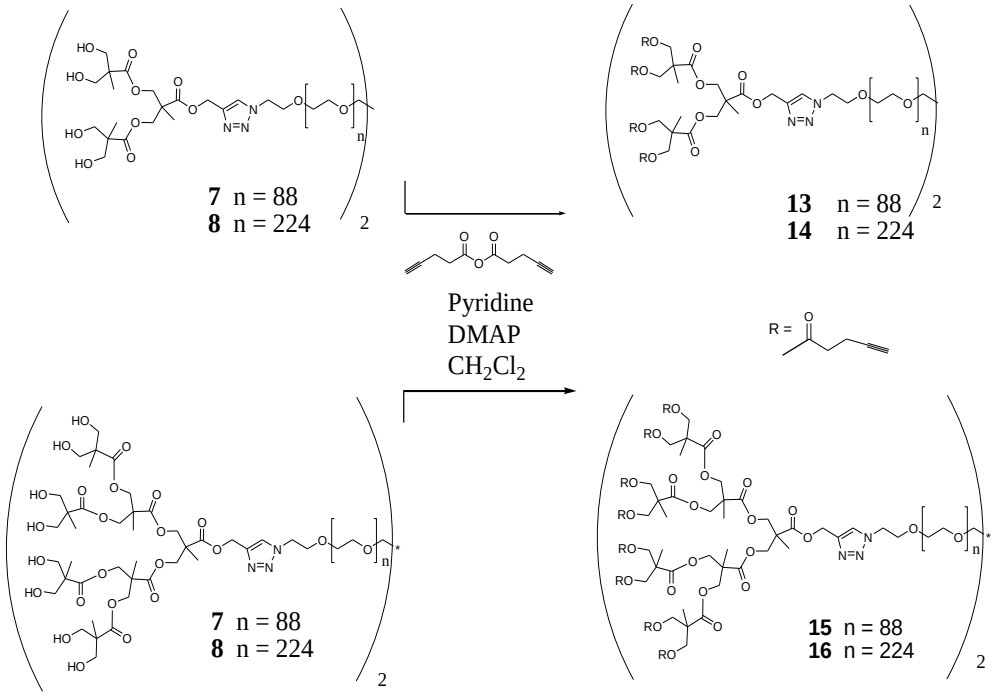

Figure 3.4. Acylation of ABA triblock copolymers.

All synthesized products were characterized via FT-IR, where the functional group changes can be tracked easily.

In click reaction azide group of the polymers and the core alkyne proton forms a triazole ring, so that for new ABA copolymer azide functional group disappears. In FT-IR, the azide functional group characteristic peak is 2100 cm^{-1}. In Figure 3.3. the FT-IR of bisazido PEG4K, due to the C-N bond stretching, shows a sharp peak at 2095 cm^{-1}(a), after the conjugation with G2 dendron , this peak disappearead and the characteristic broad peak between 3100 - 3500 cm^{-1} which represents the hydroxy groups on the surface of dendrons and also, the carbonyl stretch which belong to the carbonyl esters of dendron units at 1731 were seen. After the functionalization of the hydroxy surface, the presence of the alkyne functionality was established through the peak at 3283 cm^{-1} which was due to alkyne stretching, while the broad hydroxy bend at 3434 cm^{-1}disappeared.

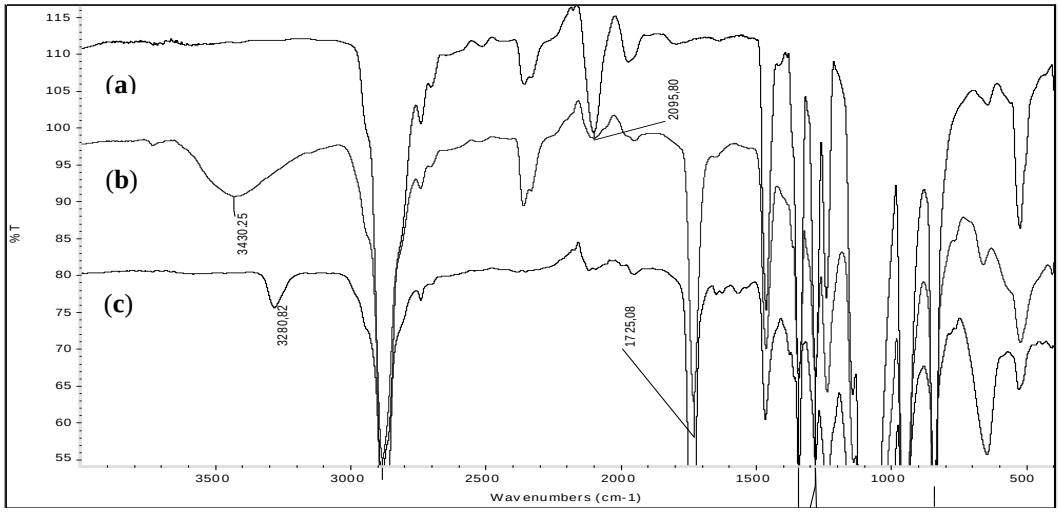

Figure 3.5. FT-IR results of a) p3, b) p9 c) p15.

The same changes on FT-IR measurement were seen for the conjugates based on PEG10K. The characteristic peak of C-N stretching azide peak at 2101.65 cm $^{-1}$ disappears after the click reaction of bisazido PEG10K and [G3]16OH dendron and a peak at 3430 cm $^{-1}$ for hydroxy groups and at 1732 cm $^{-1}$ for carbonyl groups of dendron units appearance support the triblock copolymer synthesis. After alkyne functionality obtained, appearance of the peak at 3283 cm $^{-1}$ indicates C-H stretching.

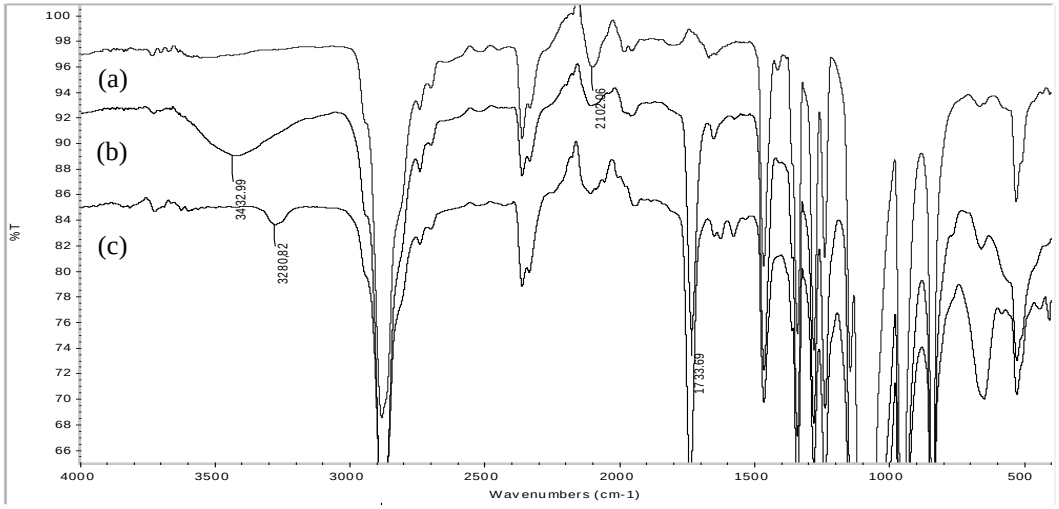

Figure 3.6. FT-IR spectrum of a) p4, b) p10 and c) p16.

The synthesis of the conjugates and their functionalization were also monitored via ^{1}H-NMR.

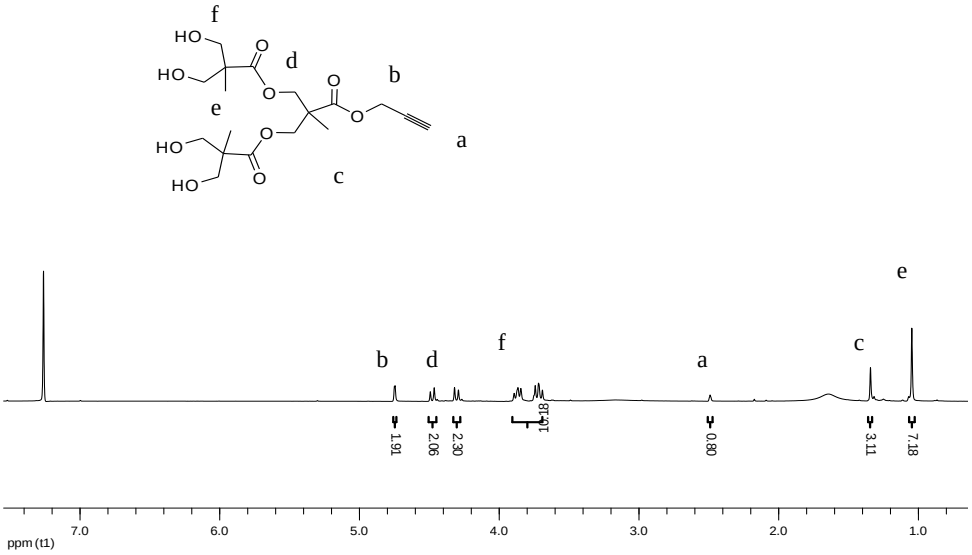

Figure 3.7. ^{1}H NMR of p5.

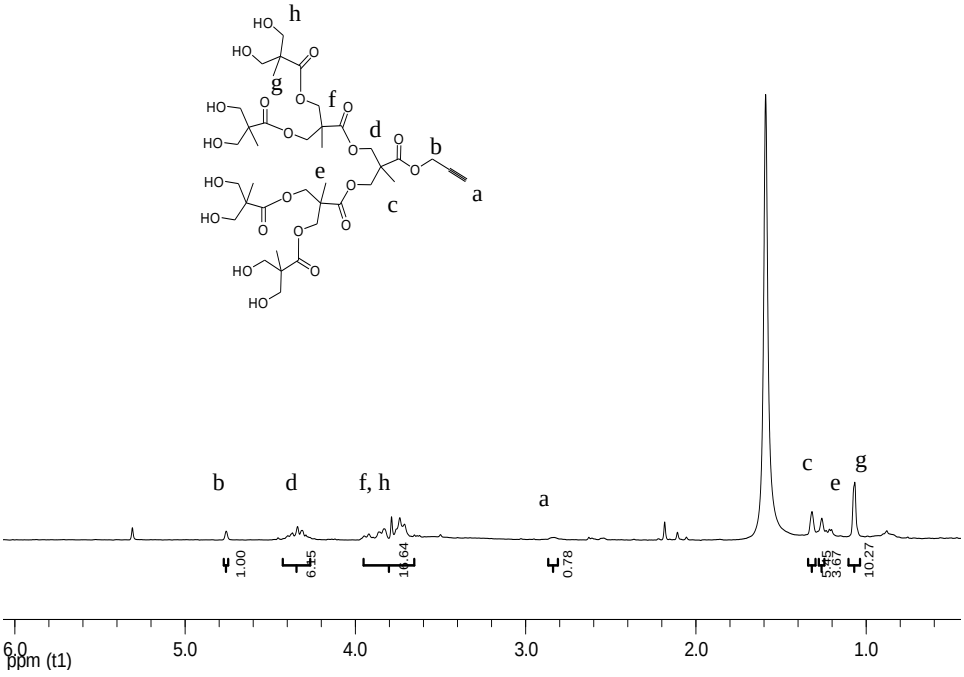

Figure 3.8. ^{1}H NMR of p6.

From the ^{1}H NMRs of G2 and G3 dendron in Figure 3.4. and Figure 3.5. , respectively, the H assignments can be seen easily. For both generations a singlet at 4.76 ppm is present that belongs to the $–CH_2$ near the –O group. Also the $–CH_2$'s of dendron arms are present for both, seen as doublet of doublet 4.40 and 4.24 ppm. The alkyne H is present for both as a singlet at 2.43 ppm and the methyl Hs give singlets at 1.2-1.0 ppm range, 2 singlets (9H) for G2 and 3 singlets (21H) for G3 dendrons.

From the 1H NMRs of bisazido-PEG 4000 and 10000 Da, just $–CH_2$ near nitrogen at 3.37 ppm and the $–CH_2$s of PEG polymer between 3.8-3.4 ppm are present.

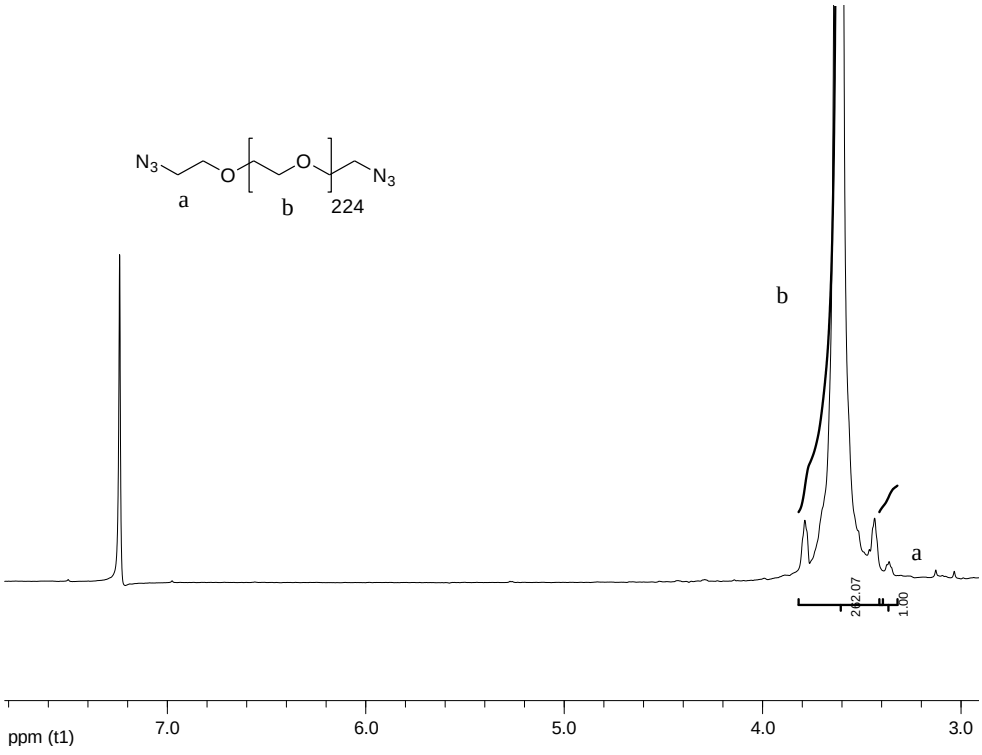

Figure 3.9. ^{1}H NMR of p4.

After the Huisgen type click reaction between the G2, G3 dendrons and bisazido-PEG 10K and 4K, 1,4-triazole formation occurs between the alkyne core of dendrons and N_3 ends of PEG polymers. This triazole hydrogen can be defined from ^{1}H NMR of ABA triblock copolymers as a singlet at 7.85 ppm. Dendrons and polymers protect the characteristic H shifts on nmr spectrum, except the singlet at 3.1 ppm for dendrons which belongs to the terminal alkyne H. Also the terminal 2Hs near –O-OC of dendron shift to

5.2 ppm from 4.78 after conjugation since its position changed to be between N and O atoms that result in a deshielded field.

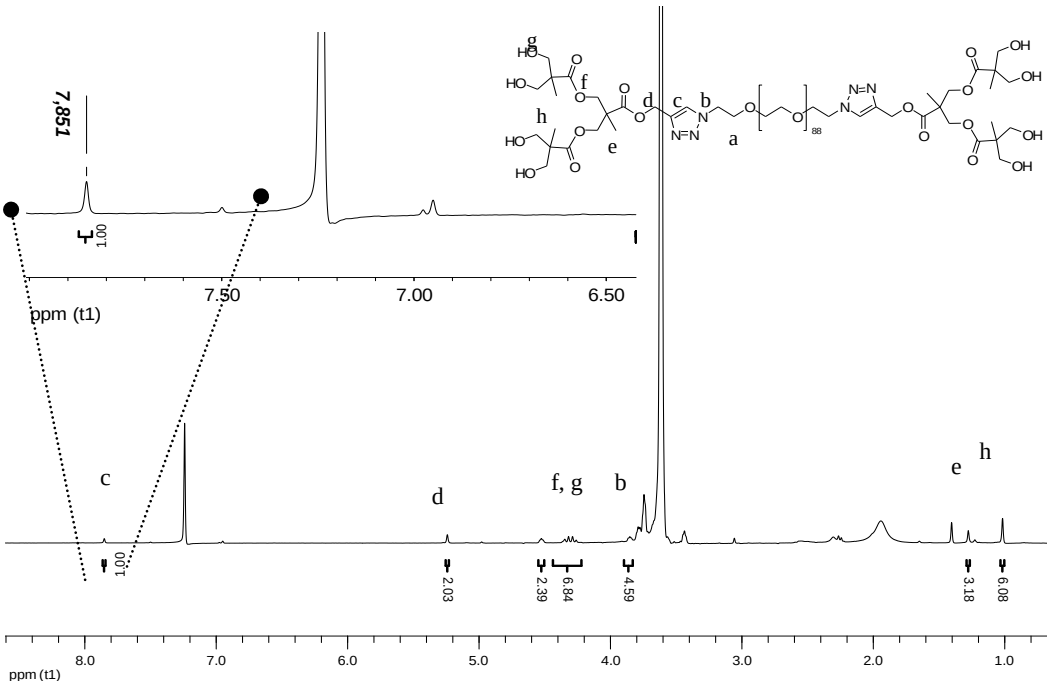

Figure 3.10. ^{1}H NMR of p7.

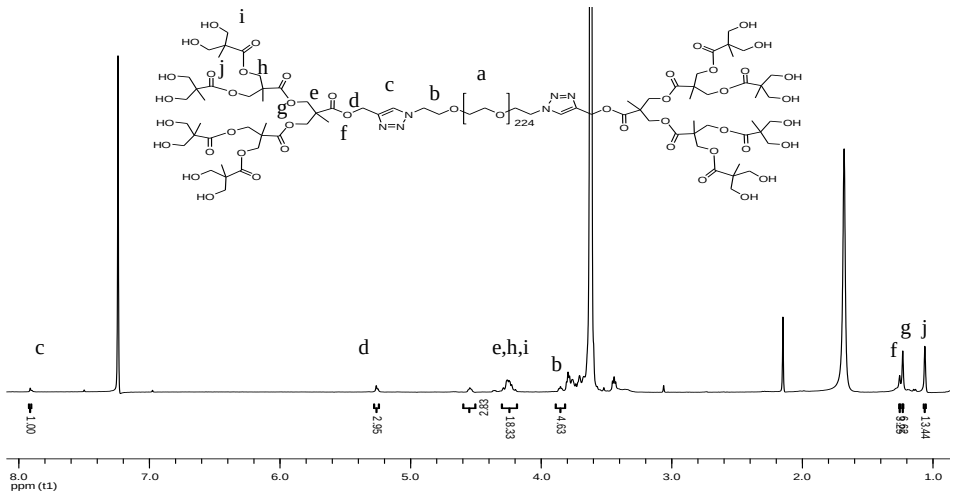

Figure 3.11. ^{1}H NMR of p8.

The ^{1}H NMR of (Figure 3.11.) also shows the same peaks for triazole and other expected H's with different H integrations due to the change of generation number.

Alkyne functionalized ABA copolymers' can also be characterized due to the new proton peaks on NMR spectrum. In Figure 3.12., proton NMR of p13 new proton peaks at 2.55 and 2.47 ppm as triplet are seen due to two neighbour $–CH_2$ groups and a singlet at 1.98 for terminal alkyne proton of pentynoic acid.

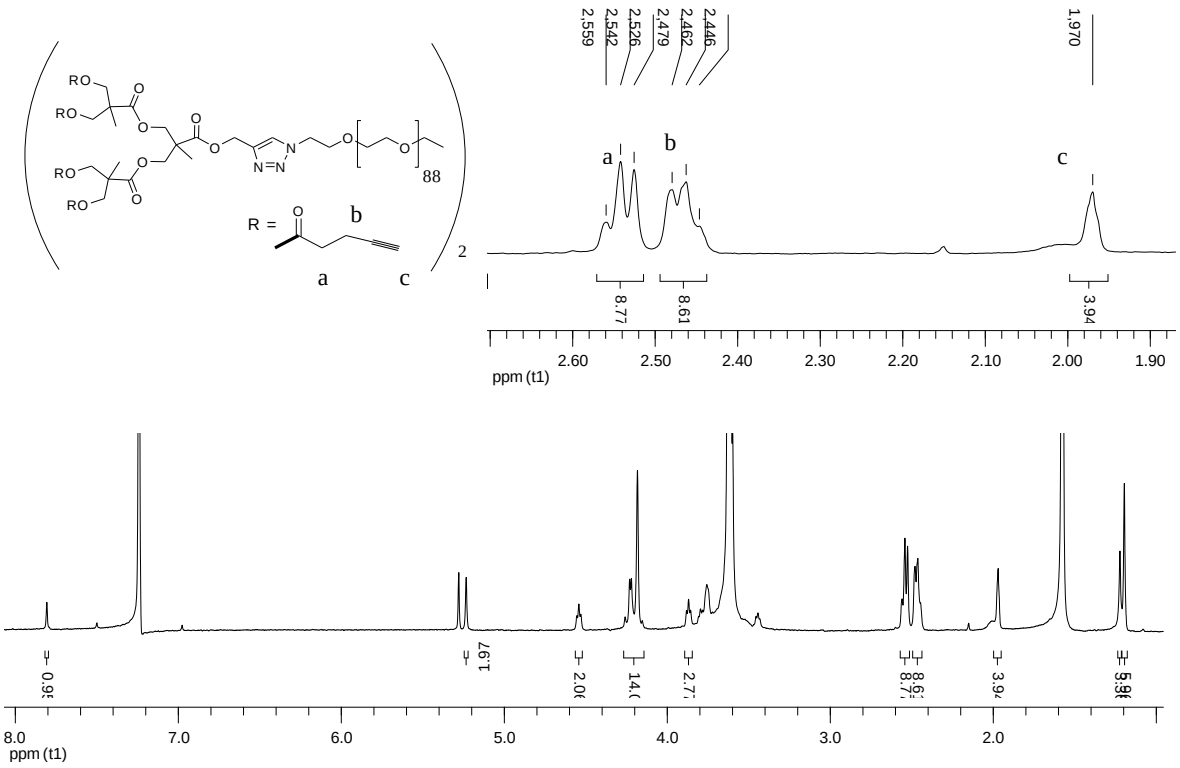

Figure 3.12. ^{1}H NMR of p13.

As it can be characterized from the proton NMR of p15 (Figure 3.13.) new peaks belong to the alkyne functional group can be seen between 2.56-2.52 ppm and 2.47-2.44 ppm as triplets from $–CH_2$ groups and a singlet at 1.97 ppm from alkyne proton.

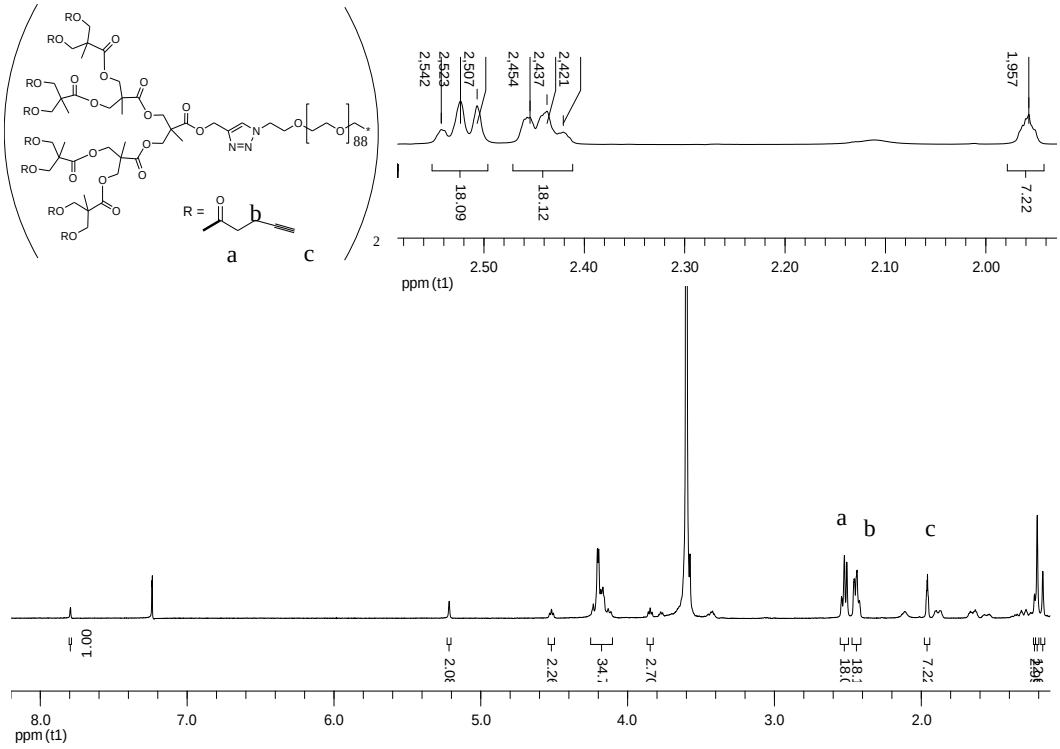

Figure 3.13. ^{1}H NMR of p15.

3.2. Drug Conjugation to the Functionalized ABA Copolymers

Alkyne functionalized ABA copolymers and azide bearing drug molecule are combined via Huisgen type [3+2] cycloaddition reaction in the presence of Cu(I)Br and PMDETA at 40 ^{o}C in THF. The general scheme for drug combination is given in Figure 3.14. For drug combination azido-Comb which is azido derivative of Combretastatin-A4 for drug molecule. For conjugation 17 and 18 were used. Conjugation efficiency for these reactions with 14 and 16 are 87.5% and 62.5%, respectively. The reason for not having 100 % conjugation may be the steric hinderence effect of drug molecule, it may not give cycloaddition reaction for each arms of dendrons. Especially for 18, there are sixteen arms and 10000 Da PEG, thus the possibility of conjugation is harder but drug combination to ten arms was a great success in these circumstances.

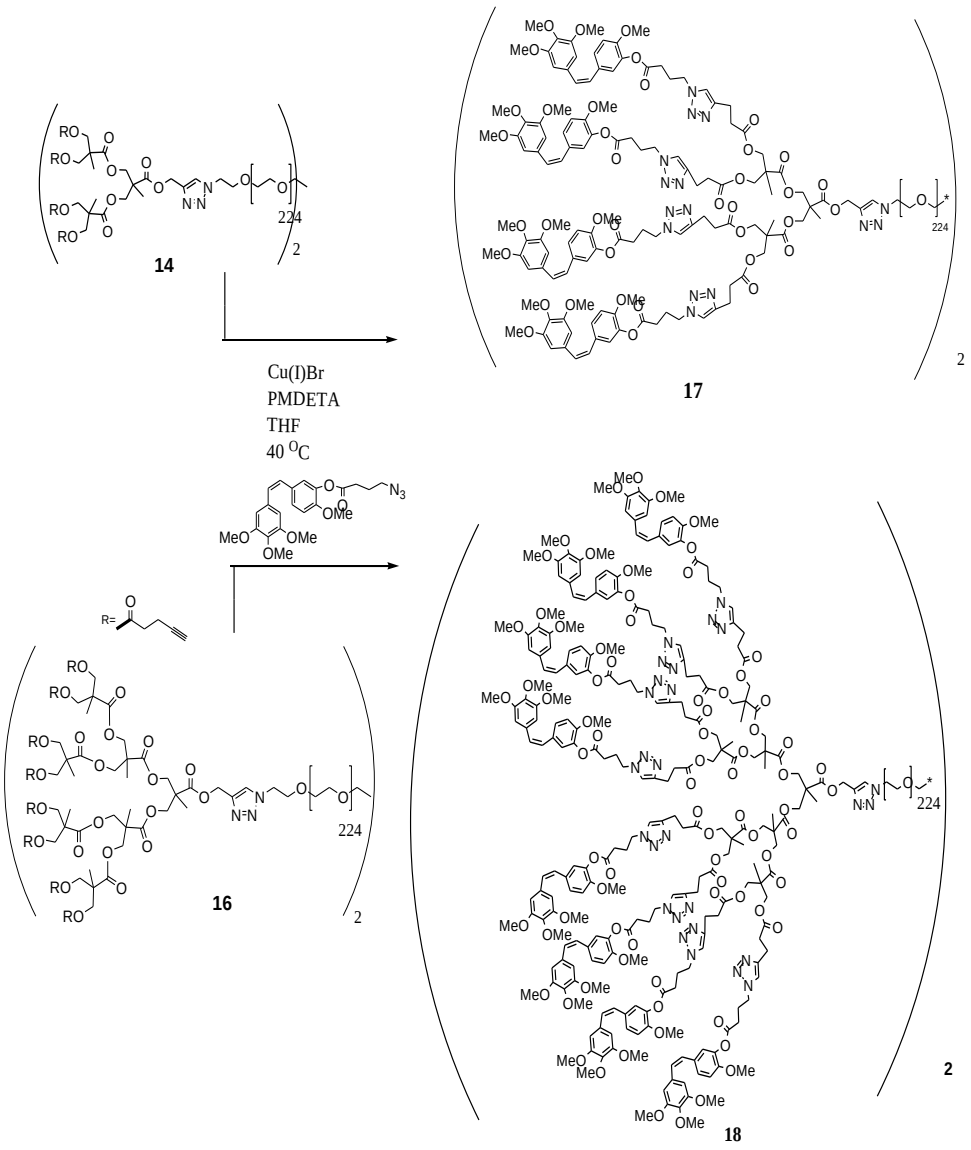

Figure 3.14. Genereal scheme for drug conjugation of ABA copolymers.

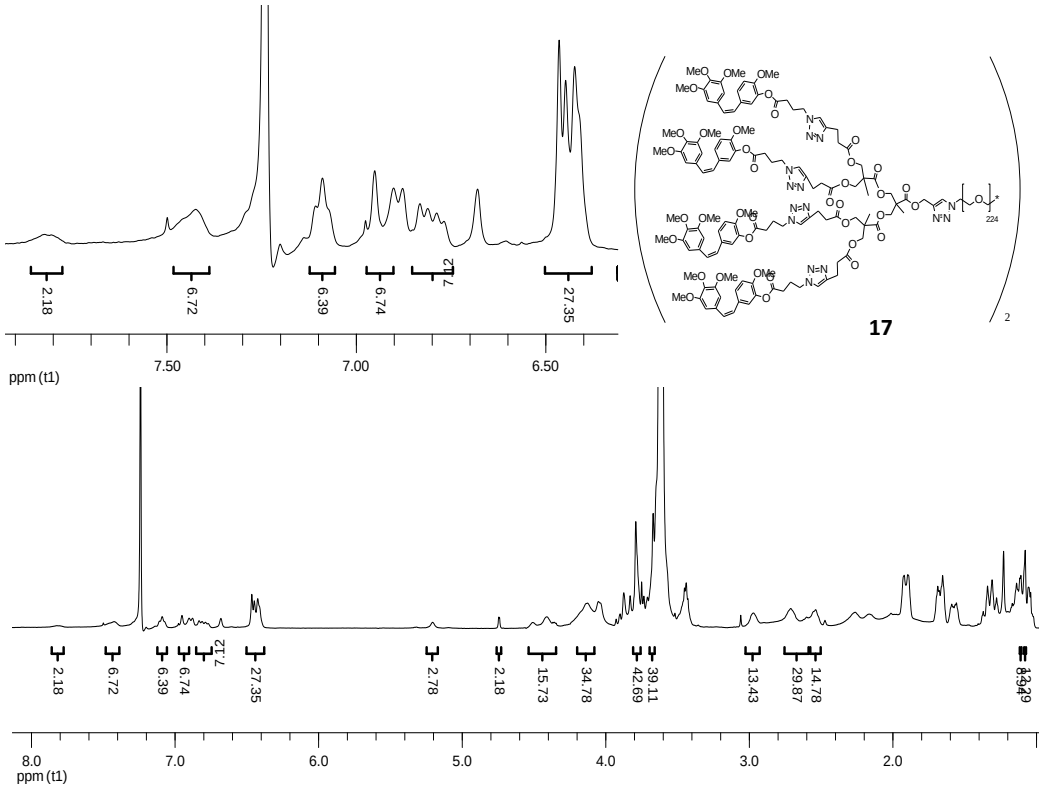

Figure 3.15. ^{1}H NMR of p17.

From ^{1}H NMR analysis drug conjugated ABA copolymers were characterized. Since new 'click' reaction introduced to the system, new triazole proton formation was expected. As it can be seen from Figure 3.15., two types triazoles are seen at 7.9 ppm and 7.4 ppm. From ^{1}H NMR of product 17 the proton peaks that belong to drug molecule can easily be seen in magnified window, new triazoles' protons appear at 7.42 ppm and the proton integration show that seven drug molecule are combined to dendrons. That drug molecules' aromatic protons appear between 7.10-6.42 ppm. From ^{1}H NMR of product 18 in Figure 3.16, the same proton peaks from drug molecules are also present. When integration of triazole 1 (between alkyne core of dendron and PEG azido) and triazole 2 (between alkyne functionalized dendron arm and Comb azido) gets into account 2 to 10 ratio is observed and this means drug conjugation is not finished but there ara ten drug molecules on the surface of dendrons.

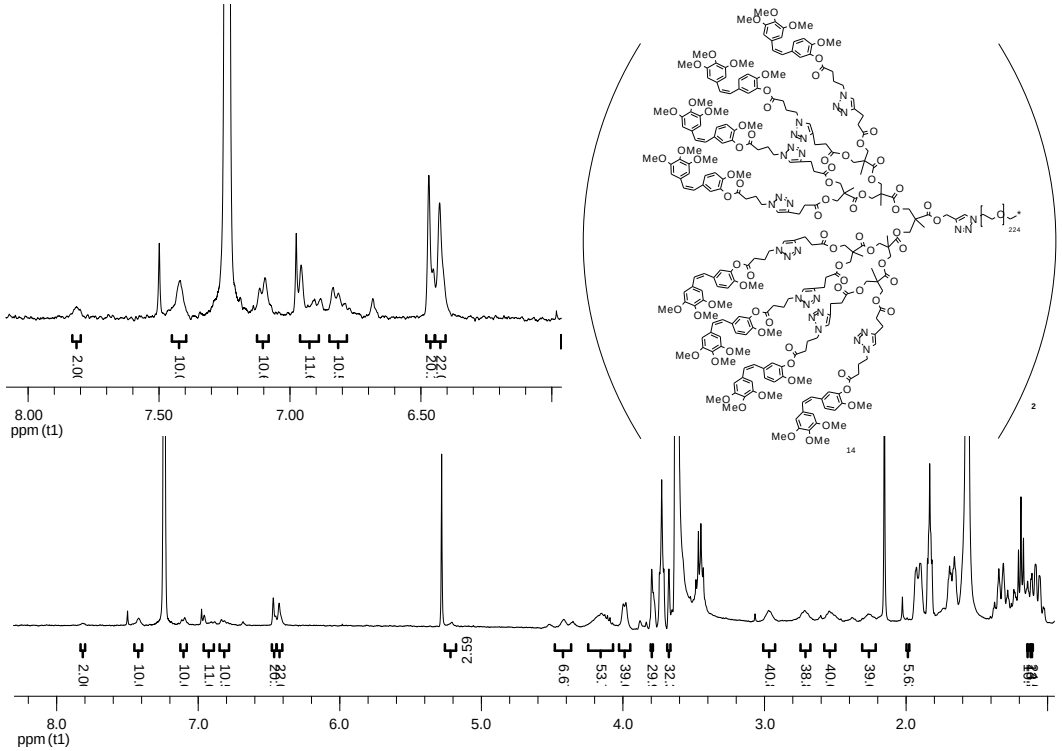

Figure 3.16. ^{1}H NMR of p18.

Drug conjugation was also done using [G1]4OR[PEG10K] (19). The 1H NMR of this product was given in Figure A.24. From integration there seems two comb drug molecule on the dendrons' surfaces.

3.3. Micelle Formation from ABA Triblock Copolymers

3.2.1. Fluorescence Experiments

After the functionalization of dendron-polymer-dendron conjugates, their tendency to form micellar structures in water was explored via fluorescence experiments since their construction composed of hydrophobic/hydrophilic/hydrophobic blocks. To confirm this assest we tried to form micelles in water using all conjugates and did their fluorescence measurements using pyrene as the probe molecule due to its giving characteristic fluorescence peaks when dissolves. Different concentrations of conjugates changing from 10^{-4} M to 10^{-9} M were prepared in distilled water.

The hydrophobic/hydrophilic molecular weight ratios of samples is given in Table 3.1. Pyrene stock solution was prepared to be 1.8 x 10^{-4} M (1.2 mg in 50 mL acetone) , for each sample 10 μL pyrene solution was placed in a vial and the acetone was removed under *vacuo* at 40 ^{o}C for 5 min. Then, polymer conjugate solution (3 mL) was placed in the pyrene containing vial. The final concentration of pyrene became 6 x 10^{-6} M. Pyrene containing polymer conjugate solutions were sonicated for 45 min.

Table 3.1. Hydrophobic/Hydrophilic ratio of conjugates in g/moL.

Product Number	Hydrophobic/Hydrophilic Ratio (g/moL)
14	1648/10100
16	2856/10100
13	1648/4100
15	2856/4100
17	4637/10100
18	7126/4100

The conjugates were then kept for 24 h. Excitation experiments were performed at 300-360 nm range using 5 nm width. The excitation data for product 15 is given in Figure 3.17. From the excitation graph of conjugate 15 it is obvious that the pyrene intensity increases as the concentration increases. The characteristic peaks of pyrene at 334 and and 338 nm wavelengths attest the experiment. Shift from these wavelengths describes the micelle formation after a certain concentration. These calculations for CMC are derived from the Log Conc vs I_{338}/I_{334} graphs.

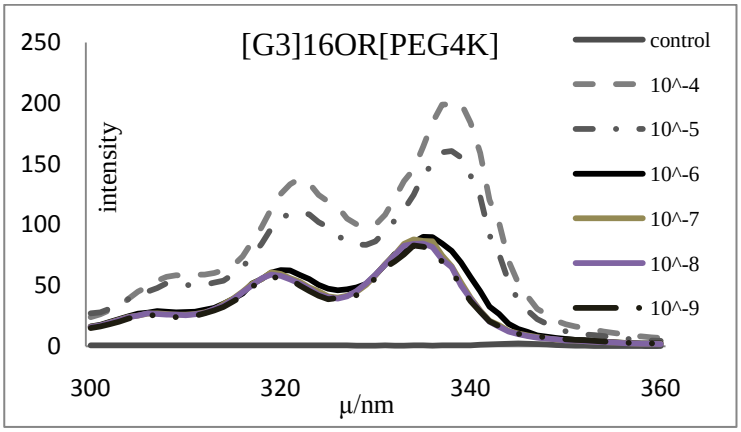

Figure 3.17. Excitation graph of p15.

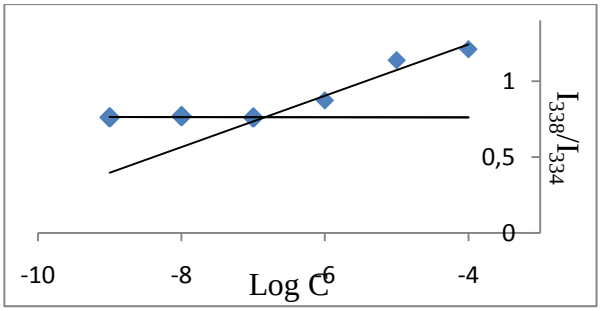

Figure 3.18. Log C vs I_{338}/I_{334} graph of p11.

Table 3.2. CMC values for dendron-polymer-dendron conjugates.

Dendron-Polymer Conjugate	CMC (M)
14	8.9×10^{-5}
16	3.8×10^{-6}
13	3.7×10^{-6}
15	1.4×10^{-7}
18	3.8×10^{-8}
17	5.2×10^{-8}

According to the Table 3.2., it is obvious that there is a trend between the conjugates related to the PEG length and the generations of dendron. The highest CMC value was seen for generation two dendron with PEG 10K as expected.

Since the hydrophobic / hydrophilic ratio determines the self assembly behavior for micelle formation, long hydrophilic / short hydrophobic part is expected to give highest CMC. On the other hand, short hydrophilic/ long hydrophobic design expected to form micelle structure at lower concentration. For drug conjugates micellar structure tend to be formed at lower concentration than copolymers. This is the result of increased hydrophobic length in copolymers.

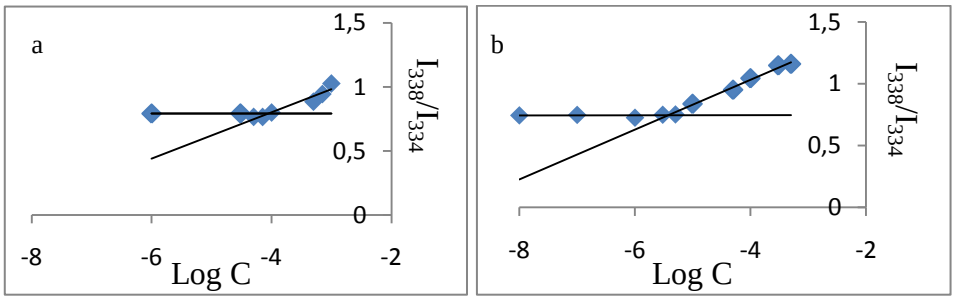

Figure 3.19. CMC graphs of copolymers; a) p14, b) p16.

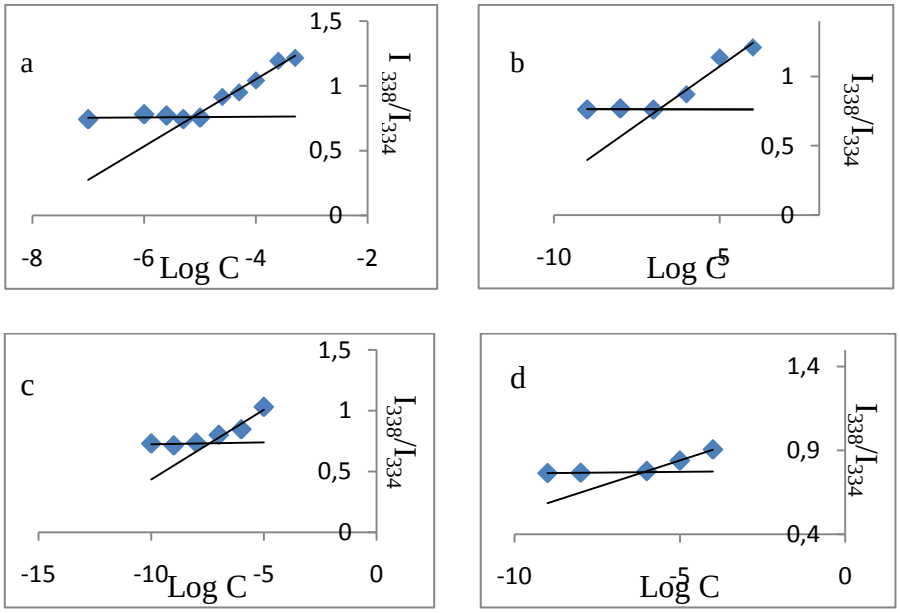

Figure 3.20. CMC graphs of a) p13, b) p15, c) p17, d) p18.

For product 19 no shift for pyrene peaks were observered, means micelle formation was not seen, so other measurements did not performed using this product.

3.2.2. Dynamic Light Scattering (DLS) Measurements

After finding the desired CMC, dynamic light scattering (DLS) experiments were performed above these concentrations. All experiments were done in water at 90^{o} angle at 25 ^{o}C. From DLS measurements the micelles' effective diameters were calculated. The detailed results for effective diameters were given at Table 3.3.

Table 3.3. Effective diameters of samples.

Product	Concentration (M)	Effective Diameter (nm)	Product	Concentration (M)	Effective Diameter (nm)
13	10^{-4}	197	16	10^{-4}	45
15	10^{-4}	290	16	10^{-5}	198
14	10^{-4}	100	17	10^{-5}	188
14	10^{-5}	140	18	10^{-5}	208

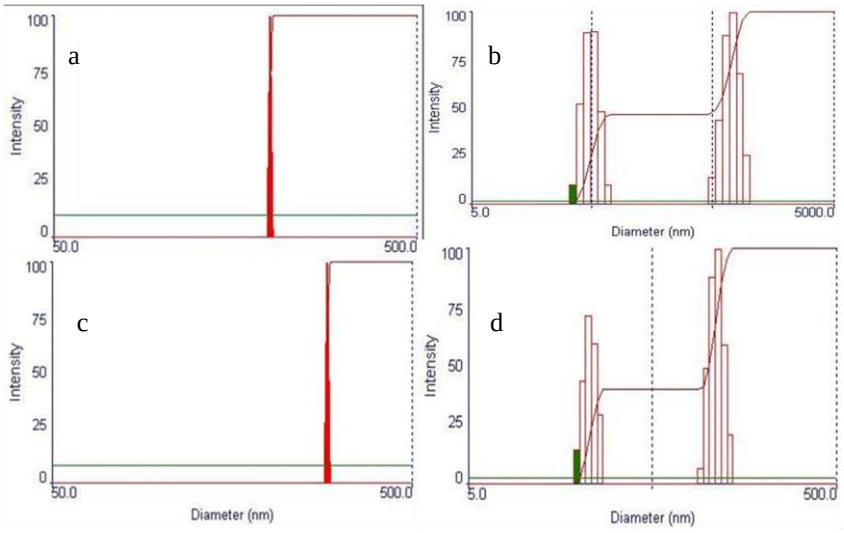

Figure 3.21. Intensity vs diameter graph of a) p14, b) p16, c) p13 and d) p15.

Since intensity vs diameter graph tells the dispersity of micellar structures at the same diameter, from these graphs micellar structures dispersion can be concluded that in a and c unimodular micelle formation, where as in c and d bimodular micelle formations are seen.

3.2.3. Scanning Transmission Electron Microscopy (STEM) Measurements

After fluorescence and DLS measurements were performed, the morphological studies of the micellar structures are done using STEM images of copolymers and drug conjugates were taken.

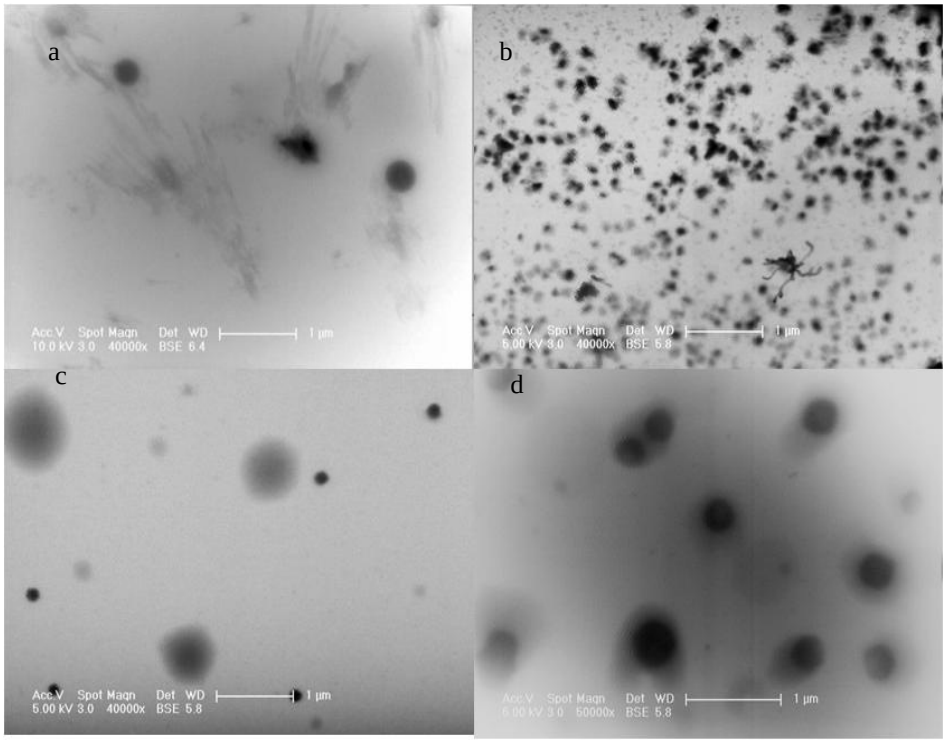

Figure 3.22. STEM images of a) p14, b) p16, c) p13, d) p15.

In the Figure 3.22. all samples were prepared at 10^{-4} M. When STEM and DLS measurements are compared there seems a consistent in them. The smallest micelle diameter was found in DLS as 45 nm for sample p16 and the biggest one is for p15. According to the STEM results it is also the same. Actually, the smallest micelle formation were expected to be formed p15 according to its hydrophobic/hydrophilic ratio but this did not observed. The reason for that ,PEG10K may more envoloped during self-assembly and more interacts with itself, the same behaviour not seen for PEG4K.

STEM images were taken also after drug conjugation to the copolymers. For these measurement samples were prepared at 10^{-5} M concentration since their CMC found to be around 10^{-8} M. In Figure 3.23. and Figure 3.24. STEM images of 17 and 18 can be seen, respectively

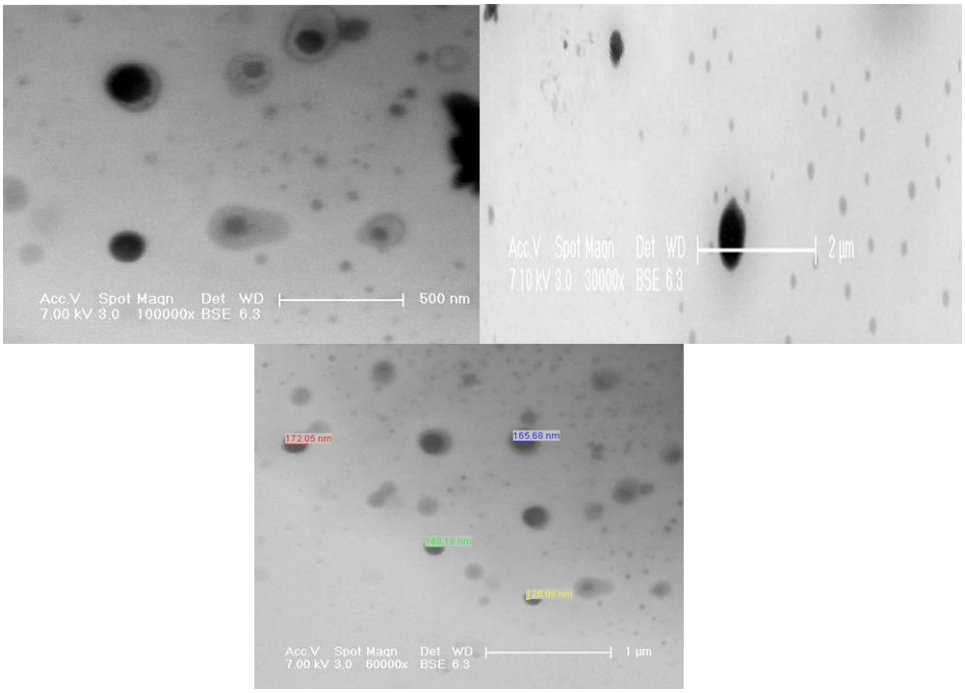

Figure 3.23. STEM images of p17.

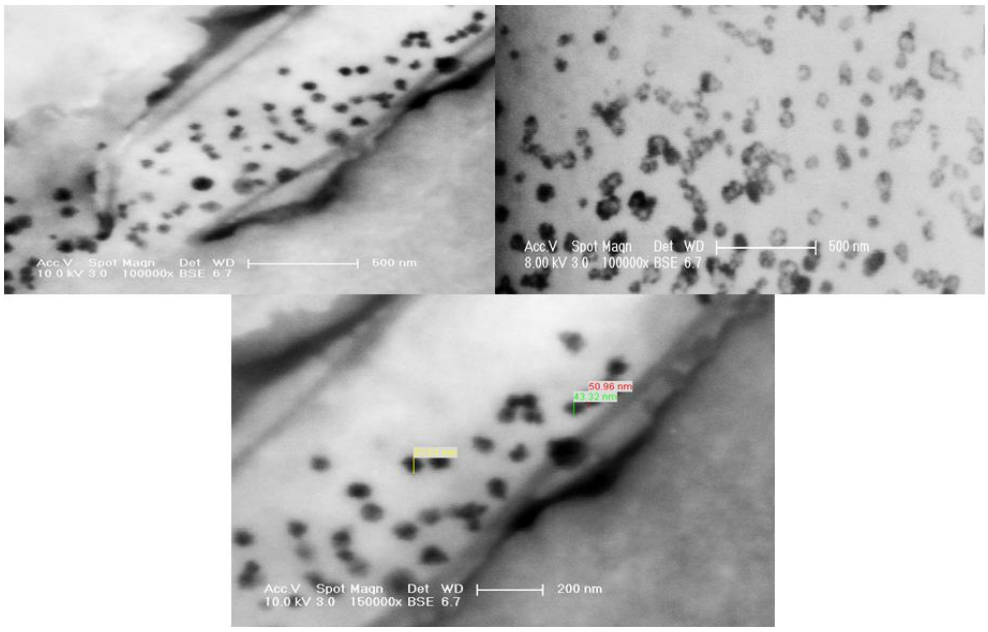

Figure 3.24. STEM images of p18.

According to the STEM images of drug conjugated copolymers the micellar structures seem to be coagulated. Introducing hydrophobic drug molecule to the system the tendency of micelle formation of copolymer increased. The diameter of non-coagulated [G3]10COMB[PEG10K] product found to be around 50 nm and micellar structures seem to be unimolecular where as in DLS experiment they showed bimolecular behaviour. Some deviations between STEM and DLS experiments can be explained by the coagulation of micellar structures in water.

4. EXPERIMENTAL

4.1. General Methods and Materials

2,2-Bis(hydroxymethyl) propionic acid (BMPA), Dowex X50WX2, Propargyl Alcohol, 4-pentynoic acid were purchased from Alfa Aesar. All polyethylene glycol were obtained from Fluka. All solvents were purchased from Merck and used as obtained without further purification unless otherwise noted. Azide functionalized PEG were synthesized according to literature procedures. Synthesis of dendrons 5 and 6 are given in supporting information. The monomer and copolymer characterizations involved 1H NMR spectroscopy (Varian 400 MHz) and Fourier transform infrared (ATR-FT-IR) spectroscopy (Thermo Fisher Scientific Inc. Nicolet 380). Micelle formations were characterized using Fluorescence spectroscopy (Cary Eclipse) , Dynamic Light Scattering 90 Plus Particle Size Analyzer instrument (Brookhaven Instruments Cooperation) and the STEM of wet micelles were taken by ESEM-FEG/EDAX Philips XL-30 (Philips, Eindhoven, The Netherlands) instrument.

4.2. Synthesis of Dendrons and Dendron-Polymer-Dendron Conjugates

Alkyne functionalized dendrons 5a and 6a were synthesized according to literature procedures. Via deprotection reaction 5 and 6 were obtained from 5a and 6a.

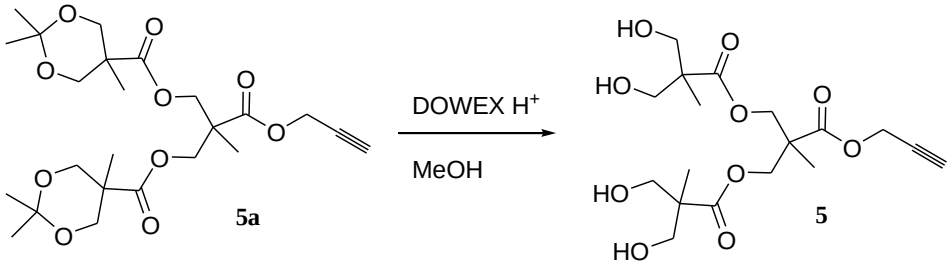

Figure 4.1. Synthesis of p5.

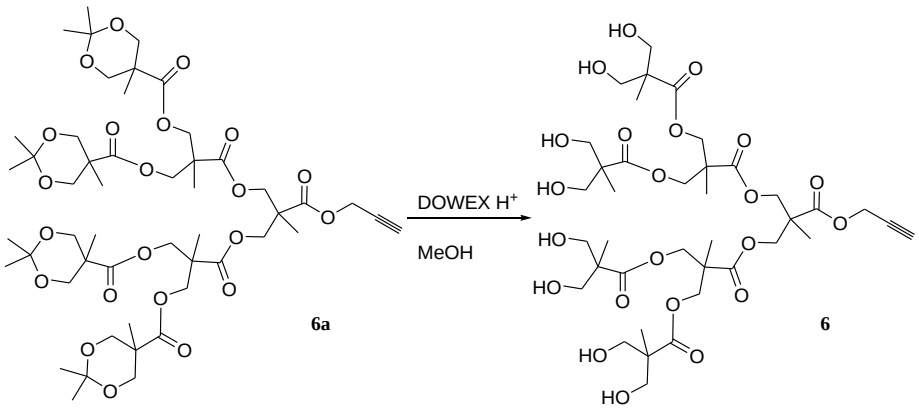

Figure 4.2. Synthesis of p6.

4.2.1. Synthesis of Generation 2 Dendron

Dowex X50WX2 (1.00g) was placed in a 100 mL Erlenmeyer flask and washed methanol (5 x 30 mL). Subsequently, 5a (6.00 g, 0.028 mmol), Dowex X50WX2 (1.00 g) and methanol (60 mL) were added to a 100 mL rb flask and stirred for 24 h. Dowex was removed via filtration and the filtrate was dried under *vacuo* yielding 5 (5.30 g, 99%) as a white solid. ^{1}H NMR (CD_3OD, δ, ppm) 4.75 (s, 2H), 4.48 (d, 2H, *J* = 11.2 Hz), 4.31 (d, 2H, *J* = 11.2 Hz), 3.9 (dd, 4H, *J* = 10.8, 8.0 Hz), 3.60 (dd, 4H, *J* = 10.8, 8.0 Hz), 2.49 (s, 1H), 1.34 (s, 3H), 1.05 (s, 6H). FT-IR (cm^1): 3260, 1718.

4.2.2. Synthesis of Generation 3 Dendron

Dowex X50WX2 (1.00g) was placed in a 100 mL Erlenmeyer flask and washed methanol (5 x 30 mL). To the 6a (3 g, 2.92 mmol), Dowex X50WX2 (1.00 g) and methanol (60 mL) was added to a 100 mL rb flask and stirred for 24 h at 40 ^{o}C. After the reaction was completed Dowex was removed via filtration and the filtrate was dried under *vacuo* yielding 6 (2.80 g, 96%) as a white solid. ^{1}H NMR (CD_3OD, δ, ppm) 4.76 (s, 2H), 4.38-4.24 (m, 12H), 3.82 (d, 8H, *J* = 10.3 Hz), 3.73 (d, 8H, *J* = 10.1 Hz), 2.43 (s, 1H), 1.23 (s, 3H), 1.16 (s, 6H), 1.14 (s, 12H). FT-IR (cm^{-1}): 3292, 1728.

4.2.3. Synthesis of bisazido PEG4K

PEG 4K diol 1 (5.0 g, 0.12 mmol) and triethylamine (4.4 g, 6.1 mL, 44 mmol) were placed in 100 mL Erlenmeyer Flask with CH_2Cl_2 (25 mL). Then MsCl (0.16 g, 0.11 mL, 1.44 mmol) was added to a flask in 0 ^oC. The reaction was stirred at 0 ^oC for 10 min than at room temperature for 24 h. After the reaction was completed, the solvent was removedunder *vacuo* and redissolved in CH_2Cl_2 (5 mL) and precipitated in isopropanol after 2 h of refrigeration. The solid was filtered and then dried under *vacuo* yielding 2 (4.98 g, 97 %). Then 2 (4.5 g, 0.11 mmol) and NaN_3 (0.07 g, 1.1 mmol) were placed in a 100 mL Erlenmeyer flask. These solid materials were purged with N_2 for 1 min. Then, DMF (30 mL) added to the flask and the reaction was stirred at 60 ^oC for 24 h. Filtrate was dried under *vacuo* and redissolved in CH_2CL_2 (10 mL) and then was poured onto cold aq HCl (6 M, 100 mL) and the solution was extracted with CH_2Cl_2 (3 x 75 mL). Polymer was precipitated in cold diethyl ether. Product was dried under high vacuum yielding 3, (4.3 g 93%) of white solid. ^1H NMR (CD_3OD, δ, ppm) 3.8-3.4 (broad s, 356 H,) 2.15 (s, 4H) . FT-IR (cm^{-1}): 2884, 2102

4.2.4.Synthesis of Bisazido PEG10K

Compund 4, synthesized in a similar manner to 3 starting from PEG 10K. . ^1H NMR (CD_3OD, δ, ppm) 3.8-3.4 (broad s, 900 H,) 2.15 (s, 4H) . FT-IR (cm^{-1}): 2881, 2095.

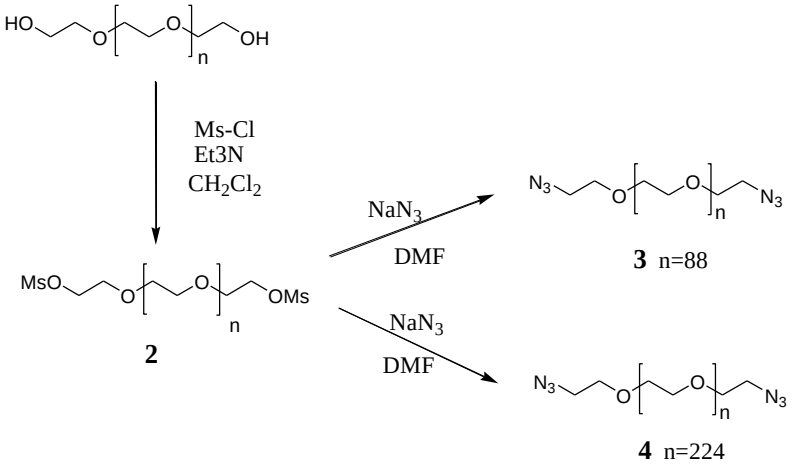

Figure 4.3. Synthesis of PEG4K and PEG10K.

4.2.5 Synthesis of [G2]8OH[PEG4K]

PEG-4K-Diazide (**3**) (400 mg, 0.1 mmol) and propargyl [G2]4[OH] (**5**) (110 mg, 0.23 mmol) were dissolved in dry THF (3 mL). In a separate flask were dissolved CuBr (1.45 mg, 0.01 mmol), PMDETA (1.78 μL, 0.01 mmol) in dry THF (2 mL) and purged with N_2. The mixture was then transferred onto azide-propargyl alcohol solution and stirred at 40 C^o for 24 h. The solvent was then evaporated and the crude product was dissolved in THF (50 mL) the solution was filtered through Al_2O_3 column to remove copper salts. The solvent was concentrated under *vacuo* and the desired product was precipitated with Et_2O, filtered and dried under *vacuo* yielding **7** (370 mg, 92%) as a yellowish white solid. ^{1}H NMR ($CDCl_3$, δ, ppm) 7.85 (s, 2H), 5.23 (s, 4H), 4.52 (t, 4H, *J* = 4.4 Hz), 4.32 (d, 4H, *J* = 10.8 Hz), 4.26 (d, 4H, *J* = 10.8 Hz), 3.85 (t, 4H, *J* = 4.8 Hz), 3.8-3.4 (bs, 356H), 1.26 (s, 6H), 1.01 (s, 12H). FT-IR (cm^{-1}): 3431, , 1732.

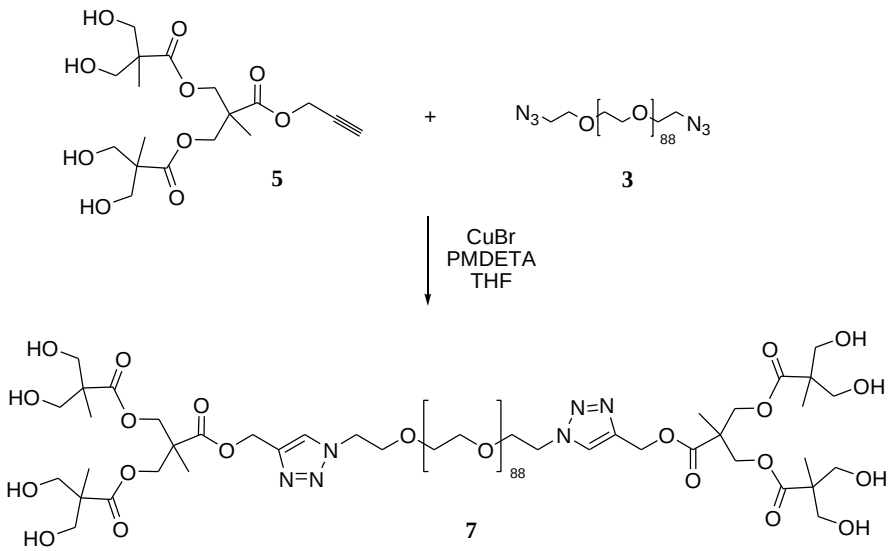

Figure 4.4. Synthesis of p7.

4.2.6. Synthesis of [G2]8OH[PEG10K]

PEG-10K-Diazide (4) (500 mg, 0.049 mmol) and propargyl [G2]4[OH] (5) (56 mg, 0.114 mmol) were dissolved in dry THF (3 mL). In a separate flask were dissolved CuBr

(0.5 mg, 0.004 mmol), PMDETA (1.7 μL, 0.004 mmol) in dry THF (2 mL) and purged with N_2. The mixture was then transferred onto azide-propargyl alcohol solution and stirred at 40 ^oC for 24 h. The solvent was then evaporated and the crude product was dissolved in THF (50 mL) the solution was filtered through Al_2O_3 column to remove copper salts. The solvent was concentrated under *vacuo* and the desired product was precipitated with Et_2O, filtered and dried under *vacuo* yielding 8 (0.470 g, 94 %) as a white solid ^1H NMR ($CDCl_3$, δ, ppm) 7.85 (s, 2H), 5.24 (s, 4H), 4.52 (t, 4H, *J* = 4.0 Hz), 4.33 (d, 4H, *J* = 11.2 Hz), 4.28 (d, 4H, *J* = 11.2 Hz), 3.85 (t, 4H, *J* = 4.4 Hz), 3.72-3.63 (bs, 900H), 1.28 (s, 6H), 1.02 (s, 12H). FT-IR (cm^{-1}): 3497, 1733.

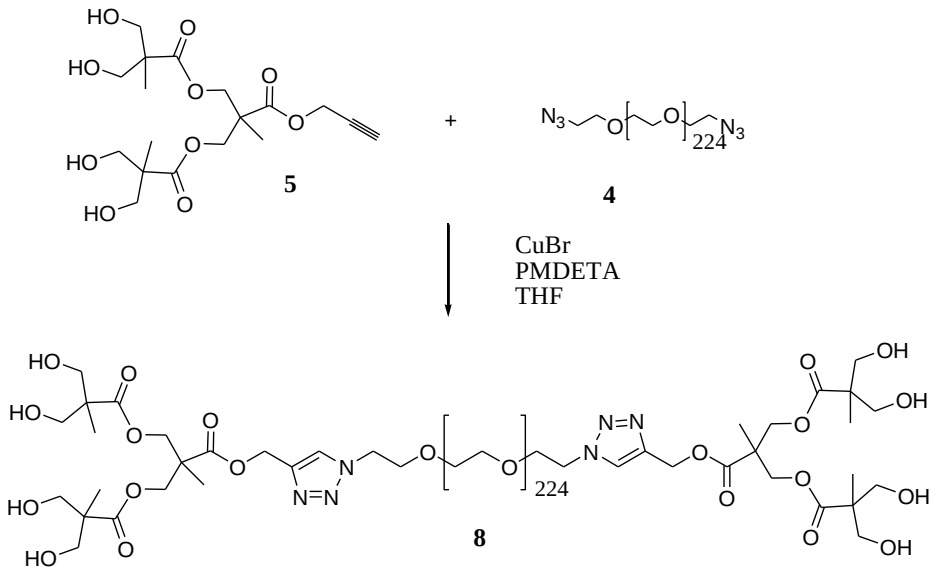

Figure 4.5. Synthesis of p8.

4.2.7.Synthesis of [G3]8OH[PEG4K]

Diazido-PEG4K (3) (0.200 g, 0.049 mmol) and propargyl [G3]8[OH] (6) (0.104 g, 0.113 mmol) were dissolved in dry THF (4 mL). In a separate flask were dissolved CuBr (0.7 mg, 0.005 mmol), PMDETA (1.8 μL, 0.005 mmol) in dry THF (3 mL) and purged with N_2. The mixture was then transferred onto azide-propargyl alcohol solution and stirred at 40 ^oC for 24 h. The solvent was then evaporated and the crude product was dissolved in THF (50 mL) the solution was filtered through Al_2O_3 column to remove

copper salts. The solvent was concentrated under *vacuo* and the desired product was precipitated in Et_2O, filtered and dried under *vacuo* yielding 9 (0.290 g, 92%) as a yellowish white solid. ^{1}H NMR ($CDCl_3$, δ, ppm) 7.92 (s, 2H), 5.27 (s, 4H), 4.54 (t, 4H, *J* = 4 Hz), 4.27 - 4.24 (m, 24H), 3.80-3.40 (bs, 356H), 3.85 (t, 4H, *J* = 4.4 Hz), 1.26 (s, 6H), 1.23 (s, 12H), 1.06 (s, 24H). FT-IR (cm^{-1}): 3433, 1733.

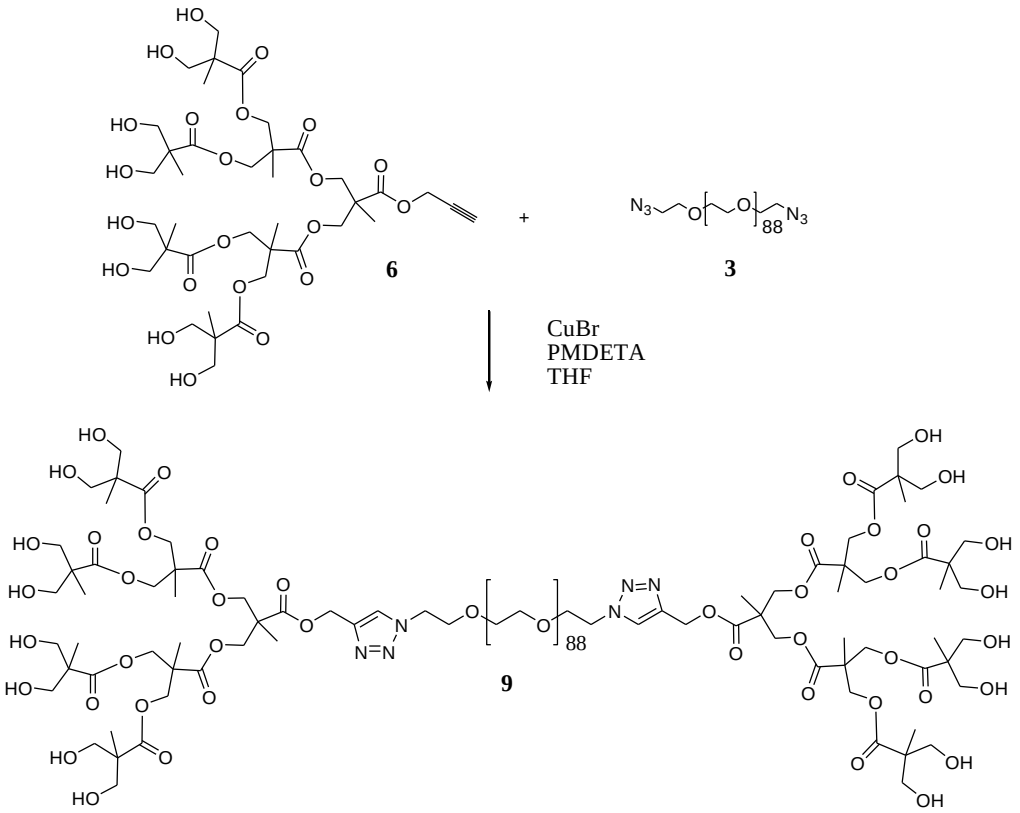

Figure 4.6. Synthesis of p9.

4.2.8. Synthesis of [G3]16OH[PEG10K]

PEG10K-Diazide (4) (0.300 g, 0.298 mmol) and propargyl [G3]8[OH] (6) (0.061 g, 0.686 mmol) were dissolved in dry THF (4 mL). In a separate flask were dissolved CuBr (0.421 mg, 0.029 mmol), PMDETA (1.4 μL, 0.029 mmol) in dry THF (3 mL) and purged with N_2. The mixture was then transferred onto azide-propargyl alcohol solution and stirred at 40 ^oC for 24 h. The solvent was then evaporated and the crude product was dissolved in THF (50 mL) and filtration done using Al_2O_3 coloumn to remove copper. The solvent was concentrated under *vacuo* and the desired product was precipitated with Et_2O, filtered and dried under *vacuo* yielding 10 (0.92 g, 71%) as a yellowish white solid. ^{1}H

NMR ($CDCl_3$, δ, ppm) 7.86 (s, 2H), 5.27 (s, 4H), 4.54 (t, 4H, *J* = 4 Hz), 4.28-4.19 (m, 24H), 3.85 (t, 8H, *J* = 4.4 Hz), 3.80-3.40 (bs, 900H), 1.25 (s, 6H), 1.23 (s, 12H), 1.06 (s, 24H). FT-IR (cm^{-1}): 3435, 2881, 1732.

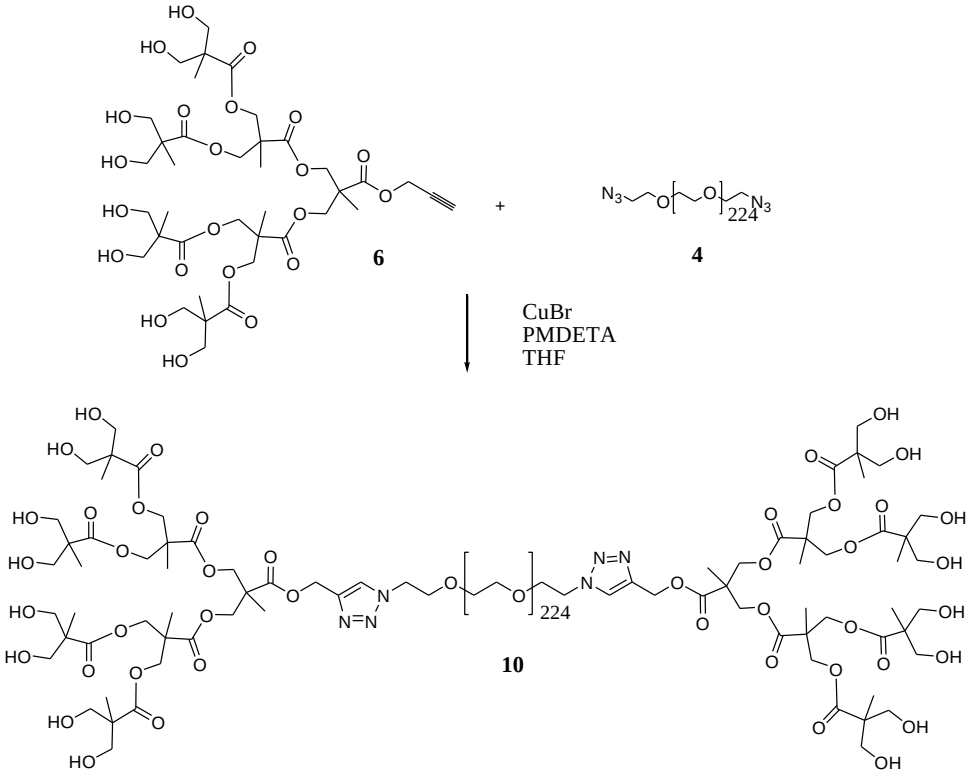

Figure 4.7. Synthesis of p10.

4.2.9. Synthesis of [G2]8OR[PEG4K]

Product 7 (0.130 g, 0.025 mmol), pyridine (0.3 mL) and DMAP (0.003 g, 0.028 mmol) were dissolved in dry CH_2Cl_2 (8 mL) in a 25 mL round bottom flask. To the stirring reaction mixture was added 5-pentynoic acid anhydride (0.075 g, 0.42 mmol) and continued stirring for 24 h at room temperature under N_2. Reaction mixture was diluted with CH_2Cl_2 (30 mL) and then extracted with 1 M $NaHSO_4$ (3 x 30 mL), 10% Na_2CO_3 (3 x 30 mL) and then with brine (1 x 30 mL). Combined organic layers were dried over anhydrous Na_2SO_4 and the residue was concentrated in *vacuo*. Crude product precipitated in diethyl ether to give 110 mg of 13 as a yellowish viscous solid (84 % yield). ^{1}H NMR ($CDCl_3$, δ, ppm) 7.82 (s, 2H), 5.25 (s, 4H), 4.56 (t, 4H, *J* = 4.8 Hz), 4.24-4.18 (m, 34H), 3.88 (t, 6H, *J* = 4.8 Hz), 3.80-3.40 (bs, 356H), 2.55 (t, 22H, *J* = 6 Hz), 2.47 (t, 22H, *J* = 6 Hz), 1.98 (s, 8H), 1.23 (s, 6H), 1.21 (s, 12H). FT-IR (cm^{-1}): 3262, 2868, 1736.

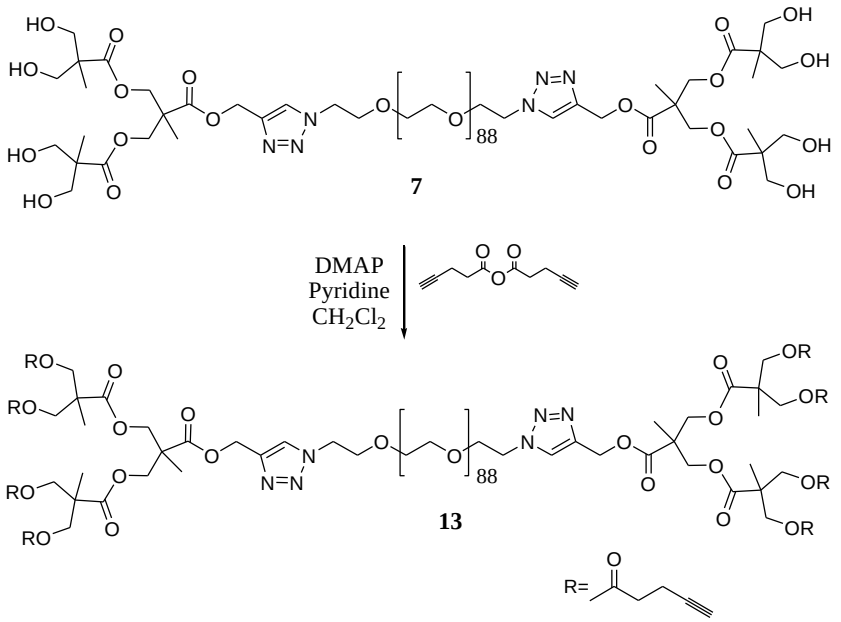

Figure 4.8. Synthesis of p13.

4.2.10. Synthesis of [G2]8OR[PEG10K]

Product 8 (0.350 g, 0.030 mmol), pyridine (0.21 mL) and DMAP (0.003 g, 0.027 mmol) were dissolved in dry CH_2Cl_2 (8 mL) in a 25 mL round bottom flask. To the stirring reaction mixture was added 4-pentynoic acid anhydride (0.043 g, 0.240 mmol) and continued stirring for 24 h at room temperature under N_2. Reaction mixture was diluted with CH_2Cl_2 (50 mL) and then extracted with 1 M $NaHSO_4$ (3 x 50 mL), 10% Na_2CO_3 (3 x 50 mL) and then with brine (1 x 50 mL). Combined organic layers were dried over anhydrous Na_2SO_4 and the residue was concentrated in *vacuo*. Crude product was purified by precipitation in diethyl ether to give 0.320 g of 14 as a white solid (90 % yield) ^{1}H NMR ($CDCl_3$, δ, ppm) 7.78 (s, 2H), 5.20 (s, 4H), 4.51 (s, 4H), 4.22-4.12 (m, 22 H), 3.88 (s, 4H), 3.80-3.40 (bs, 900H), 2.51 (bs, 16H), 2.43 (bs, 16H), 1.94 (s, 8H), 1.22 (s, 6H), 1.11 (s, 12H). FT-IR (cm^{-1}): 3265, 2882, 1740.

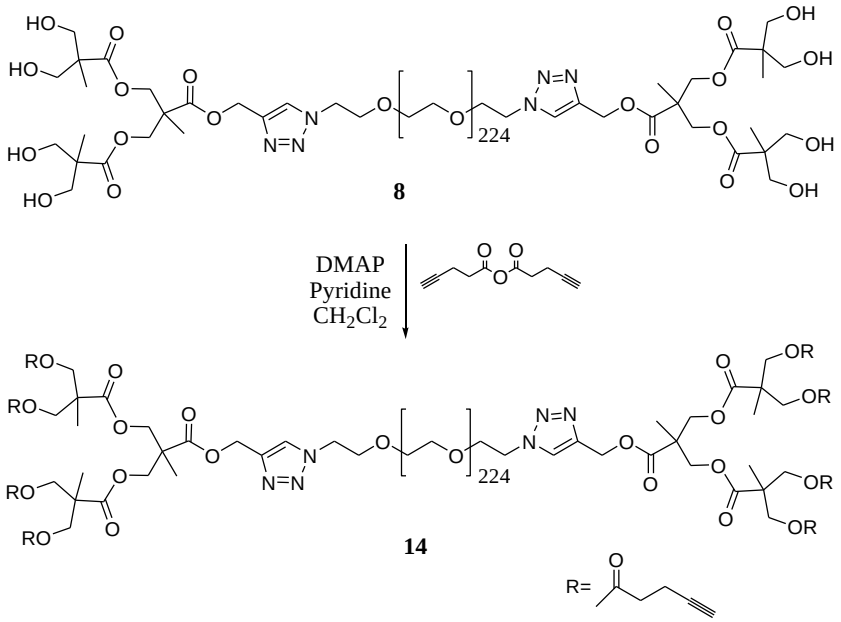

Figure 4.9. Synthesis of p14.

4.2.11. Synthesis of [G3]16OR[PEG4K]

Product 9 (0.060 g, 0.010 mmol), pyridine (0.64 mL) and DMAP (0.098 g, 0.008 mmol) dissolved in dry CH_2Cl_2 (7 mL) in a 25 mL round bottom flask. To the stirring reaction mixture was added 4-pentynoic acid anhydride (0.030 g, 0.165 mmol) and continued stirring for 24 h at room temperature under N_2. Reaction mixture was diluted with CH_2Cl_2 (30 mL) and then extracted with 1 M $NaHSO_4$ (3 x 30 mL), 10% Na_2CO_3 (3 x 30 mL) and then with brine (1 x 30 mL). Combined organic layers were dried over anhydrous Na_2SO_4 and the residue was concentrated in *vacuo*. Crude product was purified by precipitation in diethyl ether to give 50 mg of 15 as a yellowish viscous solid (81 % yield) 7.80 (s, 2H), 5.22 (s, 4H), 4.52 (t, 4H, *J* = 4.8 Hz), 4.25 - 4.18 (m, 56H), 3.85 (t, 6H, *J* = 4.8 Hz), 3.80-3.40 (bs, 356H), 2.53 (t, 32 H, *J* = 6.8 Hz), 2.46 (t, 32H, *J* = 6.8 Hz), 1.97 (s, 16H), 1.24 (s, 6H), 1.22 (s, 24H), 1.19 (s, 12H). FT-IR (cm^{-1}): 3273, 1732.

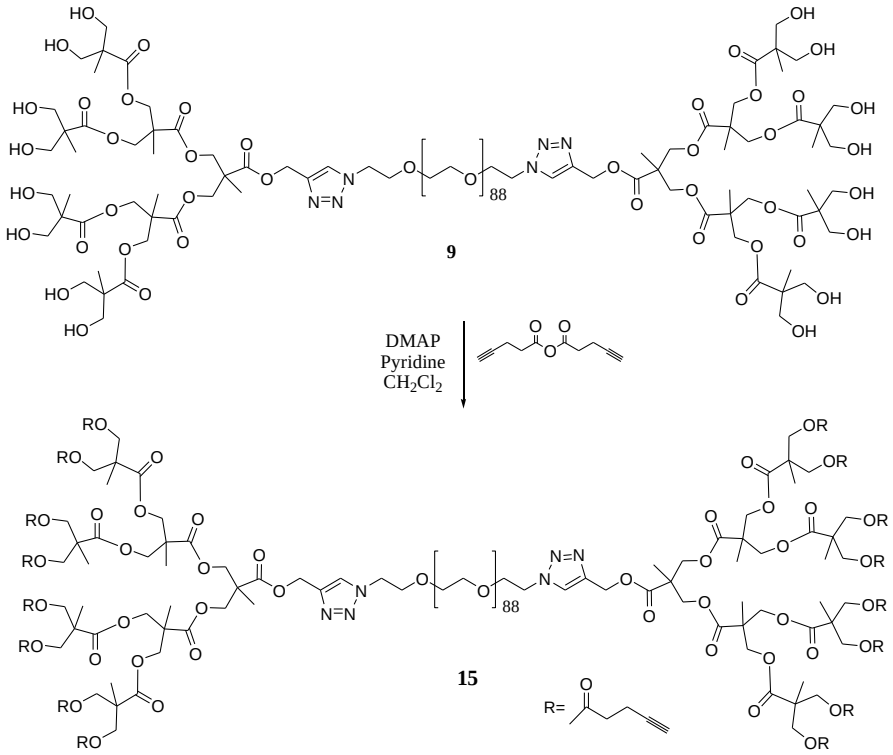

Figure 4.10. Synthesis of p15.

4.2.12. Synthesis of [G3]16OR[PEG10K]

Product 10 (0.350 g, 0.030 mmol), pyridine (0.6 mL) and DMAP (0.602 g, 0.047 mmol) dissolved in dry CH_2Cl_2 (10 mL) in a 25 mL round bottom flask. To the stirring

reaction mixture was added 4-pentynoic acid anhydride (0.084 g, 0.472 mmol) and continued stirring for 24 h at room temperature under N_2. Reaction mixture was diluted with CH_2Cl_2 (30 mL) and then extracted with 1 M $NaHSO_4$ (3 x 30 mL), 10% Na_2CO_3 (3 x 30 mL) and then with brine (1 x 30 mL). Combined organic layers were dried over anhydrous Na_2SO_4 and the residue was concentrated in *vacuo*. Crude product was purified by precipitation in diethyl ether to give 50 mg of 16 as a yellowish viscous solid (81 % yield) ^{1}H NMR ($CDCl_3$, δ, ppm) 7.80 (s, 2H), 5.22 (s, 4H), 4.53 (t, 4H, *J* = 4.8 Hz), 4.22-4.16 (m, 68H), 3.86 (t, 8H, *J* = 4.8 Hz), 3.80-3.40 (bs, 900H), 2.54 (t, 44 H, *J* = 6.8 Hz), 2.45 (t, 44H, *J* = 6.8 Hz), 1.97 (s, 16H), 1.24 (s, 6H), 1.22 (s, 24H), 1.19 (s, 12H). FT-IR (cm^{-1}): 3279, 2882, 1739.

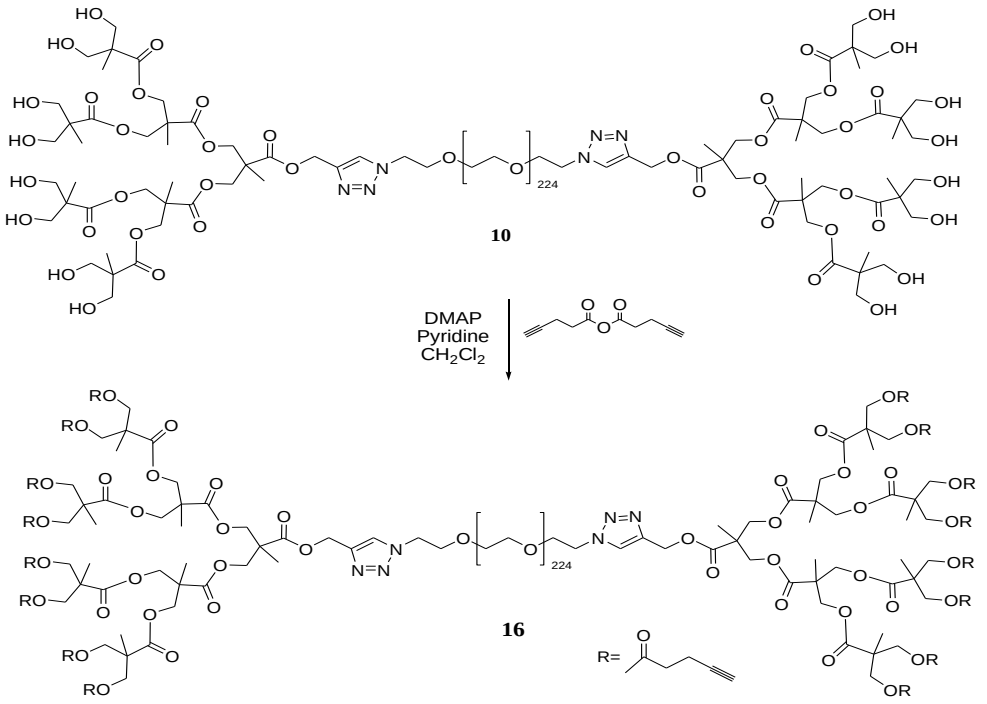

Figure 4.11. Synthesis of p16.

4.2.13. Synthesis of [G2]8COMB[PEG10K]

Product 14 (0.060 g, 0.509 mmol) and azido-Comb (0.020 g, 0.467 mmol) were dissolved in dry THF (4 mL). In a separate flask were dissolved CuBr (0.070 mg, 0.005 mmol), PMDETA (0.3 μL, 0.005 mmol) in dry THF (3 mL) and purged with N_2. The mixture was then transferred onto azide-propargyl alcohol solution and stirred at 40 ^{o}C for 24 h. The solvent was then evaporated and the crude product was dissolved in THF (50 mL) the solution was filtered through Al_2O_3 column to remove copper salts. The solvent was concentrated under *vacuo* and the desired product was precipitated with Et_2O, filtered and dried under *vacuo* yielding 17 (0.03 g, 50%) as a yellowish viscous solid. ^{1}H NMR ($CDCl_3$, δ, ppm) 7.78 (s, 2H), 7.42 (s, 6H), 7.12 (dd, 7H, *J* = 6.8 Hz), 6.95 (s, 7H), 6.83(dd, 7H, *J*= 8 Hz), 6.46(dd, 14H, *J* = 6.8 Hz) 6.42(dd, 14 H, *J* = 6.8 Hz), 5.21(s, 4H), 4.72 (s, 4H), 4.41(t, 14H, *J* = 5.2 Hz), 4.12(bs, 34H), 3.82 (s, 21 H), 3.83 (s, 21 H), 3.79(s, 42 H), 3.70-3.40 (bs, 900H), 3.00 (bs, 14H), 2.65 (bs, 32 H), 2.53(bs, 14H) ,1.11 (s, 6H), 1.07 (s, 12H).

4.2.14. Synthesis of [G3]16COMB[PEG10K]

Product 16 (0.060 g, 0.509 mmol) and azido-Comb (0.020 mg, 0.467 mmol) were dissolved in dry THF (4 mL). In a separate flask were dissolved CuBr (0.070 mg, 0.005 mmol), PMDETA (0.3 μL, 0.005 mmol) in dry THF (3 mL) and purged with N_2. The mixture was then transferred onto azide-propargyl alcohol solution and stirred at 40 ^oC for 24 h. The solvent was then evaporated and the crude product was dissolved in THF (50 mL) the solution was filtered through Al_2O_3 column to remove copper salts. The solvent was concentrated under *vacuo* and the desired product was precipitated with Et_2O, filtered and dried under *vacuo* yielding 18 (0.04 g, 50%) as a yellowish viscous solid. ^1H NMR ($CDCl_3$, δ, ppm) 7.78 (s, 2H), 7.42 (s, 10H), 7.12 (dd, 10H, *J* = 6.8 Hz, 6.95 (dd, 10H, *J* = 6.4 Hz), 6.83(s, 10H, *J*= 8 Hz),6.46(dd, 20H, *J* = 6.8 Hz), 6.42 (dd, 20 H, *J* = 6.8 Hz), 5.21(s, 3H), 4.72 (s, 4H), 4.41(bs, 40H), 4.12(m, 56H), 3.82 (s, 30 H), 3.83 (s, 30 H), 3.70-3.40 (bs, 900H), 3.00 (bs, 40H), 2.65 (bs, 80 H), 2.53(bs, 40H) ,1.11 (s, 6H), 1.07 (s, 12H).

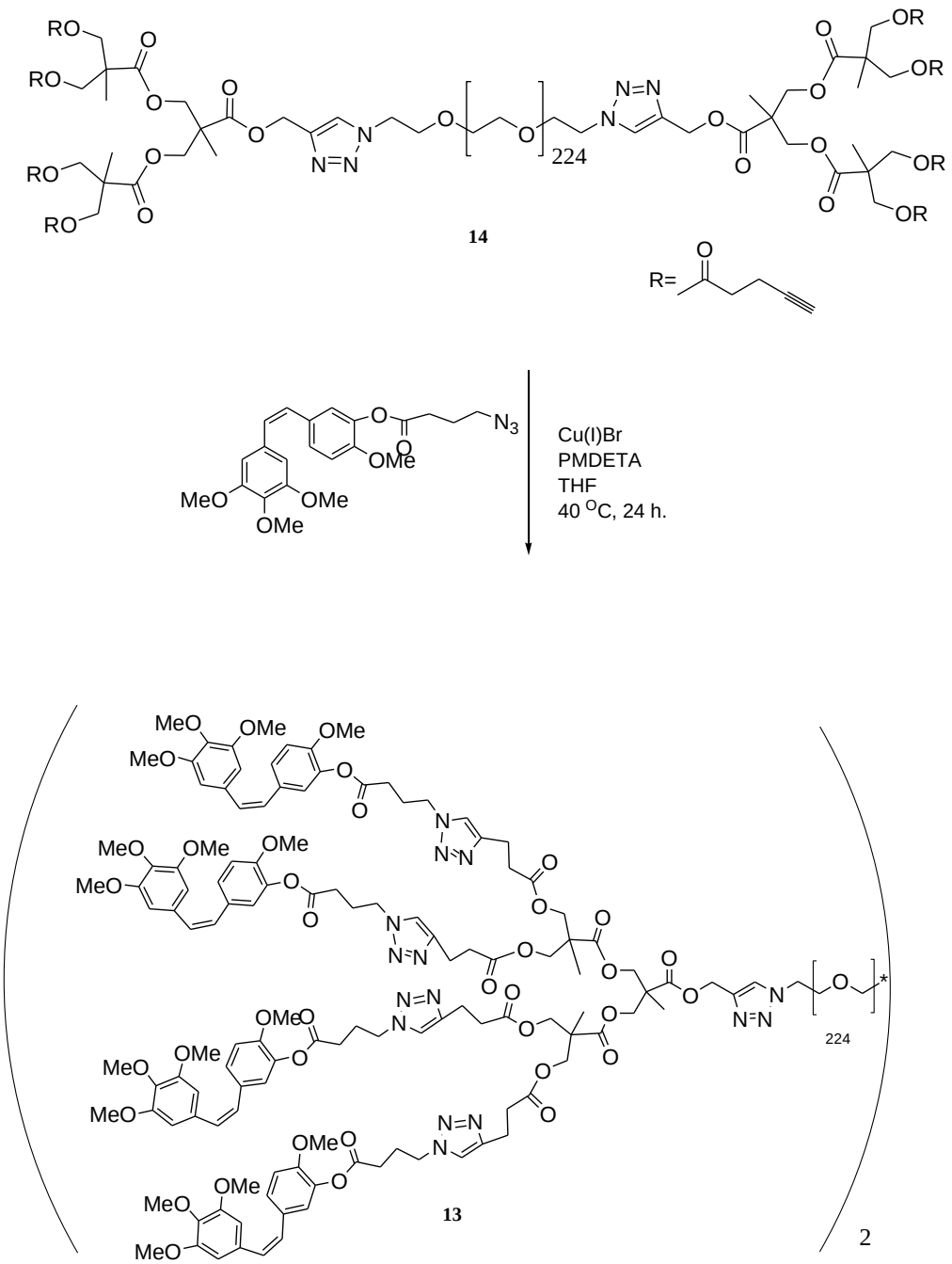

Figure 4.12. Synthesis of p17.

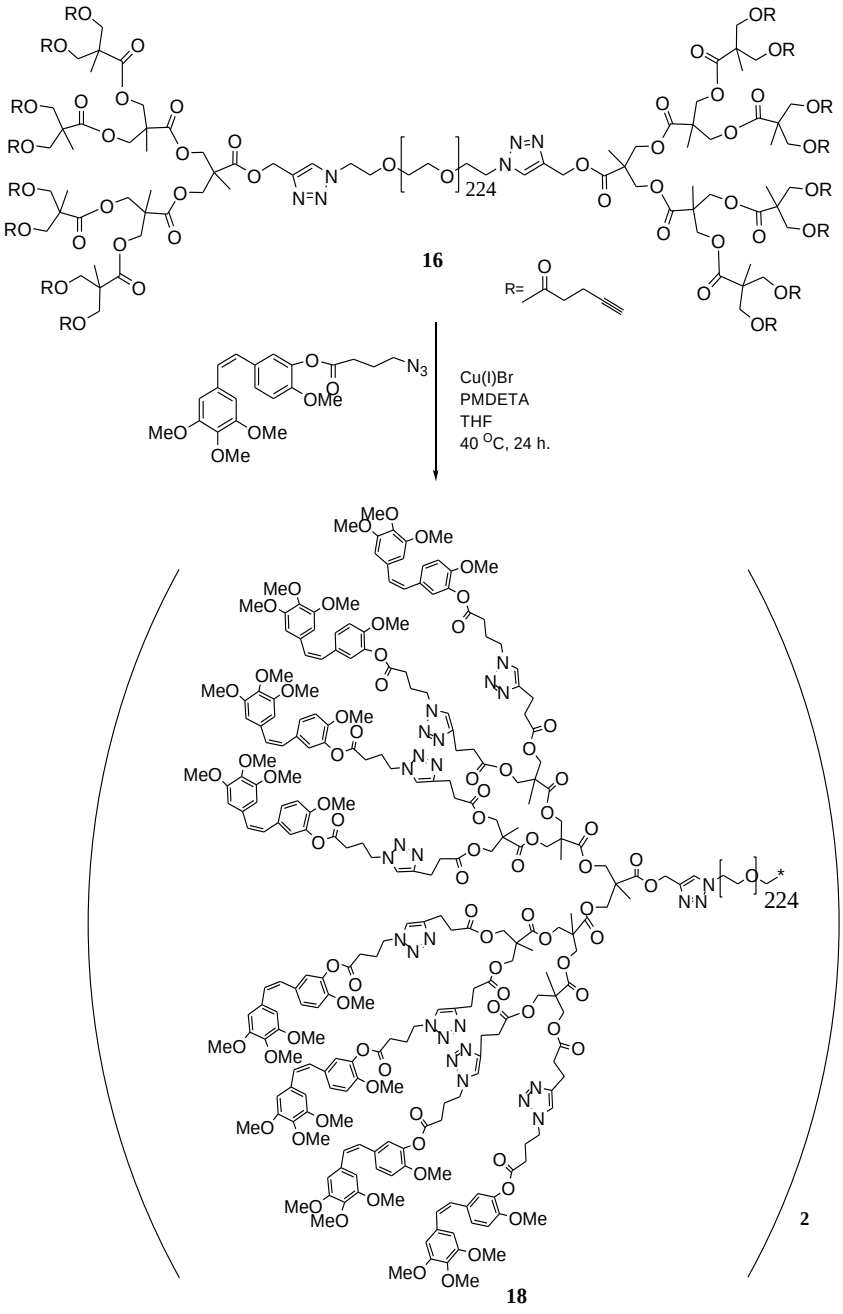

Figure 4.13. Synthesis of p18.

4.2.15. Synthesis of [G1]4COMB[PEG10K]

[G1]4OR[PEG10K] (0.020 g, 0.002 mmol) and azido-Comb (0.004 mg, 0.008 mmol) were dissolved in dry THF (2 mL). In a separate flask were dissolved CuBr (0.005 mg, 0.001 mmol), PMDETA (0.1 μL, 0.001 mmol) in dry THF (3 mL) and purged with N_2. The mixture was then transferred onto azide-propargyl alcohol solution and stirred at 40 ^oC for 24 h. The solvent was then evaporated and the crude product was dissolved in THF (50 mL) the solution was filtered through Al_2O_3 column to remove copper salts. The solvent was concentrated under *vacuo* and the desired product was precipitated with Et_2O, filtered and dried under *vacuo* yielding 19 (0.015 g, 75%) as a yellowish solid. ^1H NMR ($CDCl_3$, δ, ppm): 7.79 (s, 2H), 7.39 (s, 2H), 7.08-7.12 (dd, 4H, J =), 6.97 (s, 2H), 6.47 (s, 8H), 6.43(s, 8H), 5.21 (s, 4H), 4.50 (m, 8H), 4.41 (m, 8H), 3.78 (s, 14H), 3.68 (s, 24H), 3.65-3.40 (bs, 900H), 2.97(m, 4H), 2.65-2.60 (m, 10H), 2.25-2.30 (m, 4H), 1.18(s, 6H).

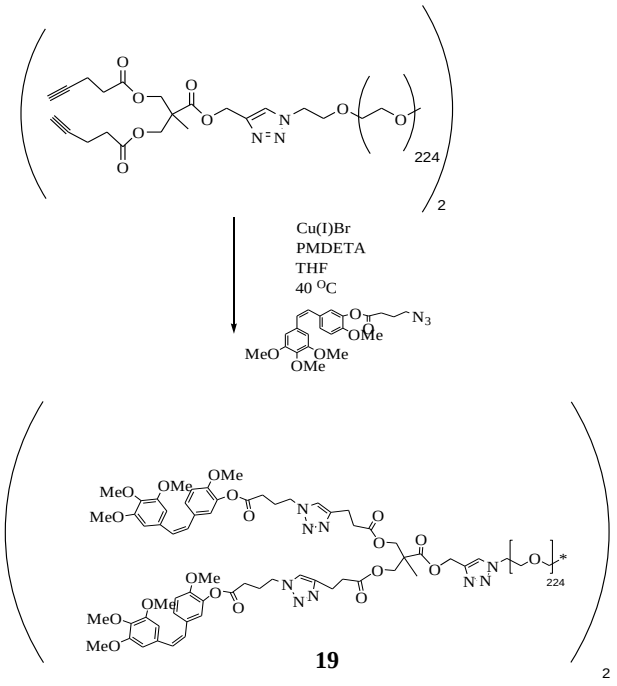

Figure 4.14. Synthesis of p19.

4.3. Measurements

4.3.1. Dynamic Light Scattering (DLS) Experiments

For finding out the effective diameter sizes and the size distribution of micelle structures alkyne functionalized dendron-polymer-dendron conjugates and drug attached conjugates' micelle solutions were prepared using H_2O at desired concentrations and sonicated at room temperature for 45 min. after than particle size analysis were done using dynamic light scattering method at 25 ^oC and 90^o angle. The size distribution were determined using intensity vs diameter graph which shows the same sized micelles' intensity at certain diameter.

4.3.2. Scanning Transmission Electron Microscope (STEM) Experiments

Micelle structures were prepared in H_2O solution at desired concentrations for alkyne functionalized and drug attached dendron-polymer-dendron conjugates and sonicated for 45 min. at room temperature than all were quickly frozen and freeze-dried under vacuum until the solvent was sublimed. Then H_2O is added to samples until get the same concentration with pre-micelle solution. Then one drop of sample solution dropped on copper grid and waited till this drop dries. Scanning transmission electron microscope analysis were studied using that copper grid to find out the microscopic images of micelle structures.

4.3.3. Fluorescence Experiments

For the determination of CMC of micelles pyrene loading studies were done and measured by fluorescence method. Micelles were prepared at different concentrations between 10^{-4} and 10^{-9} range. On the other side 1.8×10^{-3} M pyrene containing acetone solutions were prepared for all samples and acetone were removed under *vacuo* at 40 ^oC for 5 min.. Polymer samples were added to pyrene containing vials and sonicated for 45 min. than rested for 24 hours. Fluorescence experiments were done for all polymer samples and no-polymer containing blank pyrene sample for each measurements.

CONCLUSION

For this study, dendron-polymer-dendron copolymers were synthesized using generation 2 and 3 polyester dendrons with PEG 10K, 4K via Huisgen type ‘click’ reaction successfully, then alkyne functionalization to the surface of dendrons were performed. From these alkyne functionalized copolymers, micellar structures were obtained in aqueous media.

As a second study, azide functional group bearing drug molecule, namely azido-comb, was conjugated to ABA copolymers that were constructed from G2, G3 dendrons and PEG 10K polymer. Micellar structures were obtained for these drug conjugates also in aqueous media. STEM, DLS and fluorescence experiments were performed for micellar systems. As expected, the diameters of micelles obtained from the drug conjugates were found to be smaller than the micelles obtained from the alkyne appended parent triblock copolymer.

In conclusion, drug conjugated micelles were obtained via the self assembly of novel dendron-polymer-dendron triblock copolymers in aqueous solutions. As a future work, drug release studies will be done and drug conjugation to PEG4K copolymers will be performed.

APPENDIX

^{1}H NMR and FT-IR spectra of newly synthesized products.

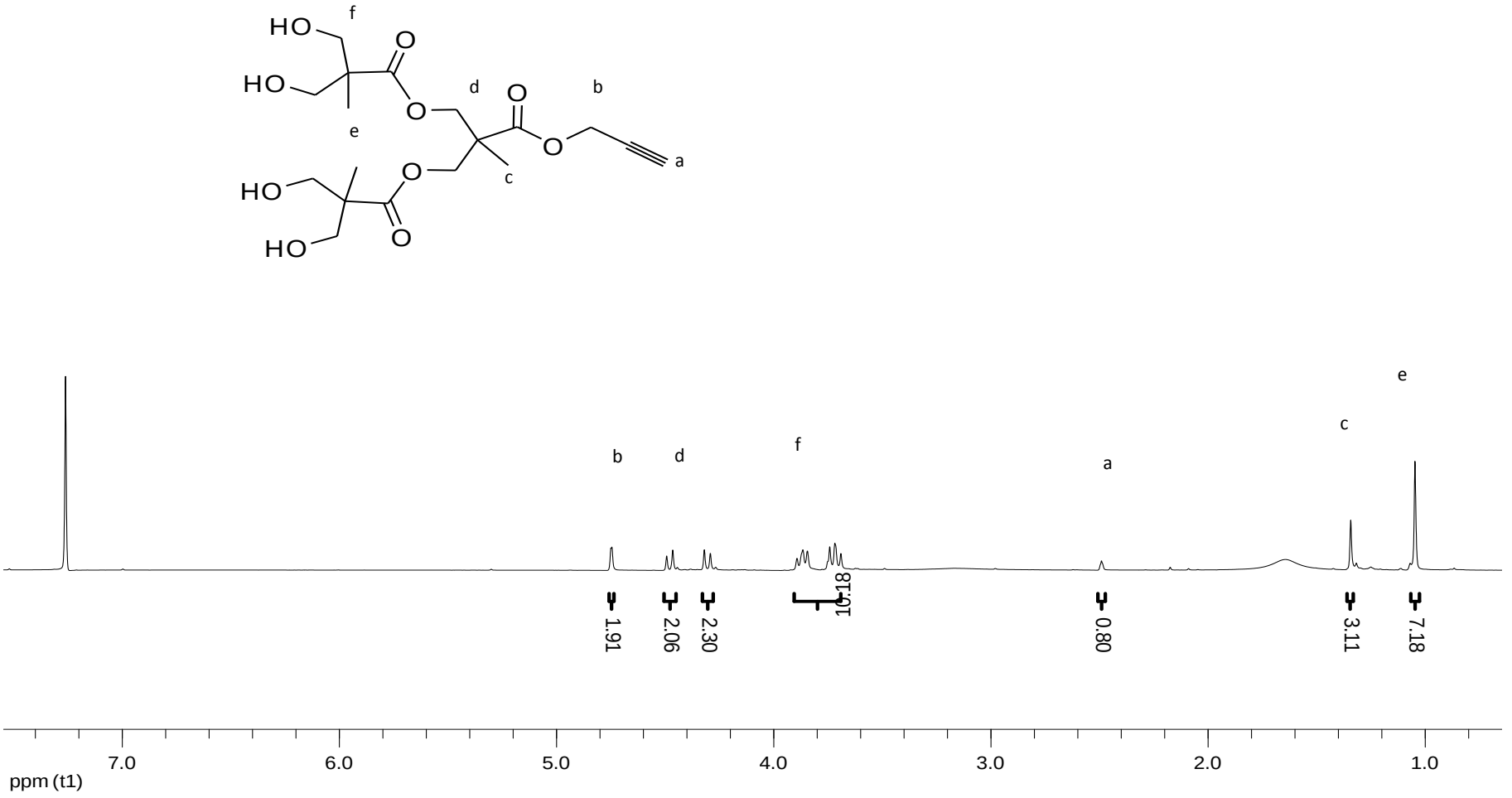

Figure A.1. ^{1}H NMR spectrum of p5.

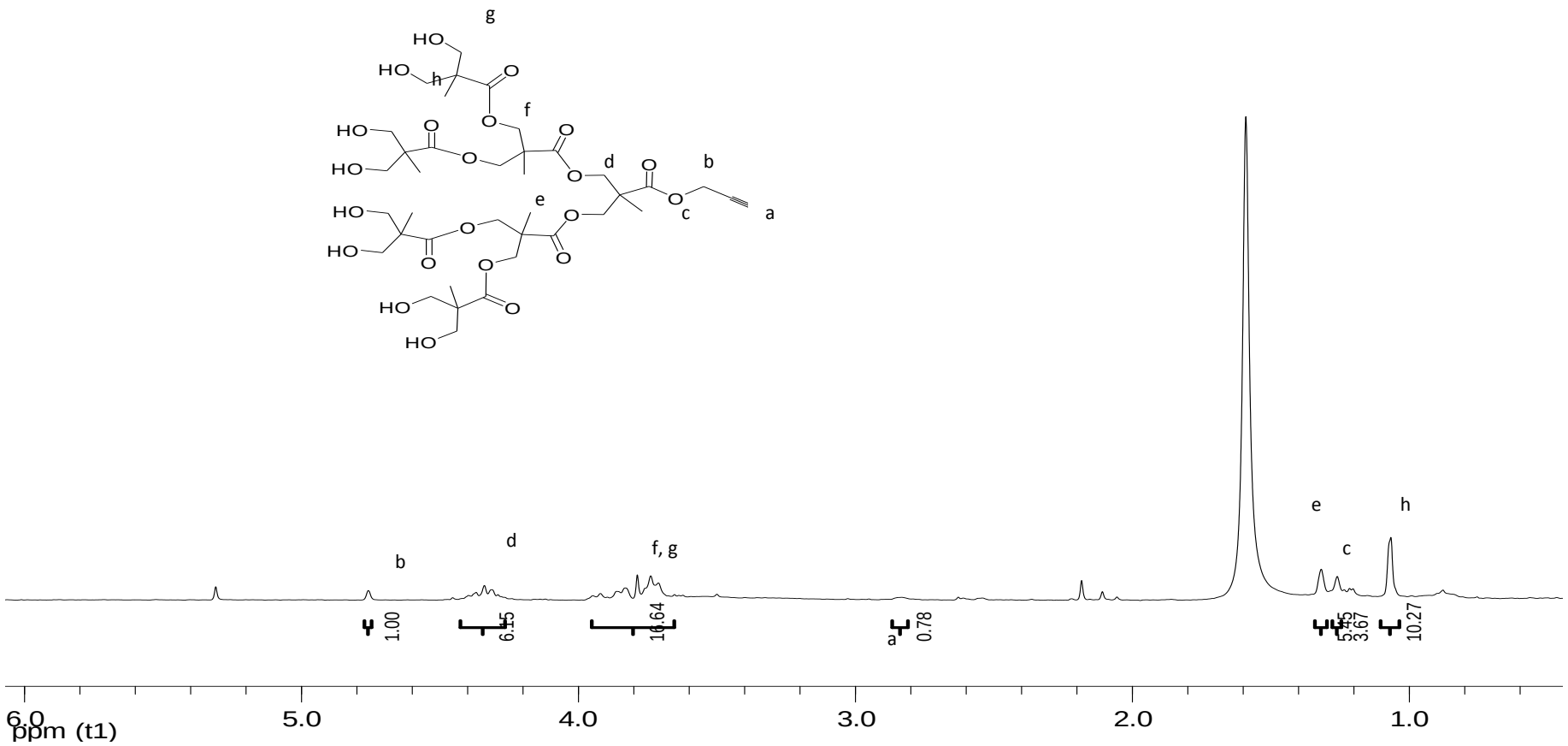

Figure A.2. ^{1}H NMR spectrum of p6.

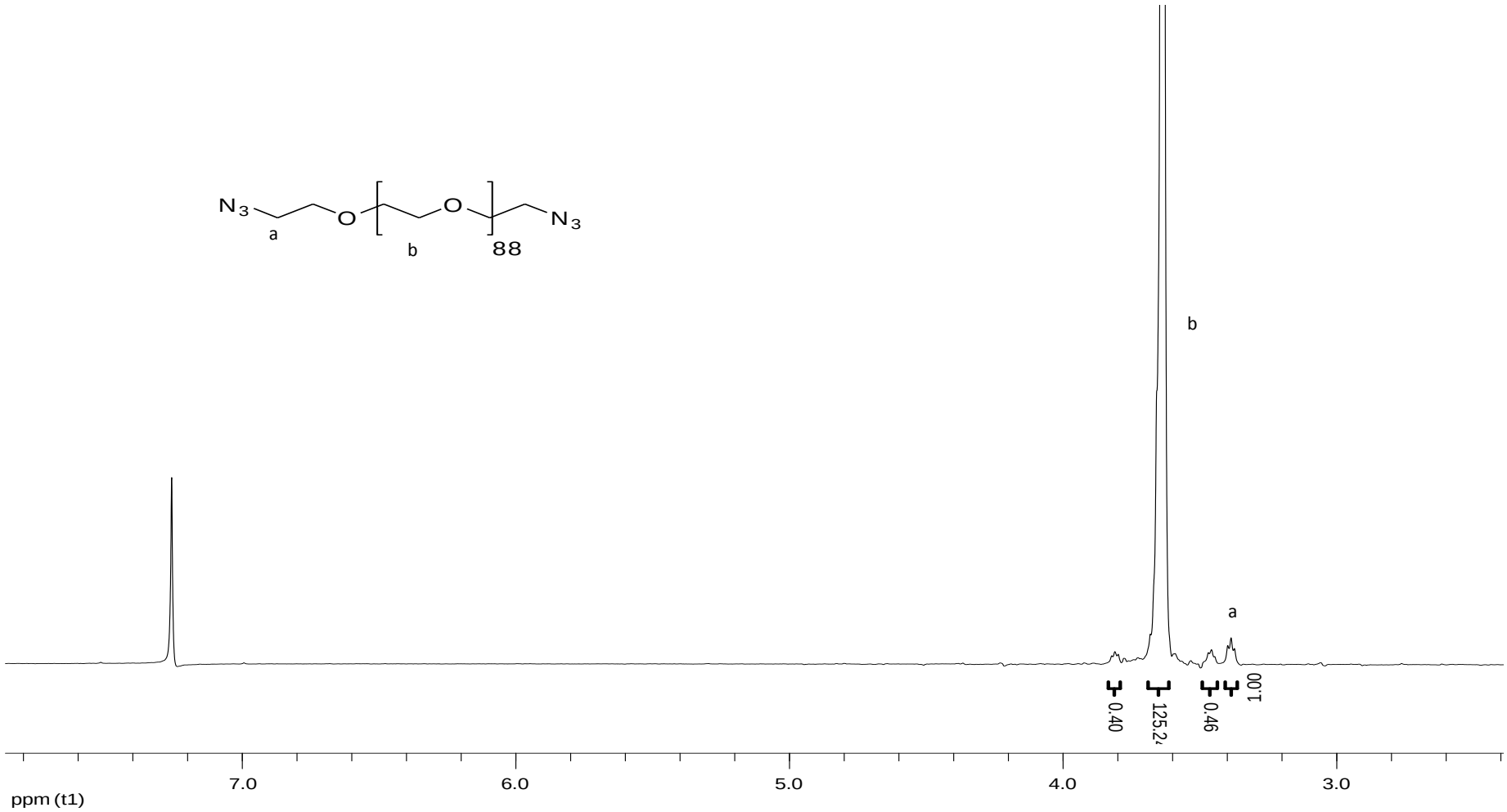

Figure A.3. ^{1}H NMR spectrum of p3.

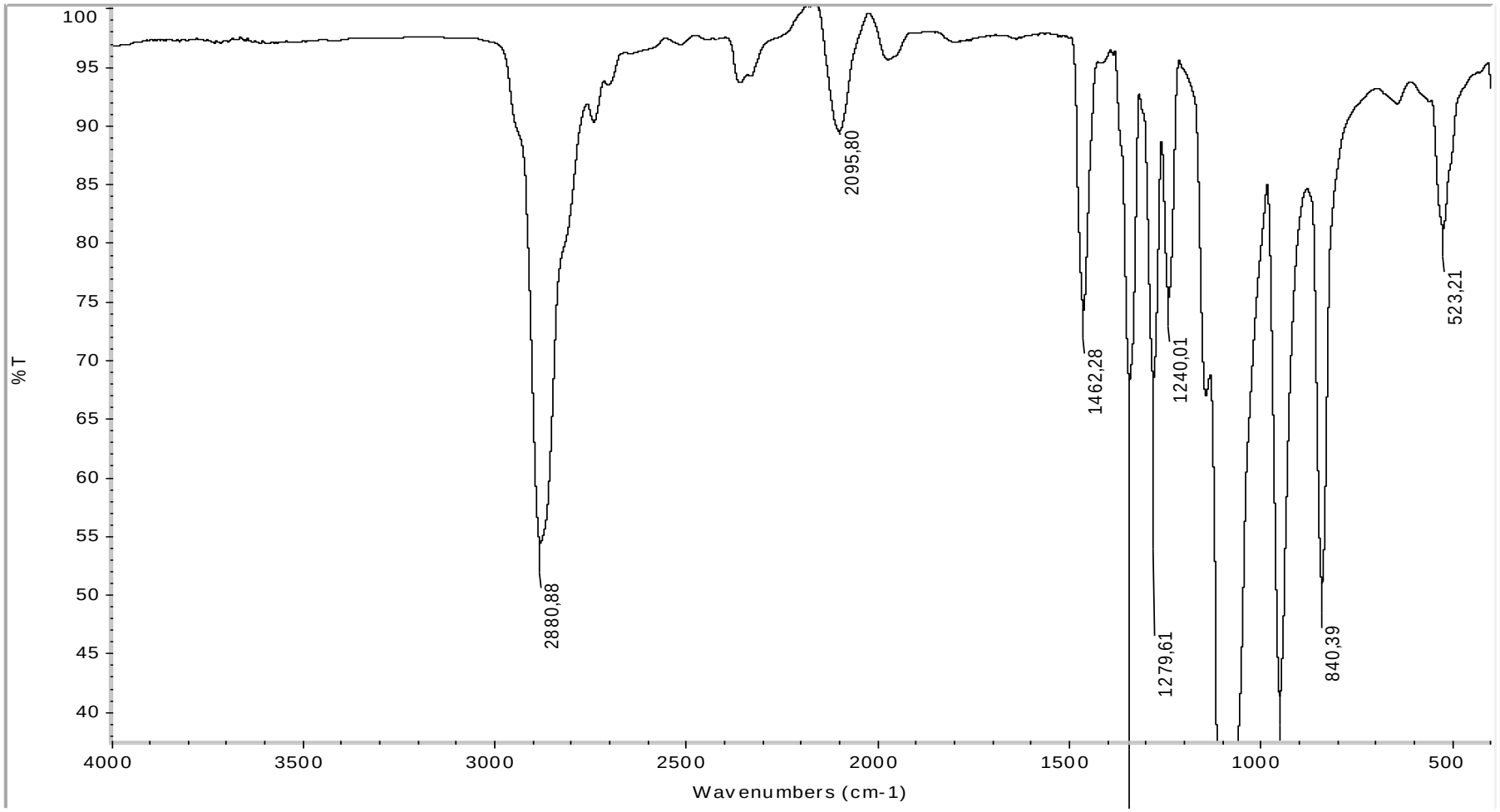

Figure A.4. FT-IR spectrum of p3.

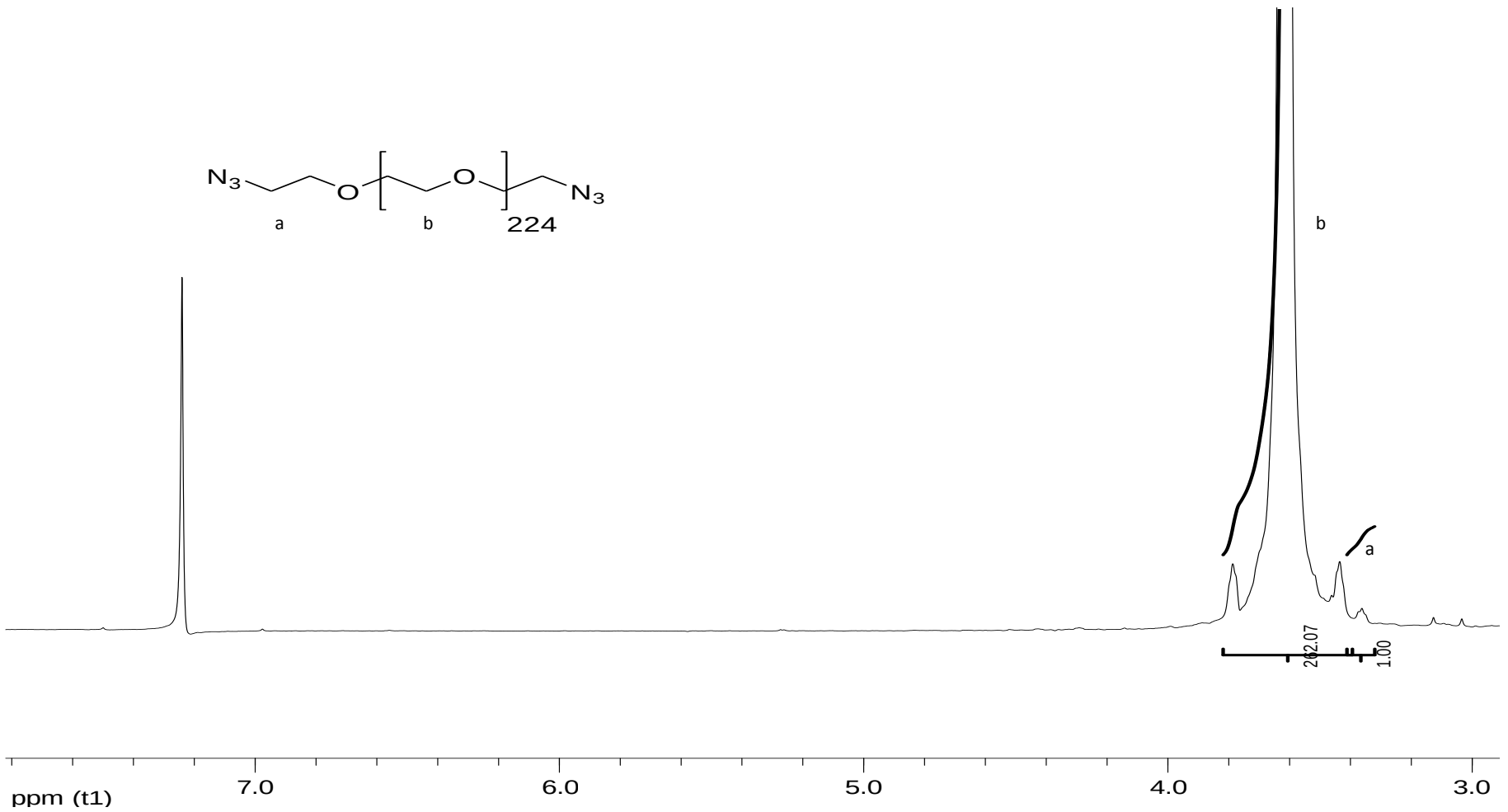

Figure A.5. ^{1}H NMR spectrum of p4.

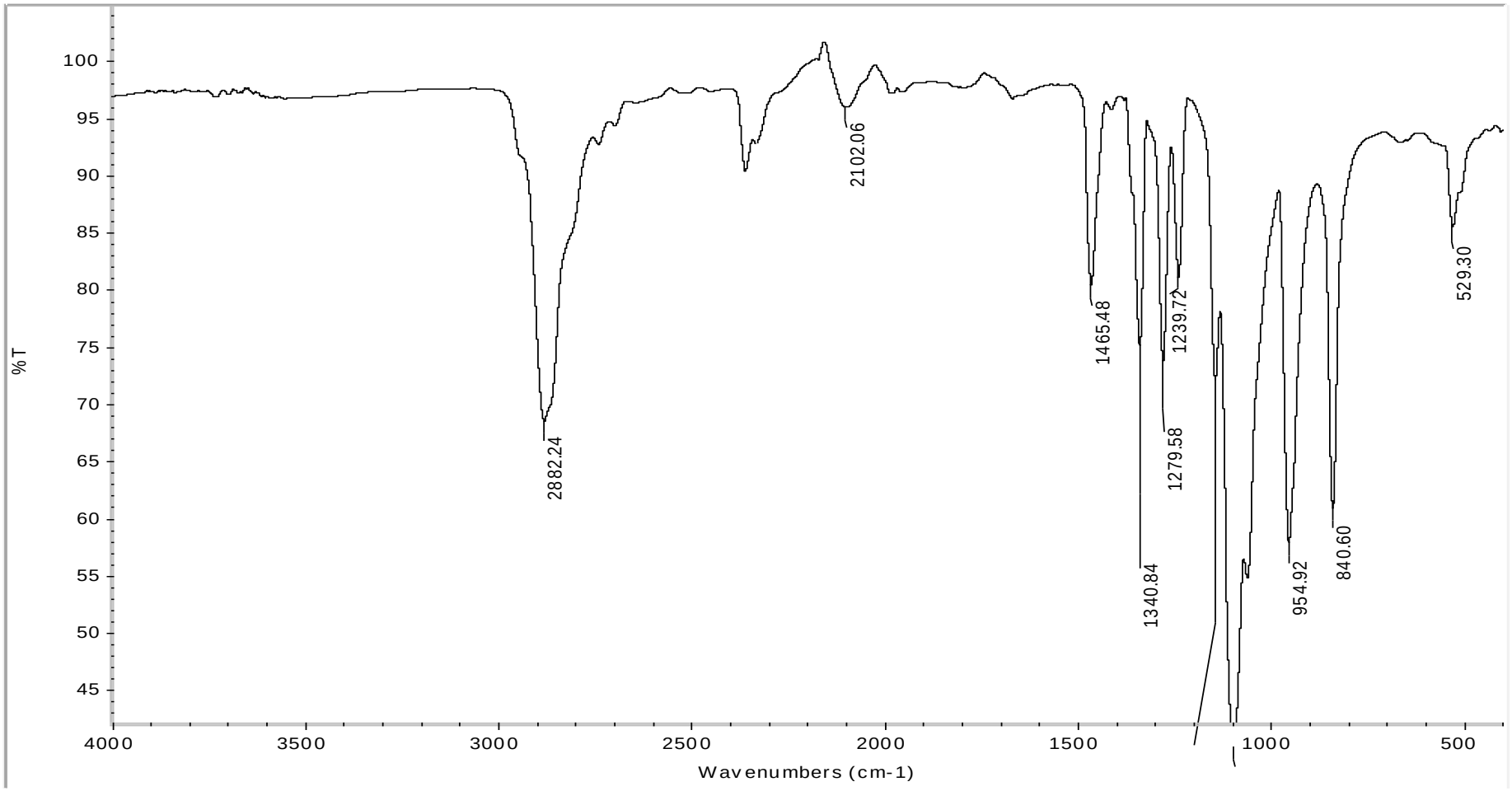

Figure A.6. FT-IR spectrum of p4.

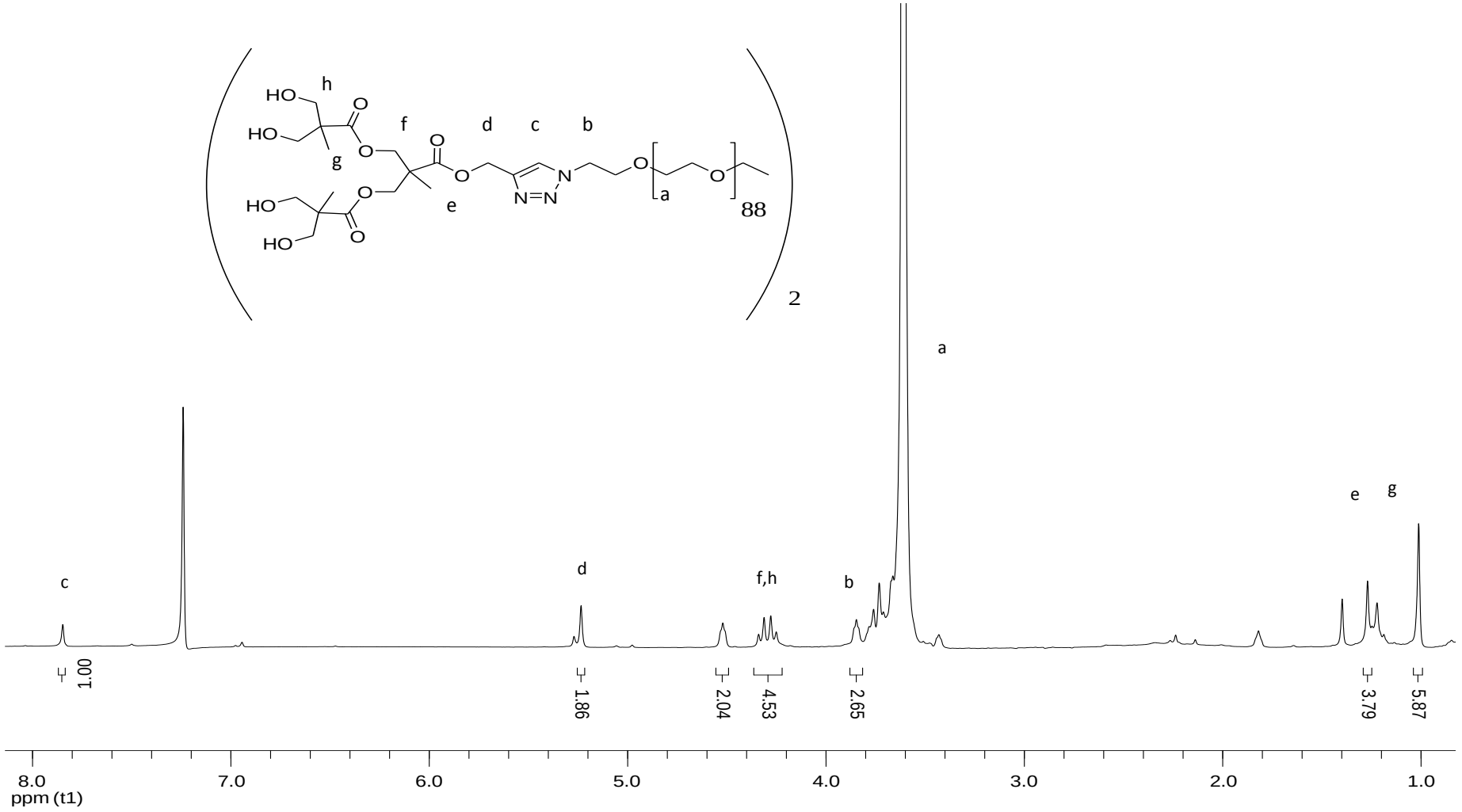

Figure A.7. ^{1}H NMR spectrum of p7.

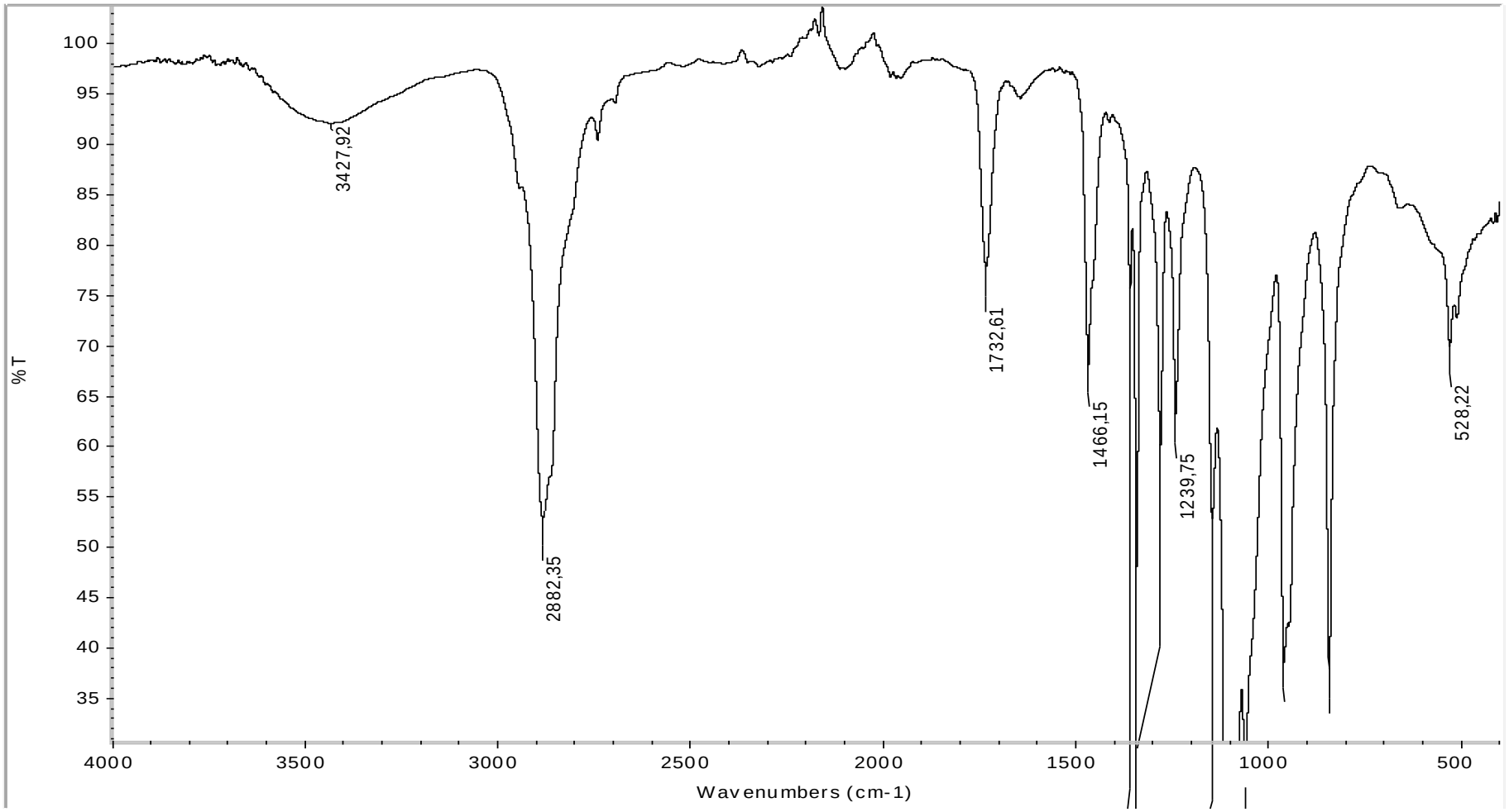

Figure A.8. FT-IR spectrum of p7.

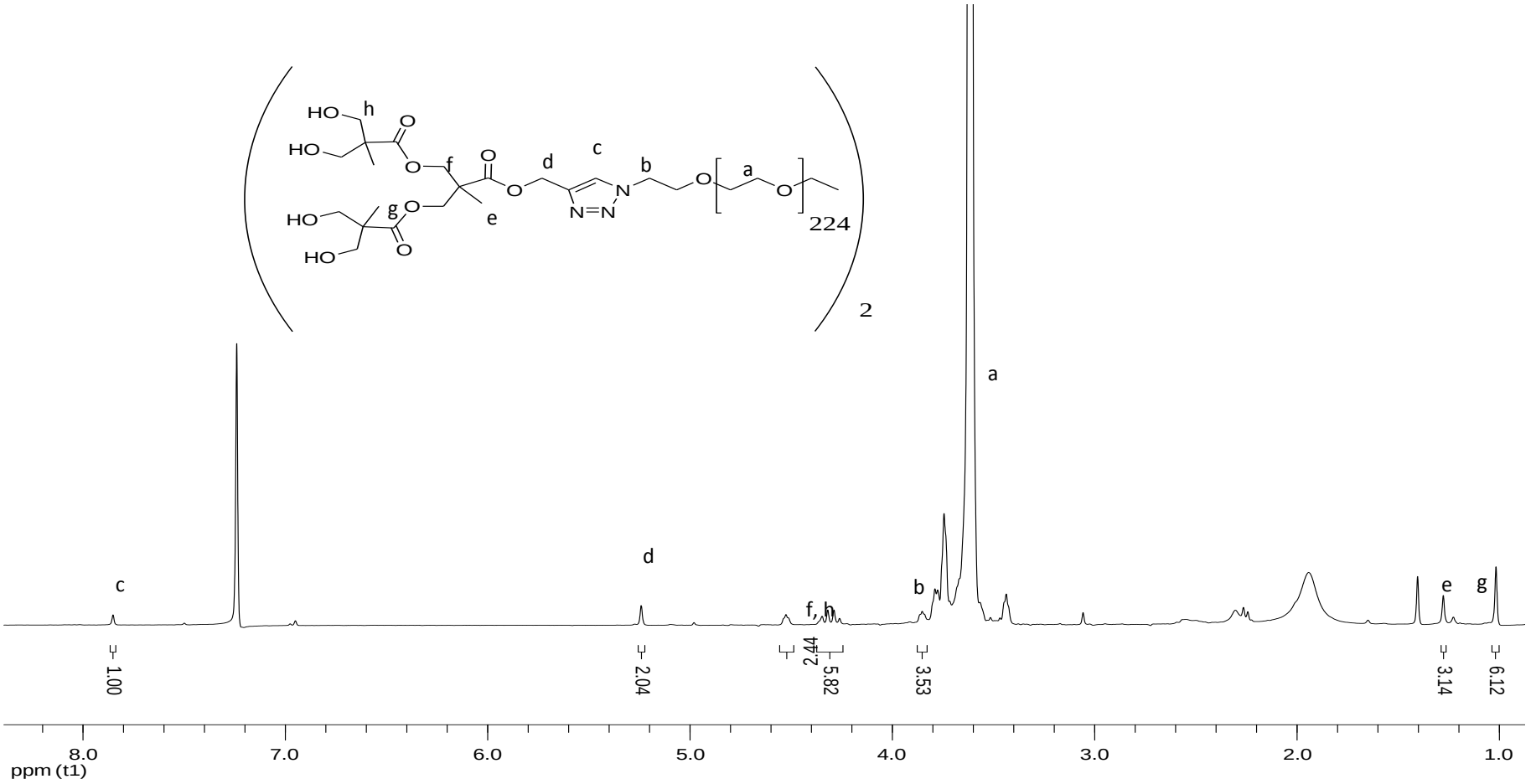

Figure A.9. ^{1}H NMR spectrum of p8.

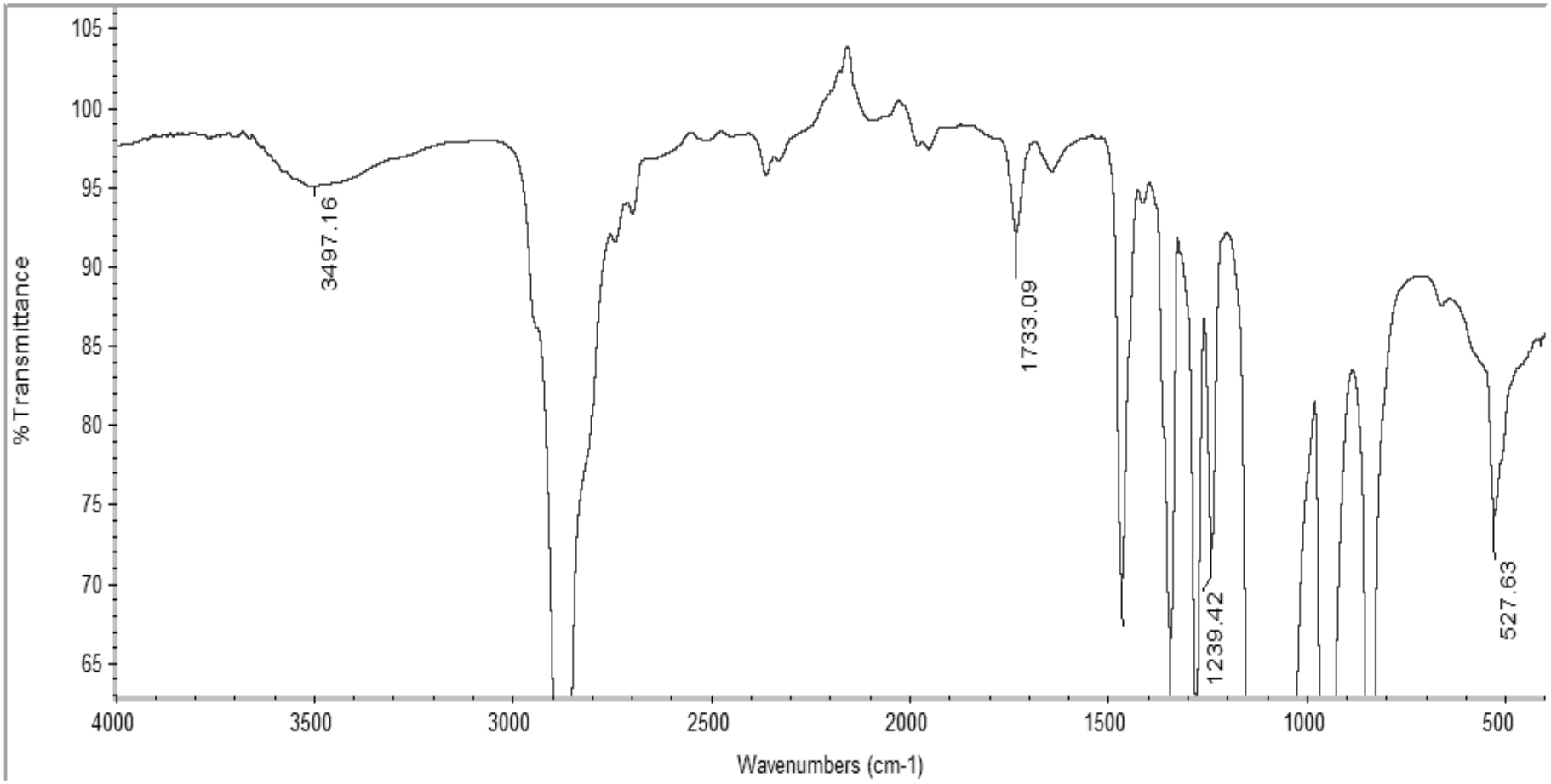

Figure A.10. FT-IR spectrum of p8.

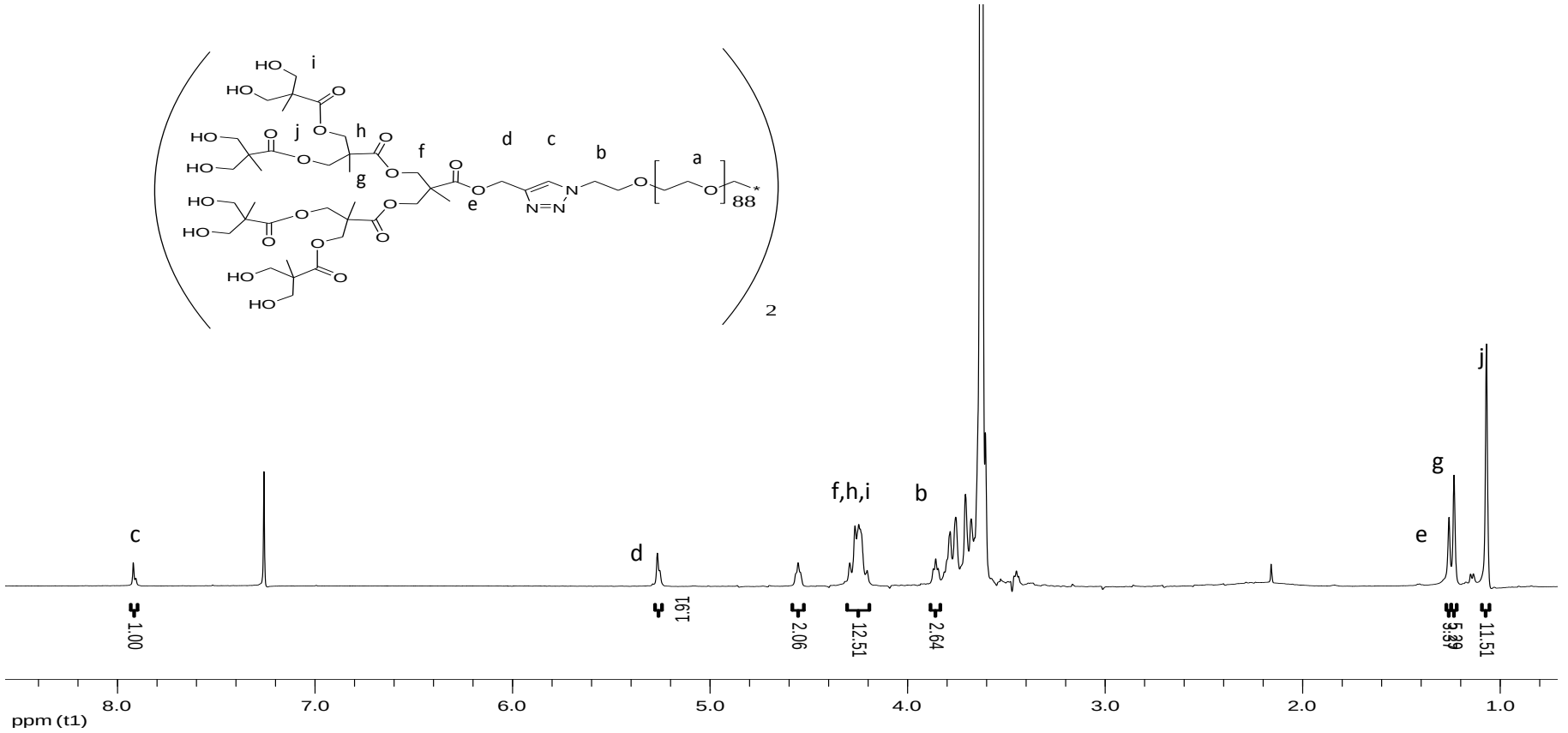

Figure A.11. ^{1}H NMR spectrum of p9.

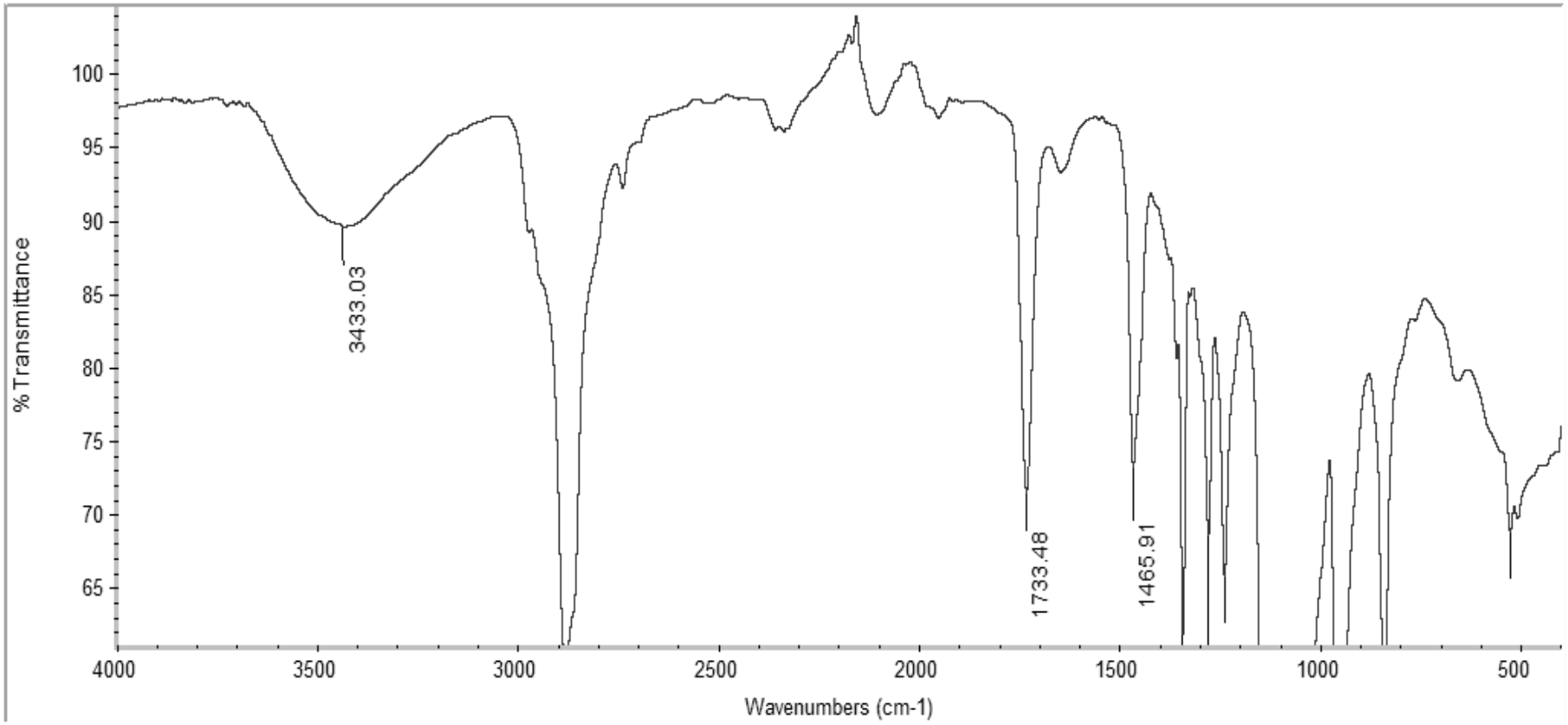

Figure A.12. FT-IR spectrum of p9.

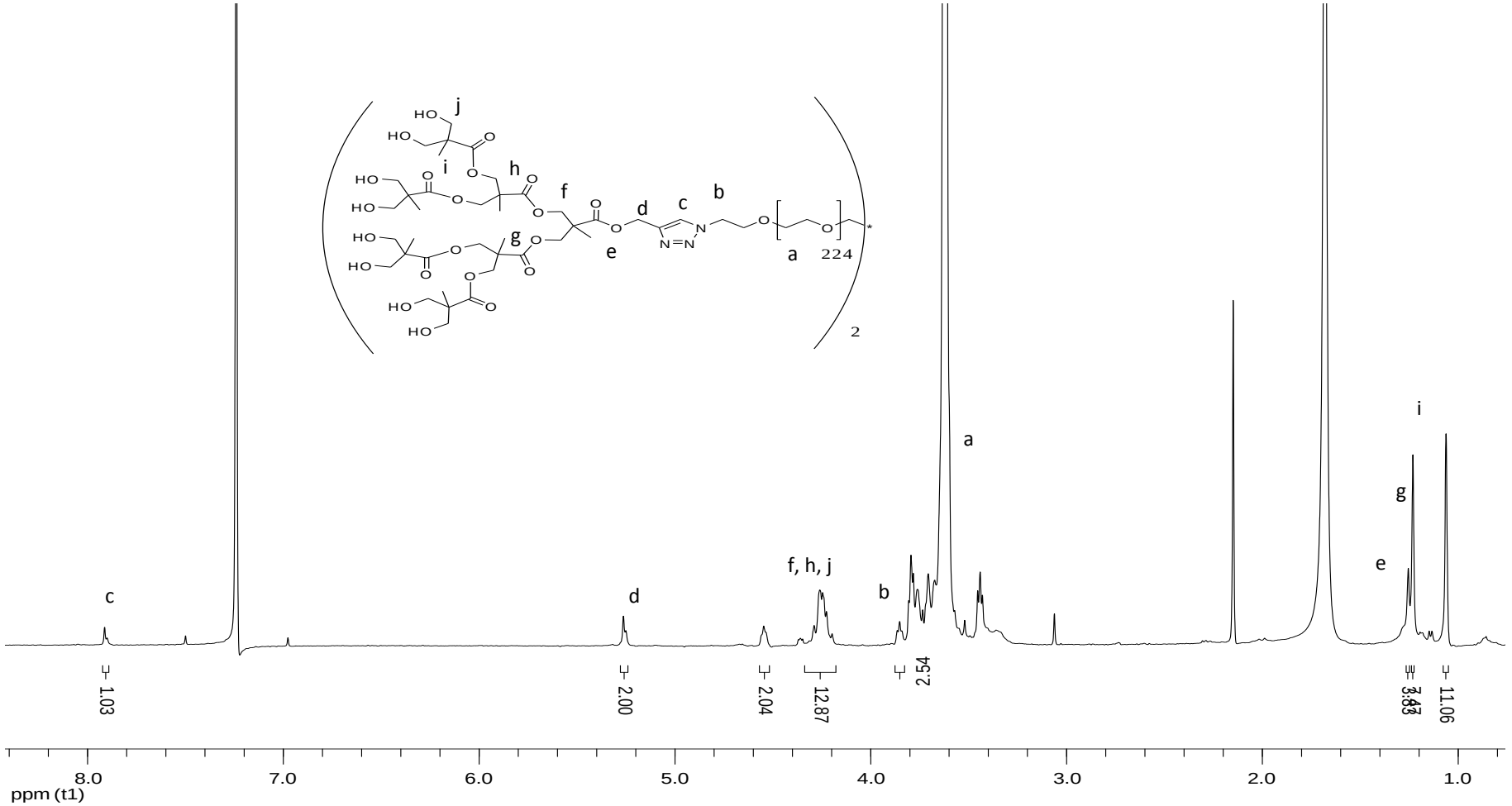

Figure A.13. 1H NMR spectrum of p10.

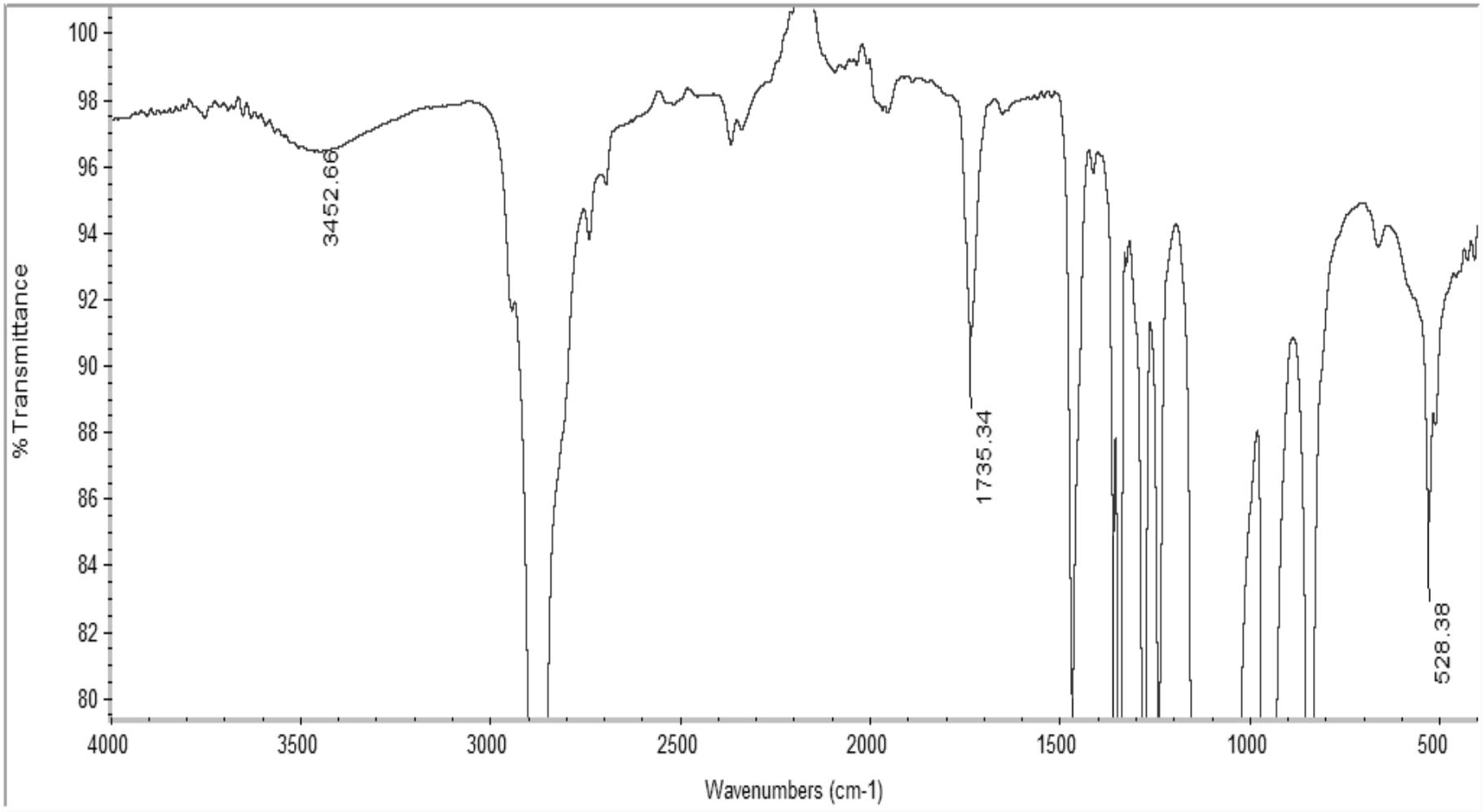

Figure A.14. FT-IR spectrum of p10.

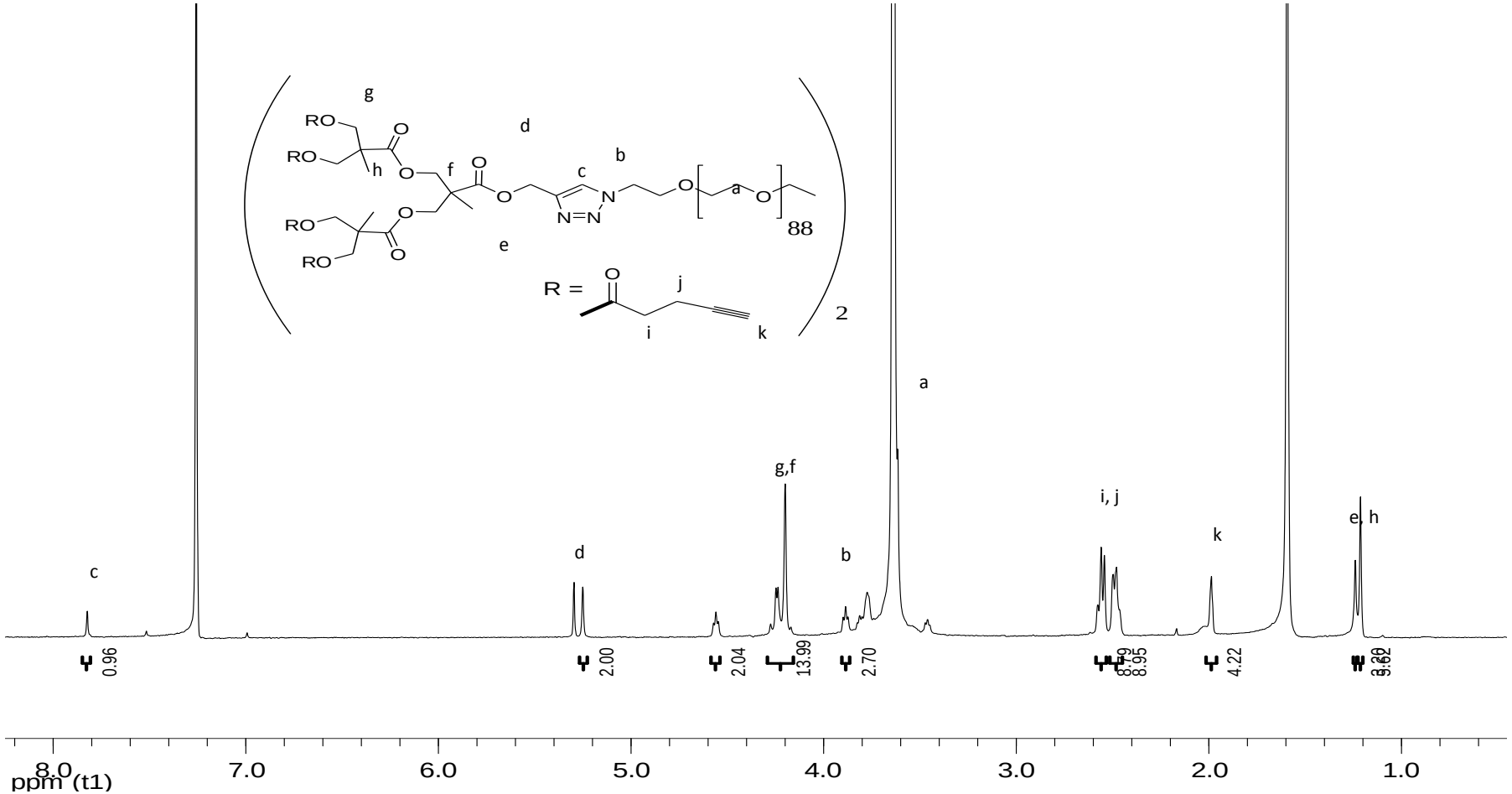

Figure A.15. ^{1}H NMR spectrum of p13.

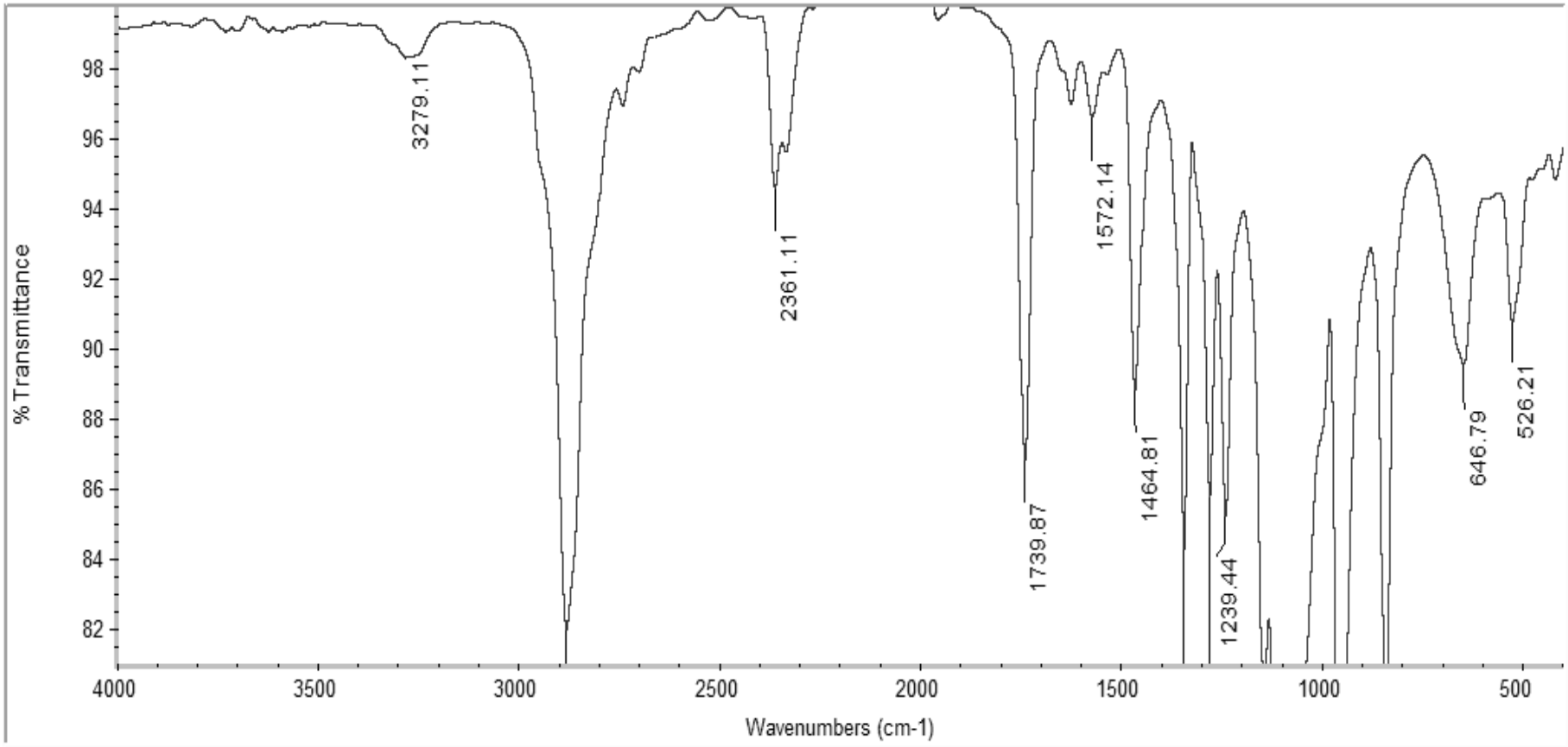

Figure A.16. FT-IR spectrum of p13.

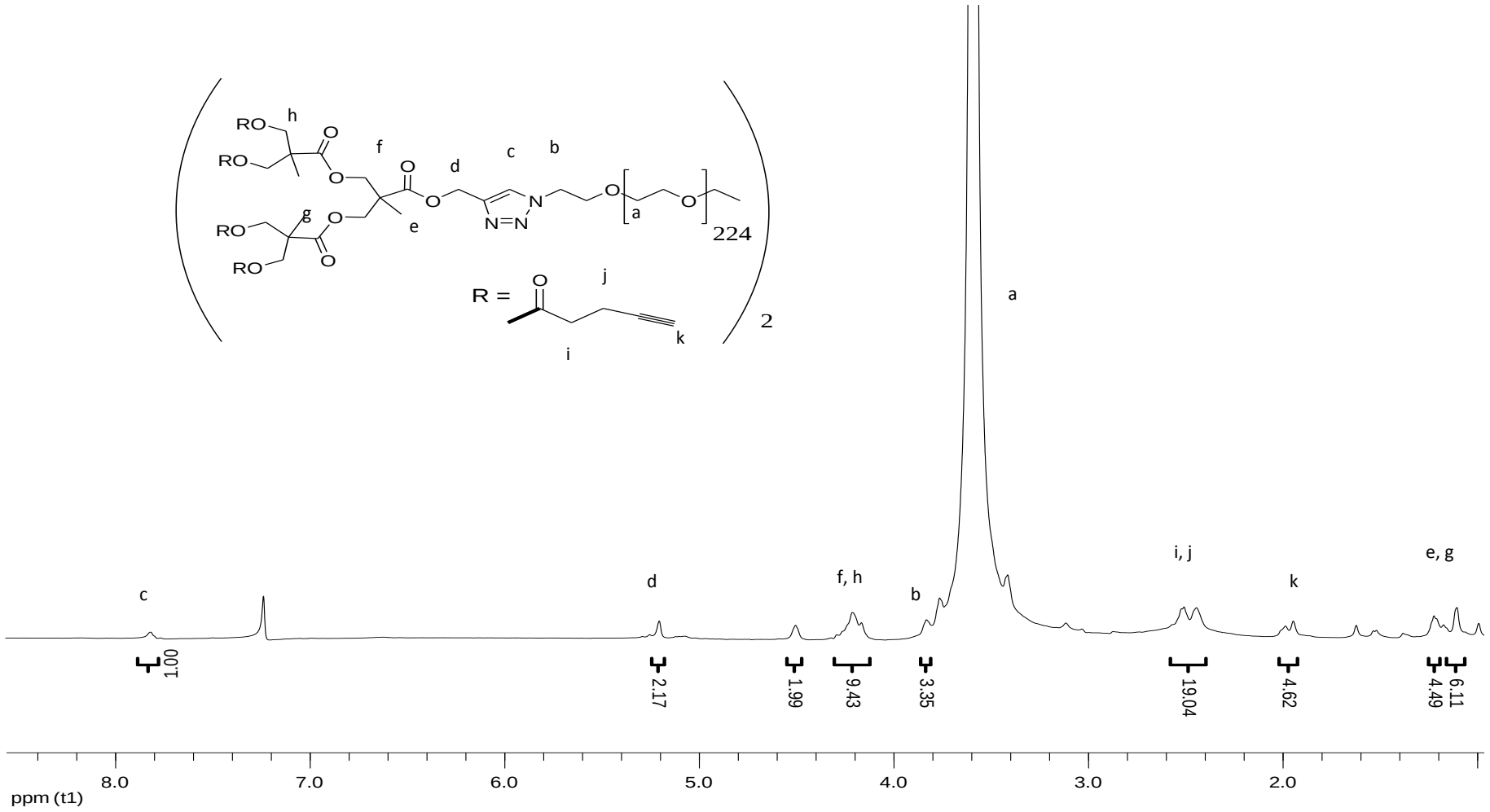

Figure A.17. 1H NMR spectrum of p14.

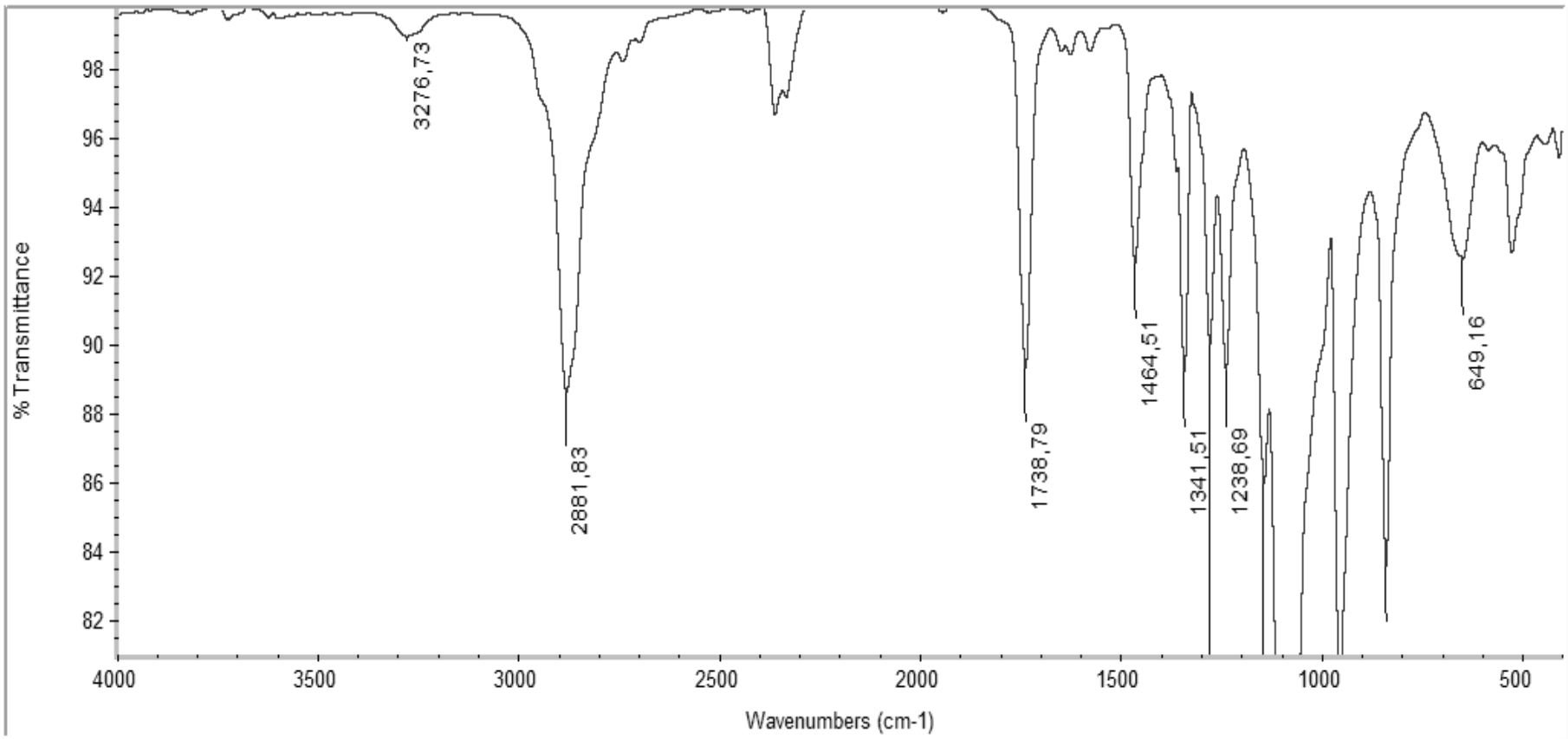

Figure A.18. ^{1}H NMR spectrum of p14.

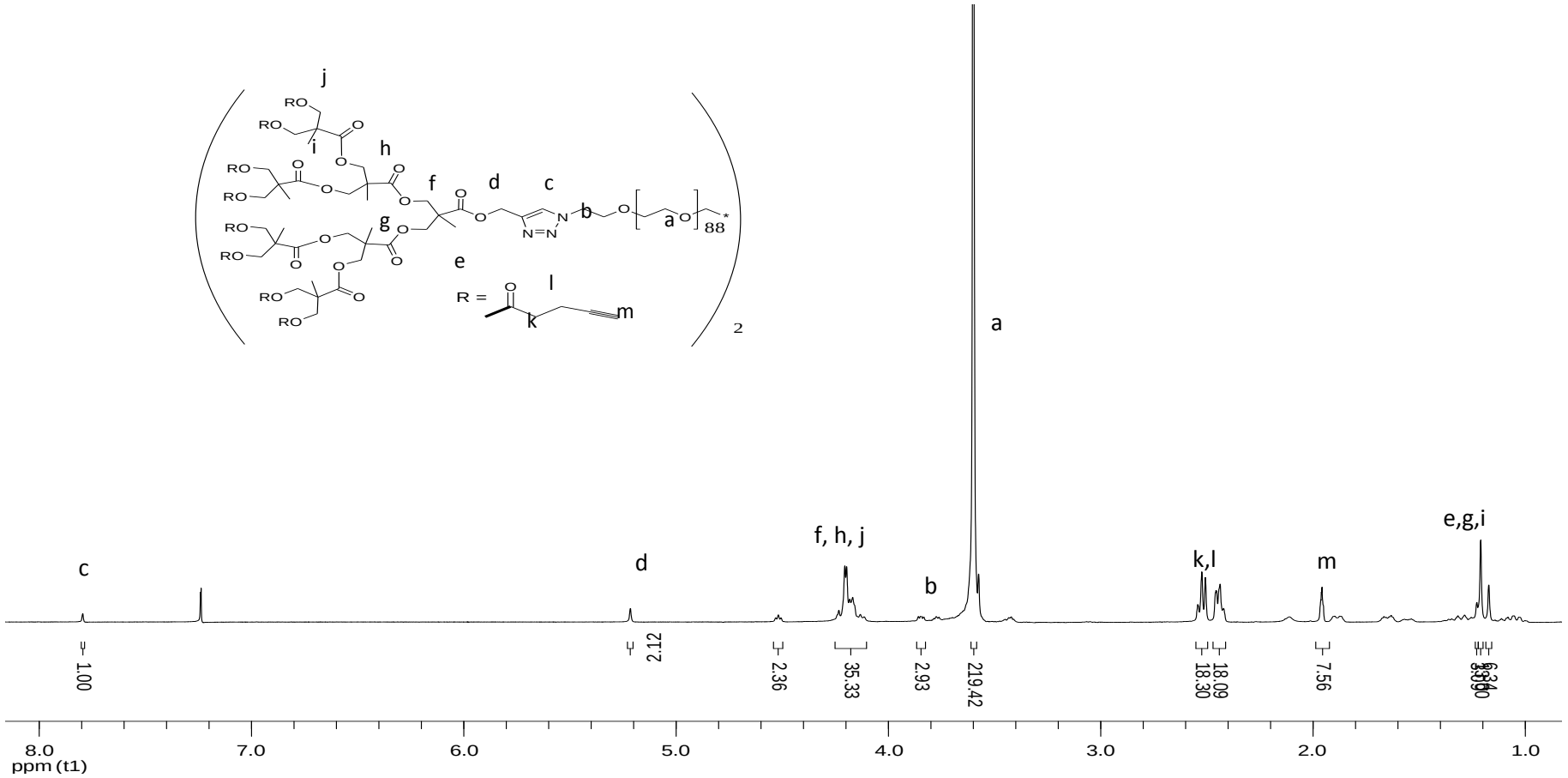

Figure A.19. ^{1}H NMR spectrum of p15.

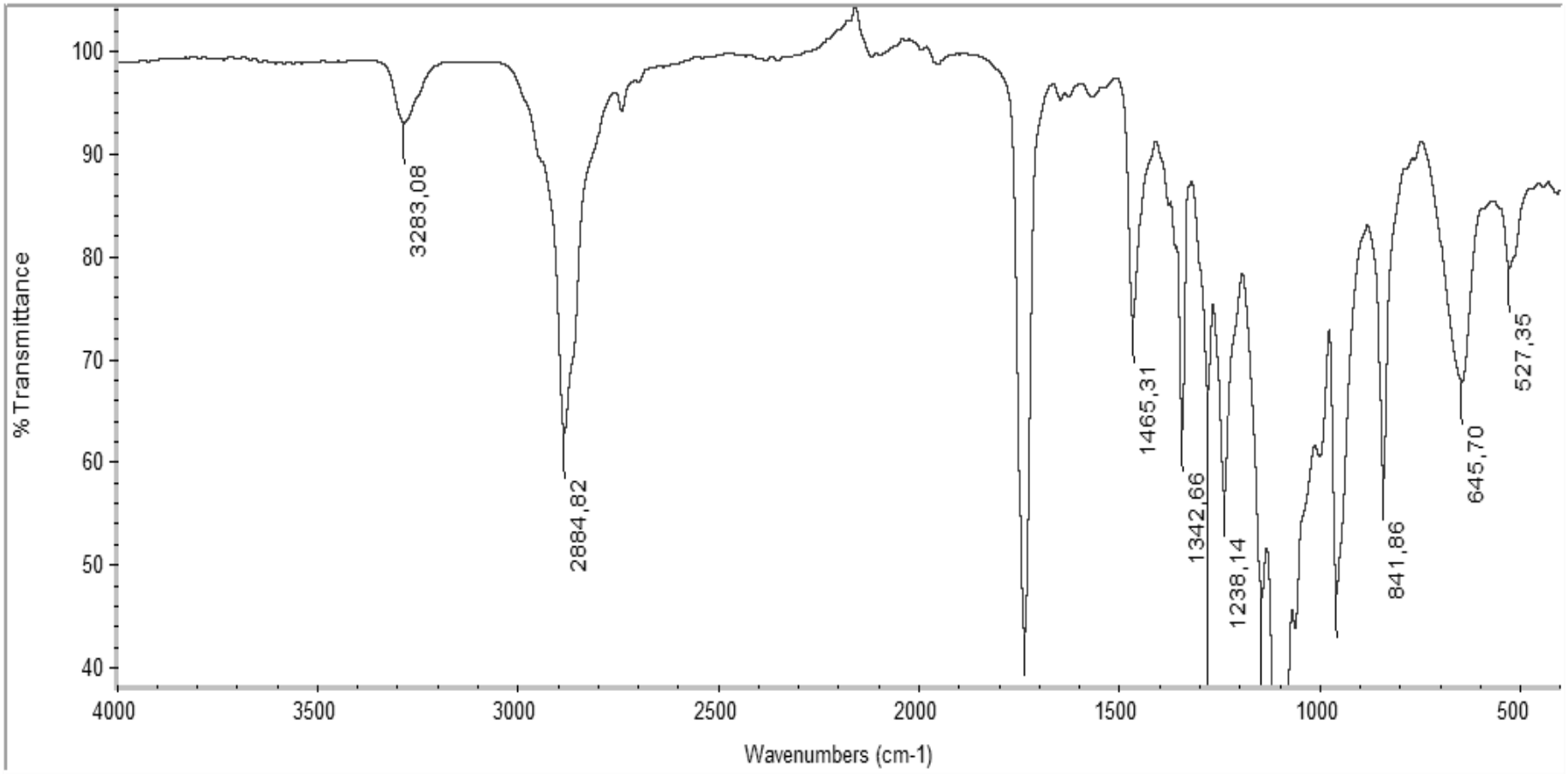

Figure A.20. FT-IR spectrum of p15.

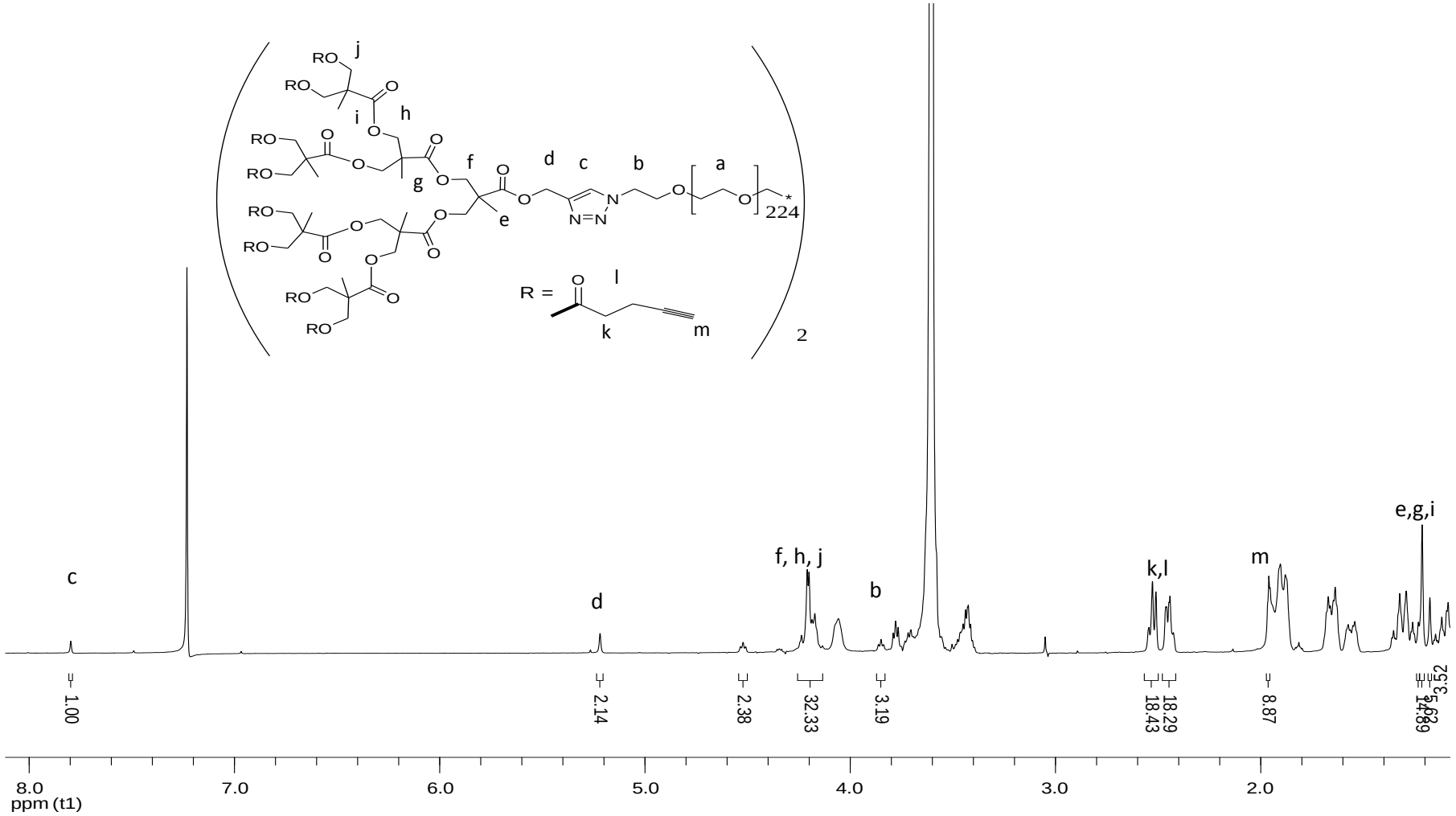

Figure A.21. 1H NMR spectrum of p16.

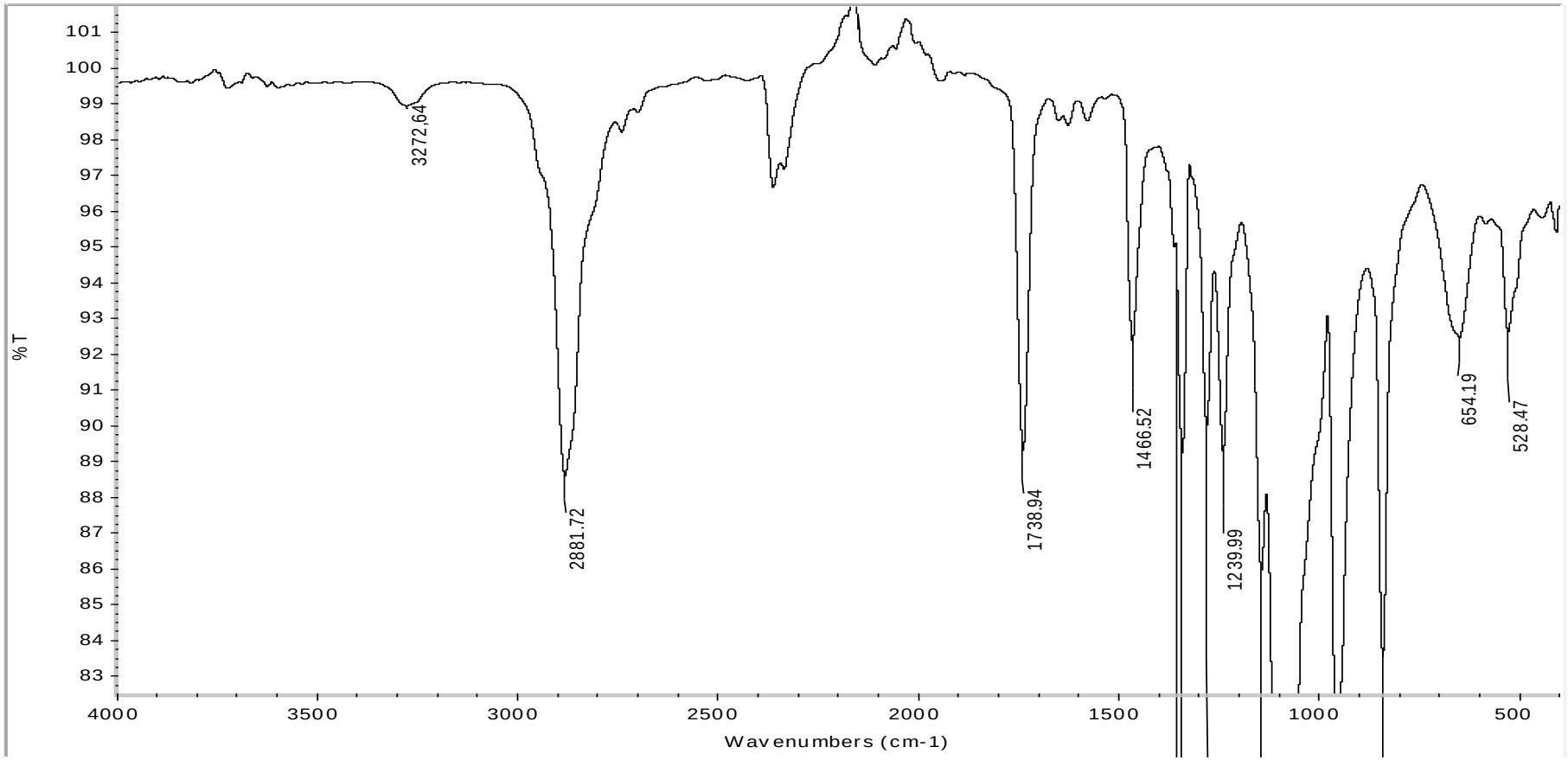

Figure A.22. FT-IR spectrum of p16.

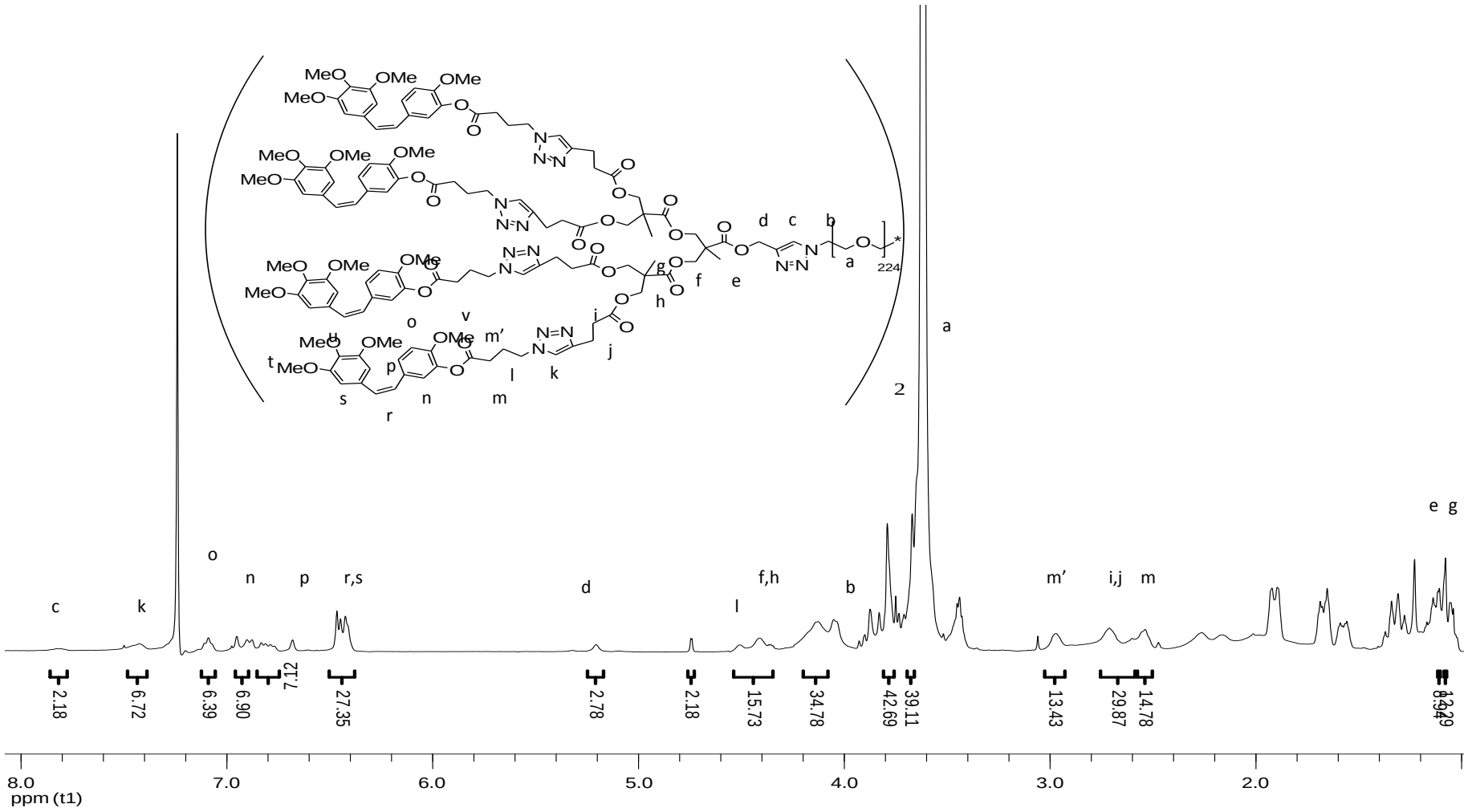

Figure A.23. ^{1}H NMR spectrum of p17.

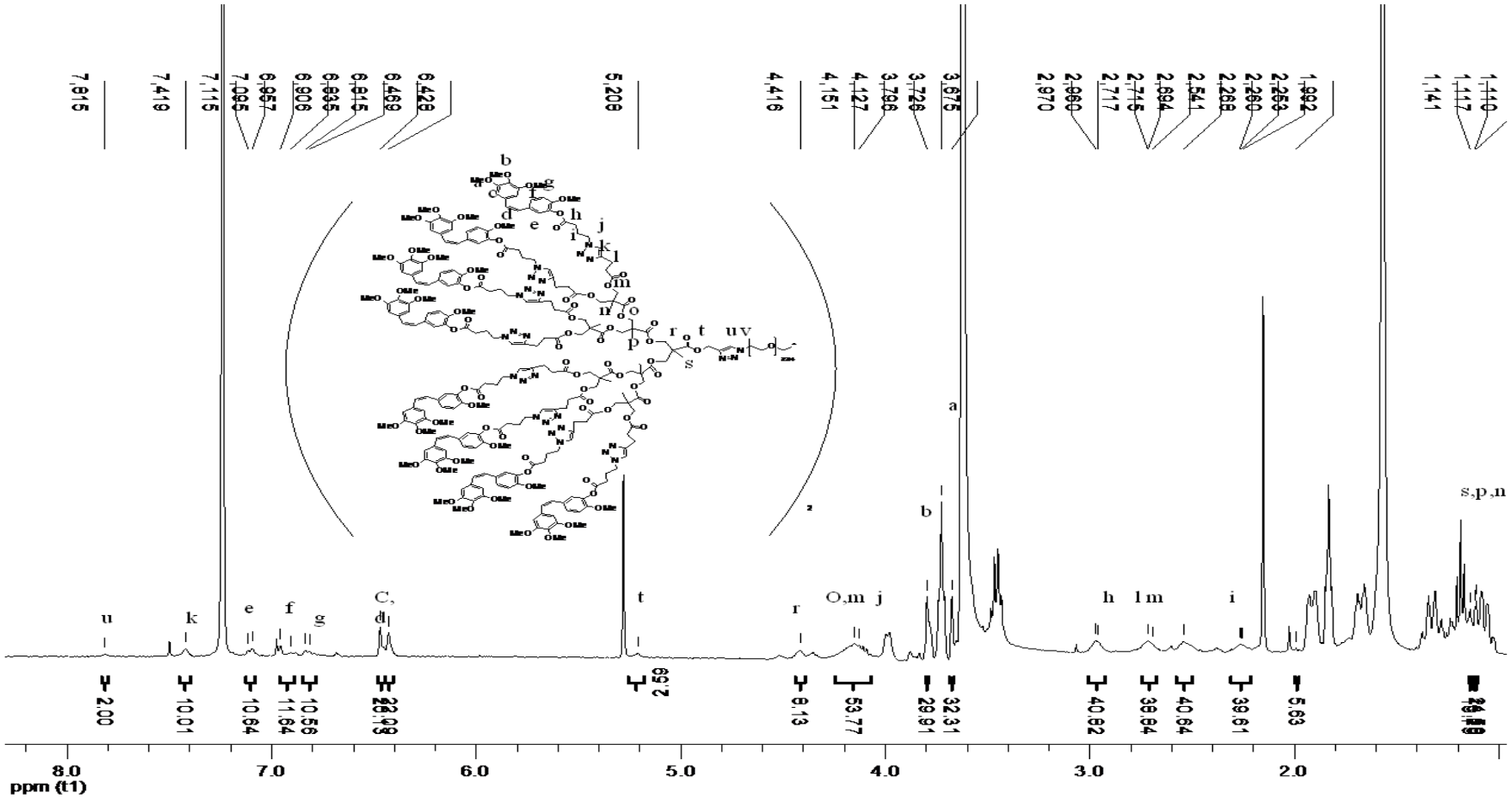

Figure A.24. ^{1}H NMR spectrum of p18.

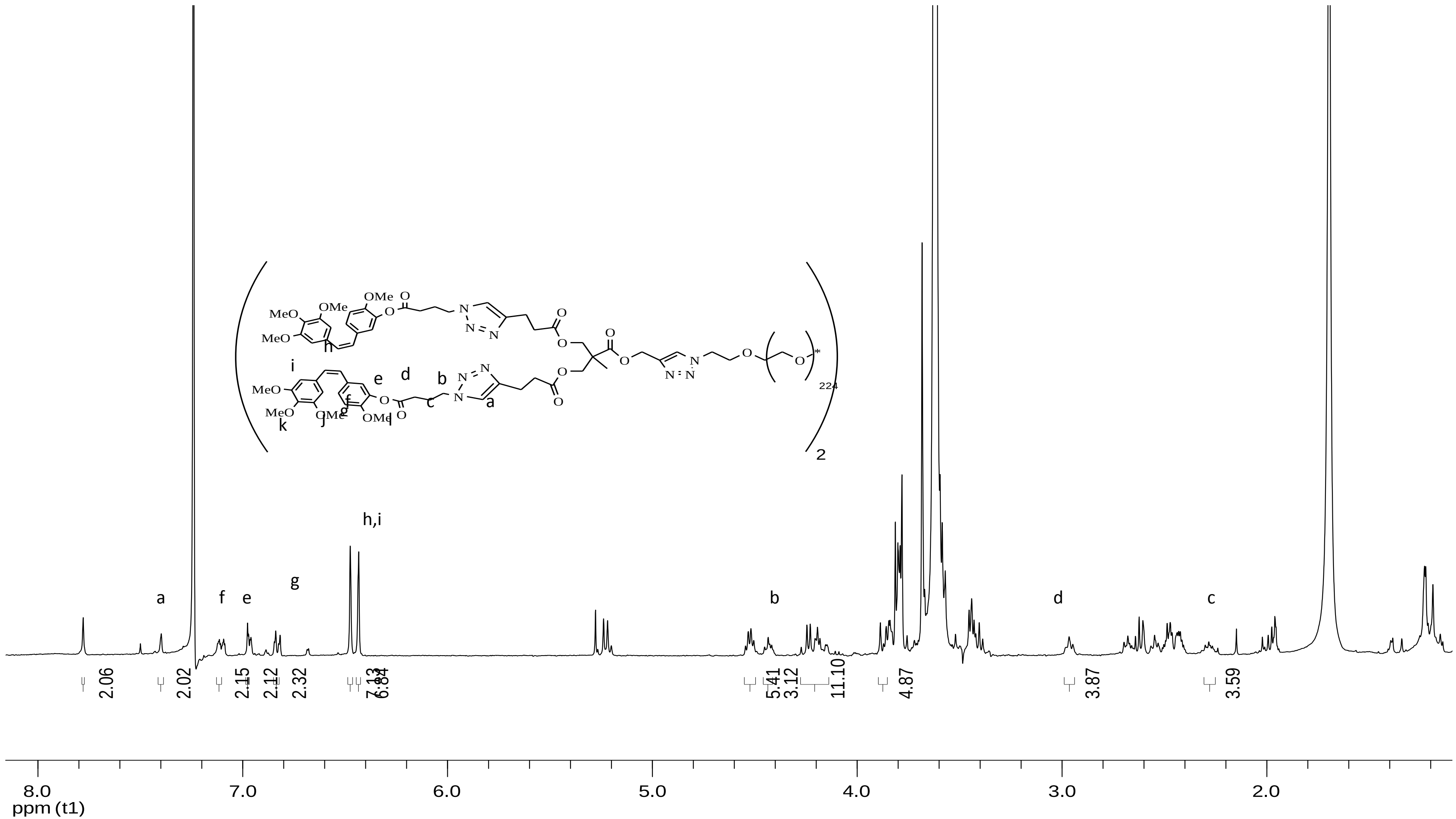

Figure A.25. ^{1}H NMR spectrum of p19.

REFERENCES

1. Bosman A. W. , H. M. Janssen, and E. W. Meijer, 'About Dendrimers: Structure, Physical Properties, and Applications' *Chemical Reviews* , Vol. 99, pp. 1665-1688 , 1999.

2. Malkoch M. , E. Malmstrolm and Anders Hult, 'Rapid and Efficient Synthesis of Aliphatic Ester Dendrons and Dendrimers', *Macromolecules,* Vol. 35, No. 22, pp. 8307–8314, 2002.

3. Medina S. H. and E. H. El-Sayed, 'Dendrimers as Carriers for Delivery of Chemotherapeutic Agents', *Chemical Reviews,* Vol.109, pp. 3141-3157, 2009.

4. Meldal M. and C. W. Tornøe, 'Cu-Catalyzed Azide-Alkyne Cycloaddition', *Chemical Reviews* , Vol. 108, pp. 2952–3015, 2008.

5. Kolb H. C. , M. G. Finn, and K.B.Sharpless, 'Click Chemistry', *Angewandte Chemie International Edition*, Vol. 40, pp. 2004–2021, 2001.

6. Helms B. , J. L. Mynar, C. J. Hawker, and J. M. J. Frechet, 'Dendronized Linear Polymers via "Click Chemistry", *Journal of the American Chemical Society*, Vol. 126, pp. 15020-15021, 2004.

7. Altin H. , I. Kosif, and R. Sanyal, 'Fabrication of "Clickable" Hydrogels via Dendron-Polymer Conjugates ', *Macromolecules*, Vol. 43, pp. 3801-3808, 2010.

8. Maeda H. , J. Wu., T. Sawa, Y. Matsumura and K. Hori, 'Tumor vascular permeability and the EPR effect in macromolecular therapeutics: a review', *Journal of Controlled Release* , Vol. *65*, pp. 271-284, 2000.

9. Lee C. C. , J. A. Mackay, J. M. J. Frechet and F. C. Szoka, 'Designing Dendrimers for Biological Applications', *Nature Biotechnology*, Vol. 23, No. 12, pp. 1517-1527, 2005.

10. Gillies E. R. and J. M. J. Frechet, 'Designing Macromolecules for Therapeutic Applications: Polyester Dendrimer – Poly(ethylene oxide) "Bow-Tie" Hybrids with Tunable Molecular Weight and Architecture*', Journal of the American Chemical Society,*Vol. 124, pp.14137-14146, 2002.

11. Gillies E. R. and J. M. J.Fréchet, 'Dendrimers and dendritic polymers in drug delivery', *Drug Discovery Today*, Vol. 10, No. 1, pp. 35-43, 2005.

12. Ihre H. R. , O. L. Padilla De Jesus, F. C. Szoka, and J. M. J. Frechet, ' Polyester Dendritic Systems for Drug Delivery Applications: Design, Synthesis, and Characterization', *Bioconjugate Chemistry*, Vol. 13, pp. 443-452, 2002.

13. Pasut G. , F.M. Veronese , 'PEG Conjugates in Clinical Development or Use as Anticancer agents: An overview', *Advanced Drug Delivery Reviews,*Vol. 61, pp. 1177-1188, 2009.

14. Yokoyama *et al*. , 'Polymeric Micelles Drug Carriers for Tumor Targeting', *Polymeric Drug Delivery*, pp. 27-36, 2006.

15. Gitsov I., K. R. Lambrych, V. A. Remnant, R. Pracitto, ''Micelles with Highly Branched Nanoporous Interior: Solution Properties and Binding Capabilities of Amphiphilic Copolymers with Linear Dendritic Architecture', *Journal of Polymer Science.: Part A: Polymer Chemistry*, Vol. 38, pp. 2711–2727, 2000.

16. Ganta S., H. Devalapally, A. Shahiwala, M. Amiji, 'A Review of Stimuli-Responsive Nanocarriers for Drug and Gene Delivery', *J. Controlled Release,* Vol. 126, pp. 187 – 204, 2008.

17. Maeda H., G. Y. Bharate, J. Daruwalla, 'Tumor-selective Delivery of Macromolecular Drugs via The EPR Effect: Background and Future Prospects', *European Journal of Pharmaceutics and Biopharmaceutics*, Vol. 71, pp. 409 –419, 2009.

18. Meng F. H. , Y. Zhong, J. Feijen, 'Stimuli-responsive polymersomes for programmed drug delivery', *Biomacromolecules* , Vol. 10, pp. 197 –209, 2009.

19. Torchilin V. P. , 'Cell penetrating peptide-modified pharmaceutical nanocarriers for intracellular drug and gene delivery ', *Biopolymers*, Vol. 90, pp. 604 – 610, 2008.

20. Yokoyama M. , T. Okano, Y. Sakurai, S. Suwa, and K. Kataoka, ' Introduction of Cisplatin into Polymeric Micelles', *Journal of Controlled Release,* Vol. 39, pp. 351-6, 1996.

21. Gref R. , Y. Minamitake , M.T. Percocchia, V. Trubetskoy, V.P. Torchillin, and R. Langer , 'Biodegradable Long-Circulating Polymeric Nanospheres', *Science* Vol. 263, pp. 1600-3, 1994.

22. Kim S. and K. Park, 'Targeted Delivery of Small and Macromolecular Drugs', Chp.19, *Polymer Micelles Drug Delivery*, pp. 513-552, CRC Press, 2010.

23. Tian L. and P. T. Hammond , 'Comb-Dendritic Block Copolymers as Tree-Shaped Macromolecular Amphiphiles for Nanoparticle Self-Assembly', *Chemical Mateials,* Vol. *18*, pp. 3976-3984, 2006.

24. Liu M. *et al.* , 'Water-Soluble Dendritic Unimolecular Micelles: Their Potential as Drug Delivery Agents', *Journal of Controlled Release,* Vol. 65, pp. 121 –131, 2000.

25. Kataoka K. , A. Harada, Y. Nagasaki, 'Block Copolymer Micelles for Drug Delivery: Design, Characterization and Biological Significance', *Advanced Drug Delivery Re*views, Vol. 47, pp. 113-131, 2001.

26. Klok *et.al.* , 'Advanced Drug Delivery Devices via sSelf-Assembly of Amphiphilic Block Copolymers', *Advanced Drug Delivery Re*views, Vol. 53, pp. 95-108, 2001.

27. Kwon G. S. , 'Poly (ethylene oxide)-Block-Poly (-amino acid) Micelles for Drug Delivery', *Advanced Drug Delivery Re*vievs, Vol. *54*, pp. 169-190, 2002.

28. Hubbell , J. A., ‘Enhancing drug function ’, *Science,* Vol. 300, pp. 595-596, 2002.

29. Anger P. , P. Bharadwaj and L. Novotny, ‘Enhancement and quenching of single-molecule fluorescence’, *Physical Review Letters,* Vol. 96, pp. 113002-113006, 2006.

30. Winnik F. M., ‘Fluorescence studies of aqueous solutions of poly (N-isopropylacrylamide) below and above their LCST ’, *Macromolecules*, Vol. 23, pp. 233-242, 1990.

31. Farinha J. P. S , S. Picarra, K. Miesel and J. M. G. Martinho, ‘Fluorescence Study of the Coil-Globule Transition of a PEO Chain in Toluene ’, *Journal of Physical Chemistry,* Vol. 105, pp.10536-10545, 2001.

32. Picarra S. , P. Relogio, C. A. M. Afonso, J.M.G. Martinho and J. P. S. Farinha, ‘Coil−Globule Transition of Poly(Dimethylacrylamide): Fluorescence and Light Scattering Study’, *Macromolecules*, Vol. 36, pp. 8119-8129, 2003.

33. Yang H. *et al*., ‘Polyethylene glycol–polyamidoamine dendritic micelle as solubility enhancer and the effect of the length of polyethylene glycol arms on the solubility of pyrene in water ’, *Journal of Colloid Interface Science*, Vol. 273, pp. 148–154, 2004.